STABILIZING CONTROL AND CONTROLLABILITY:

CONTROL SOLUTIONS TO AVOID SLUG FLOW IN PIPELINE-RISER SYSTEMS

by

Espen Storkaas

A Thesis Submitted for the Degree of Dr. Ing.

Department of Chemical Engineering
Norwegian University of Science and Technology

7 June 2005

ISBN: 82-471-7072-8 (printed version),
82-471-7070-1(electronic version)

Abstract

Riser slugging is a flow regime that can occur in multiphase pipeline-riser systems, and is characterized by severe flow and pressure oscillations. The irregular flow caused by riser slugging can cause large operational problems for the downstream receiving facilities, and an effective way to handle or remove riser slugging is needed. Recently, anti-slug control systems that stabilize the flow in the pipeline at the same operating conditions that uncontrolled would yield riser slugging has emerged as the preferred solution to avoid riser slugging. This thesis offers a comprehensive analysis of the system characteristics that are relevant to control and, based on that controllability analysis, robust anti-slug controllers are designed.

The controllability analysis is done using two different models. Initially, a simplified two-fluid model is used, and the analysis shows that riser slugging can be avoided by a simple control system that manipulates the valve at the top of the riser. The type and location of the measurement to the controller is, however, critical, and the best choice is to use a pressure measurement located either at the pipeline inlet or at the riser base. A flow measurement at the top of the riser can also be used, but, because the steady-state gain is close to zero, it should only be used in combination with another measurement.

The analysis with the two-fluid model also revealed that the, for control purposes, an even simpler model can be used. Based on this conclusion, a simple nonlinear dynamic model with only three states is developed. This model covers both riser slugging, and, more importantly, the unstable but preferred non-oscillatory flow regime that exists at the same boundary condition. The three-state model is verified throughout the thesis by providing the same controllability results as the more complicated two-fluid model, by showing the same dynamic behavior as both the two-fluid model and OLGA, and finally by the fact that controllers based on the three-state model show excellent performance when they are tested on the other models.

The valve used as manipulated input for anti-slug controllers is large and often slow-acting. A too slow valve can result in saturations problems, and we derive conditions that give a lower bound on the input rate for stabilizing control and perfect disturbance rejection. The required input rate can be combined with the input magnitude limitations to form a frequency-dependent bound on the input that can be used directly in a controllability analysis or in controller design.

Both simple PID controllers and model based $\mathcal{H}_\infty$ controllers are designed and tested by simulations with all three models (three-state, two-fluid and OLGA). If an upstream pressure measurement is used as input, a PID controller is close to optimal and provides good performance and robustness. Controllers that are based only on topside measurements (e.g. pressure drop over valve, flow or even valve position) can also provide robust stability, but if fast setpoint tracking is required, a MISO (multiple-input single-output) $\mathcal{H}_\infty$ controller must be used.

Finally, the scope for pipeline control is extended to cover other multiphase phenomena than only riser slugging. In an industrial case study, an extended slug controller is introduced that, in addition an anti-slug controller, contains flow controllers to minimize the effect of transient slugs such as surge waves and startup slugs.

Acknowledgment

As I am writing these final words on this thesis, I find my self looking back on the almost five years I have spent working on it and trying to summarize the experience. The work has been an invaluable learning experience, both personally and professionally, because of the challenges it presented and also because it has given me the chance to get to know and work with interesting and knowledgeable people. Thus, at this point, there is a lot of people that I would like to thank for their help and guidance.

First and foremost, my deepest gratitude goes to to my supervisor, professor Sigurd Skogestad, whose insight, enthusiasm and ability to see both the finer details and the bigger picture has been invaluable during the work on this thesis. He has always taken an active interest in my work, and I am proud to have been given the opportunity to work under his supervision.

Second, I would like to thank my friend and co-worker Vidar Alstad. We have shared an office during our graduate studies, and he has always been willing to provide help or discuss parts of my work. By also being a good and trusted fried, he has made my work a lot easier and a lot more fun.

Furthermore, I would like to thank the rest of the Process control group and all the other people I have be fortunate enough to work with. A special thanks goes to the members and organizers of the Petronics program for including me as an associate member, to the Process Control group at the Statoil Research center at Rotvoll for the time I spent there and the many things they taught me, and to Professor Dale Seborg at the Process Control group, UC Santa Barbara, for allowing me to come and work with his group during the spring of 2002.

I would also like to thank all my friends, both in Trondheim and elsewhere. A special thanks goes to Kristin Tøndel, who has encouraged and inspired me throughout my graduate studies.

My family has always been there for me, and for that, they have my gratitude. Even though the physical distance between Trondheim and Skien at times may have seemed large, they have always been supportive and caring, and through that, we have remained close.

Finally, I would like to dedicate this thesis to the memory to my grandmother, Ester Hegna, whose love of life and positive attitude have been a great inspiration to me and to everybody that was fortunate enough to get to know her.

Contents

Chapter 1

Introduction

1.1 Motivation

Flow assurance technology has played a key role in the development of the offshore oil and gas industry for the past 20 years. The term flow assurance covers the entire spectrum of design tools, methods, equipment, knowledge and professional skills needed to ensure the safe, uninterrupted and simultaneous transport of gas, oil and water from reservoirs to the processing facilities (Buller et al., 2002). The background for the important role of flow assurance is that the North Sea is becoming a mature region in terms of hydrocarbon production. The majority of the new discoveries are now, and are likely to be in the future, too small to be developed as independent, stand-alone fields. Also, as existing fields are entering their tail-phase production, spare processing capacity is becoming available on the existing offshore processing facilities. Thus, the smaller fields are being tied in to existing infrastructure as satellite fields both to make the production from these fields economically viable and to utilize the existing production capacity.

The tie-in lines from the satellite fields are transporting the untreated wellstream, consisting of a mixture of gas, oil, water and in some cases sand, from the wellhead clusters into the production platforms. The flow assurance challenges associated with the transport of this mixture over long distances involves handling physical flow-impeding phenomena such as slug flow and sand transport and physio-chemical flow-impeding phenomena such as hydrates, scale, asphaltenes, wax and emulsions. In addition to the flow-impeding phenomena, corrosion problems has to be addressed and equipment for metering, pumping/compression and flow restriction/control have to be designed and optimized (Buller et al., 2002).

The topic of this thesis is slug flow, or more precisely, how to avoid slug flow. Slug flow is a flow regime in multiphase pipeline flow that is characterized by varying or irregular flows and surges of gas and liquid through any cross-section of a pipeline. The irregular flow conditions can create severe problems for the downstream processing facilities, and a means for removing or reducing the undesirable slug flow in the pipeline is sought.

1.2 Flow regimes in multiphase pipelines

The spatial distribution of the phases in multiphase flow is dependent on operating conditions such as phase velocities and pipeline angle. The different configurations the flow can arrange itself in are called flow regimes or flow patterns (Baker, 1954; Mandhane et al., 1974; Taitel and Dukler, 1976; Taitel et al., 1980; Barnea, 1987; Weisman et al., 1979). The possible flow patterns include stratified flow, annular flow, bubbly flow, slug flow and churn flow. Various intermediate flow patterns can also be present in pipelines.

Slug flow can occur on different time- and length scales depending on the underlying mechanism for the slug flow formation. In this work, the definitions in Buller et al. (2002) are used to divide slug flow in pipeline-riser systems into four different types:

- *Hydrodynamic slugging* develops in horizontal parts of the pipeline when liquid waves grow on the gas-liquid interface and eventually close the cross-section, thus forming liquid slugs
- *Riser slugging* occurs when liquid blocks the low-point where a down-sloping pipeline is attached to a riser. The blockage initiates the slug, which thereafter grows upward in the riser and back through the pipeline. This continues until the pressure build-up over the slug is sufficiently high to blow it out of the riser, whereupon the entire cycle is repeated.
- *Terrain slugging* involves slug development where pipelines traverse rough seafloor terrain. The slug picks up liquid accumulated in inclined sections and may become very extensive
- *Transient slugging* is caused by increased liquid flow rates at pipeline exit to processing facilities in response to changes in operating conditions

Of these four, riser slugging, possibly combined with or initiated by terrain slugging, is the most serious for oil/water-dominated systems. For the most serious cases, the riser slugs can fill up the entire riser and be several hundred meters long. The inlet separator on the receiving facilities is not large enough to receive these slugs. If such a large slug were to arrive into the separator it would cause overfilling which would trip the production. Even smaller riser slugs can be problematic, as the uneven feed to the process will lead to poor separation, varying compressor load and wear and tear on the equipment. Hence, riser slugging must be avoided in pipeline-riser systems.

1.3 Anti-slug control

Control systems that are designed to avoid riser slugging in pipeline-riser systems are often called slug controllers. This term is misleading, as it suggests that the riser slugs still exist in the pipeline, and that the control system is only trying to limit or suppress them. The real role of these control systems are to completely remove the riser slugs by stabilizing a desired, but unstable, flow regime that exists at the same boundary conditions as riser slugging. We will use the term *anti-slug* control with the following definition:

Definition 1.1 ***An anti-slug controller*** *is a controller that stabilizes a desired, non-oscillatory flow regime that exists at the same boundary conditions as riser slugging and thereby avoids the formation of riser slugging in the system.*

1.3.1 Previous work

Up until the last few years, the preferred solution to avoid or reduce the problems associated with riser slugging has been to design the system such that the slugging potential is minimized or to change the boundary condition (that is, reducing the topside choke valve opening) to remove the slug flow from the system (Sarica and Tengesdal, 2000). None of these solutions are optimal. Design changes often involve installation of expensive equipment such as slug catchers and reducing the topside choke valve opening introduces extra pressure drop that will limit production when the reservoir pressure goes down as the reservoir is depleted.

An alternative approach based on feedback control to avoid riser slugging was first proposed by Schmidt et al. (1979*a*). The key concept in that paper was to avoid riser slugging by automatically adjusting the topside choke valve position based on an algorithm with a pressure measurement upstream of the riser and a flow measurement in the riser as inputs. Hedne and Linga (1990) used a more conventional PI controller based on an upstream pressure measurement to avoid riser slugging. Both these papers are based on experimental work in medium scale flow loops and show the potential for using control solutions to avoid riser slugging in pipeline-risers systems. The benefits of using a control solution are that no expensive equipment is needed and that no significant pressure drop is added to the system. However, the work of Schmidt et al. (1979*a*) and Hedne and Linga (1990) did not result in any reported industrial applications.

In the last ten years or so, there has been a renewed interest in control based solutions to avoid riser slugging. Courbot (1996) presents a control system to prevent riser slugging implemented on the Dunbar pipeline. The approach in this paper was to implement a control system that uses the topside choke valve to keep the pressure at the riser base at or above the peak pressure in a the riser slug cycle, thus preventing liquid accumulation in the bottom of the riser. This approach effectively removed riser slugging in the system, but it did so by automating the old choking strategy rather than affecting the stability of the flow regimes in the pipeline. This means that an extra pressure drop was introduced in the system due to the high setpoint for the pressure controller. Henriot et al. (1999) presents a simulation study for the same pipeline as Courbot (1996), where the setpoint for the riser base pressure is set considerably lower. In this work, the controller is probably stabilizing an unstable operating point rather than just keeping the process away from the riser slugging region, although this is not shown explicitly.

The first industrial implementation of an anti-slug controller is reported by Havre et al. (2000), who presents an anti-slug control system for the Hod-Valhall pipeline and illustrates its performance both with simulations and actual field data. The simulation results illustrate an interesting fact; by turning the control system off and keeping the same valve opening as was implemented (on average) by the control system, the riser slugging returns in the system. This proves that the control system stabilizes an unstable operating point. This

unstable operating point, where the flow in the pipeline is steady, exists at the same boundary condition as would normally result in riser slugging. Havre and Dalsmo (2002) give a more detailed treatment of the control system introduced in Havre et al. (2000).

Skofteland and Godhavn (2003) use conventional PID controllers to stabilize the flow in pipeline-riser systems and reports both field experience from the Heidrun field and experimental results from Sintef Petroleum Research Multiphase Flow Laboratory. A main contribution in this paper is the introduction of a cascade control system, where an inner flow loop is combined with an outer pressure loop to suppress bot severe and moderate slugging. Additional experimental work is reported in Godhavn, Mehrdad and Fuchs (2005) and Fard et al. (2003). Godhavn, Strand and Skofteland (2005) reports an application at the Tordis field, where an anti-slug controller is combined with model predictive control to also handle slugs that enter the inlet separator.

Hollenberg et al. (1995) presents a different approach for removing severe slugging form a pipeline-riser system. By introducing a small separator on top of the riser, the gas and liquid flow can be controlled separately above a certain frequency. This structure, called the S^3® Slug Suppression System also allows for accurate measurement of the gas and liquid rate, and by controlling the total mixture flow rate and the pressure in the small separator, the system can be stabilized. Kovalev et al. (2003) report that the S^3 system has been successfully implemented at the North Cormorant and Brent Charlie platforms in the North Sea.

As this brief literature review shows, most of the published results regarding avoiding riser slugging are from either oil companies or engineering companies. These companies, which have been active in this field of research for some time, may have in-house expertise regarding the slug control that are not published and hence not available as background material for this work.

1.4 Contributions and thesis outline

This thesis offers a comprehensive analysis of the controllability properties of a pipeline-riser system at riser slugging conditions. Based on the controllability analysis, robust anti-slug controllers that stabilize the flow and thus avoid riser slugging are designed. A number of different control structures and controller designs are considered, with the primary aim of stabilizing the flow whilst avoiding input saturation and providing low-frequency performance.

The scope of this thesis is, except for the case study in chapter 7, limited to two-phase flow, where the oil and water phase is treated as one continuous phase. Water can, especially in cases where the water cut is high, have a significant impact on the riser slugging problem, but this effect is not included in this work. Also, the scope is limited to tie-in lines from subsea templates with respect to pipeline geometry. Other typical pipeline geometries, such as a pipeline from a wellhead platform to a production platform, are not considered.

1.4.1 Model development and controllability analysis

Chapter 2

A simplified two-fluid model based on distributed mass and momentum conservation equations for each phase is developed and fitted to a simulated OLGA test case. From an analysis of the model, we find that the transition from stable flow (at low choke valve openings) to riser slugging (at higher valve openings) is through a Hopf bifurcation, and that the system contains a pair of complex conjugate unstable poles p_i. A controllability analysis reveals that the system can be stabilize by simple controllers provided that the right measurements are used.

Chapter 3

The main contribution in chapter 3 is the introducing of the simplified three-state model. The model is fitted to both experimental data and to data from a simulated OLGA test case with good results. The model is further verified by comparing open-loop step responses to both the two-fluid model and OLGA and by comparing local (linear) behavior and results from a controllability analysis with the two-fluid model.

The three-state model is well suited for analysis and controller design because of its limited complexity and its ability to predict the system characteristics important for control, and is thus an important tool for designing anti-slug controllers for pipeline-riser systems.

1.4.2 Effect of input rate limitations

Chapter 4

Stabilizing control of the pipeline-riser system is based on manipulating the topside choke valve. These choke valves are big and often slow-action, and the opening time for the valve can be a limiting factor for an anti-slug controller. Therefore, we introduce a method for calculating the required valve rate for stabilizing control, as well as for perfect disturbance rejection. The limitations on the input rate is then combined with the input magnitude limitations to form a frequency-dependent bound on th input usage that can be used directly in controllability analysis and controller design.

1.4.3 Controller design

Chapter 5

The controllability analysis performed in chapters 2 and 3 gave clear answers as to which measurements should be used for the anti-slug control. In chapter 5, we design PID controllers based on these controllability findings and test them on the three models that are used in this thesis (three-state, two-fluid and OLGA). Using three different models provides some insight into the robustness properties of the model. The controllers designed in this

chapters generally perform very well, but cascade controllers based on only topside measurements are fundamentally limited by unstable zeros dynamics in the process, and are thus slower than controllers that are based on an upstream pressure measurement.

Chapter 6

In this chapter we use $\mathcal{H}_\infty$ optimization based on the 3-state model to design anti-slug controllers. We use a S/KS mixed-sensitivity optimization, which means that we are minimizing the input usage and optimizing the performance (in terms of the sensitivity function S). MISO (multiple-input single-output) $\mathcal{H}_\infty$ controllers based on topside measurements are not limited by the same unstable zeros that limited the bandwidth of the cascade controllers and significantly improved low-frequency performance is achieved.

Attempts are also made to design a stabilizing LQG controller with an extended Kalman filter. The controller manages to stabilize the process, but the resulting performance is poor.

Chapter 7

Chapter 7 contains an industrial case study where the scope of the control system is extended from only avoiding riser slugging to also suppressing transient slugs such as surge waves and startup slugs. This is done by combining the anti-slug controller with individual flow controllers that are designed to average out the flow and thus avoid large peaks in the production. The controllers are combined through a minimum select function that implements the lowest signal from the different controllers, and, provided that the controllers are properly tuned, prioritizes between the different tasks.

1.4.4 Publications

The following publications have so far resulted from this work:

Chapter 2 and 3

E.Storkaas, S. Skogestad and V. Alstad, ”Stabilizing of desired flow regimes in pipelines”, AIChE Annual meeting, Paper 287d, Reno, Nevada, November 5-9, 2001.

E. Storkaas and S. Skogestad, ”Stabilization of severe slugging based on a low-dimensional nonlinear model”, AIChE Annual meeting, Paper 259e, Indianapolis, 3-8 Nov. 2002.

E. Storkaas, J.-M. Godhavn and S. Skogestad, ”A low-dimensional dynamic model of severe slugging for control design and analysis”, Proc. 11th International Conference on Multiphase flow (Multiphase’03), San Remo, Italy, 11-13 June 2003, Published by BHR Group, ISBN 1-85598-048-7, pp. 117-133.

E. Storkaas and S. Skogestad, ”Controllability analysis of an unstable, non-minimum phase process”, accepted for publication at IFAC world congress Prague, Czech Republic, July 2005.

Chapter 4

E. Storkaas and S. Skogestad, ”Effect of Input Rate Limitation on Controllability”, AIChE Annual Meeting, Austin, Texas, Nov. 2004, Presentation 406d.

Chapter 5

E. Storkaas and S. Skogestad, ”Cascade control of unstable systems with applications to stabilization of slug flow”, Proc. of 7th international symposium on advanced control of chemical processes, Hong Kong, 11-14 Jan. 2004.

Chapter 7

E. Storkaas and J.-M. Godhavn, ”Extended slug control for pipeline-riser systems”, accepted for publication at 12th International Conference on Multiphase flow (Multiphase’05), Barcelona, Spain, 25-27 May 2005.

Chapter 2

Controllability Analysis of Two-phase Pipeline-riser Systems at Riser Slugging Conditions

Espen Storkaas and Sigurd Skogestad

Based on a paper submitted to IEE Proceedings Control Theory and Applications

Abstract

A PDE-based two-fluid model is used to investigate the controllability properties of a typical pipeline-riser system. Analysis of the model reveals a very interesting and challenging control problem, with the presence of both unstable poles and unstable zeros.

We show that riser slugging in pipeline-riser systems can be avoided with a simple control system that manipulate the valve at the top of the riser. The type and location of the measurement to the controller is critical. A pressure measurement located upstream of the riser (that is, at the riser base or pipeline inlet) is a good candidate for stabilizing control. On the other hand, a pressure measurements located at the top of the riser cannot be used for stabilizing control because of unstable zero dynamics. A flow measurement located at the top of the riser can be used to stabilize the process, but, because the steady state gain is close to zero, it should in practice only be used in an inner control loop in a cascade.

The analysis of the system properties reveals that the dominating dynamical behavior of riser slugging probably can be described by a simpler model than the PDE-based model used in this chapter.

2.1 Introduction

Stabilization of desired fluid flow regimes in pipelines offers challenges of immense potential value. The opportunities for control engineers in this field are large, as control technology has only just started to make a significant impact in this area. Pipeline flow has commonly been analyzed based the on the flow regimes that develops in the pipeline under different boundary conditions. However, with feedback control, the stability of the flow regimes can be changed to facilitate improved operation.

The best known example of an open-loop flow regime change is probably the transition from laminar to turbulent flow in single-phase pipelines which is known to occur at a Reynolds-number of about 2300. It is well known that by carefully increasing the flow rate one may achieve laminar flow at much larger Re-numbers, but that in this case a small knock at the pipeline will immediately change the flow to turbulent. This indicates that the laminar flow region exists for higher Re-numbers, but that it is unstable. In theory, stabilization of the laminar region should be possible, and some attempts have been made in applying control to this problem (e.g. see Bewley (2000) for a survey), but short time and length scales make practical applications difficult.

Another unstable flow phenomenon occurs in multiphase pipelines, where pressure-flow fluctuations known as slug flow can be induced both by a velocity difference between the gas and liquid phase (hydrodynamic slugging) and by the pipeline geometry (terrain induced slugging, riser slugging). The latter slugging phenomenon occurs at a time and length scale that makes control a viable option and is the focus of this thesis.

A typical flow regime map for a pipeline-riser system is shown in figure 2.1. The flow regime map is taken from Taitel (1986), and includes some theoretical stability conditions. It is important to notice that flow regime maps such, as the one in figure 2.1, apply without control. With feedback control, we can move the boundaries, thereby stabilizing a desirable flow regime where riser slugging ”naturally” occurs.

Traditionally, undesirable slugging has been avoided in offshore oil/gas pipelines by other means than control, for example, by changing the operating point or making design modifications (Sarica and Tengesdal, 2000). Up until very recently, the standard method for avoiding this problem was to change the operating point by reducing the choke valve opening. However, the resulting increase in pressure results in an economic loss.

In many cases the problems with unstable flow regimes occur as the oilfields get older and the gas-to-oil ratio and water fraction increases. Since these transport systems are highly capital cost intensive, retrofitting or rebuilding is rarely an option. Thus, an effective way to stabilize the desired unstable flow regimes is clearly the best option.

The first study that applied control to this problem and by that avoided the formation of riser slugging was reported by Schmidt et al. (1979*a*). The use of feedback control to avoid severe slugging was also proposed and applied on a test rig by Hedne and Linga (1990), but this did not result in any reported implementations. More recently, there has been a renewed interest in control-based solutions (Havre et al., 2000; Hollenberg et al., 1995; Henriot et al., 1999; Skofteland and Godhavn, 2003). These applications are either experimental or based on simulations using commercial simulators such as OLGA. None of the control systems are based on a first principles dynamic model and subsequent analysis and con-

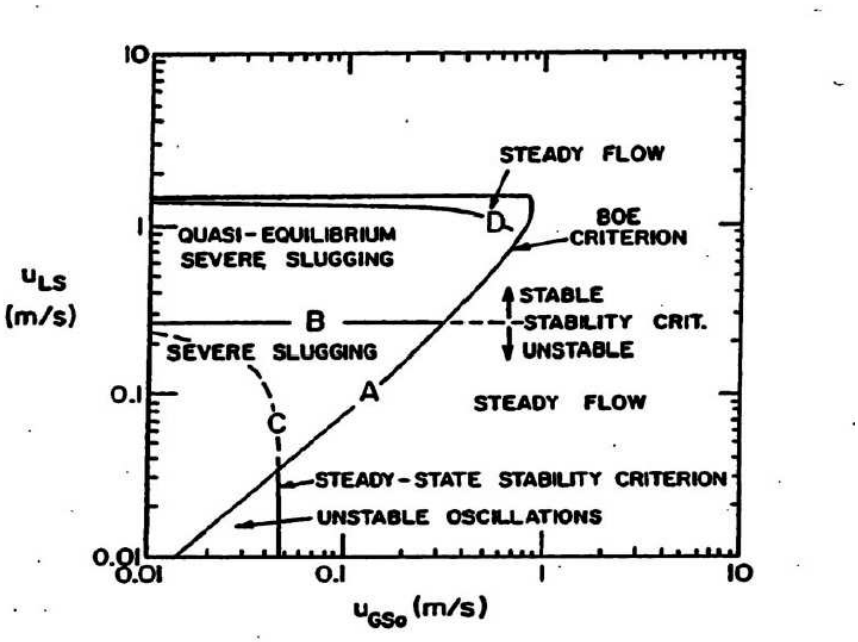

Figure 2.1: Flow regime map for an experimental pipeline-riser system (Taitel, 1986). The map shows the flow regime in the pipeline as function of superficial gas and liquid velocities. Low gas and liquid velocities results in riser slugging.

troller design. Several industrial applications are also reported (Havre et al., 2000; Courbot, 1996; Skofteland and Godhavn, 2003; Havre and Dalsmo, 2002; Kovalev et al., 2003).

In this chapter, we analyze, based on a simple first-principles model, a typical riser slugging case, and present a controllability analysis that highlight the system characteristics that are important from a control point of view. This analysis gives information on sensor/actuator selection, hardware requirements and achievable performance that are critical for a successful design of a stabilizing controller for the system.

2.2 Riser Slugging Phenomenon

The cyclic behavior of riser slugging is illustrated schematically in figure 2.2. It can be broken down into four parts. First, gravity causes the liquid to accumulate in the low point (step 1), and a prerequisite for severe slugging to occur is that the gas and liquid velocity is low enough to allow for this accumulation. The liquid blocks the gas flow, and a continuous liquid slug is formed in the riser. As long as the hydrostatic head of the liquid in the riser increases faster than the pressure drop over the riser, the slug will continue to grow (step 2).

When the pressure drop over the riser overcomes the hydrostatic head of the liquid in the slug, the slug will be pushed out of the system and the gas will start penetrating the liquid in the riser (step 3). Since this is accompanied with a pressure drop, the gas will expand and further increase the velocities in the riser. After the majority of the liquid and the gas has

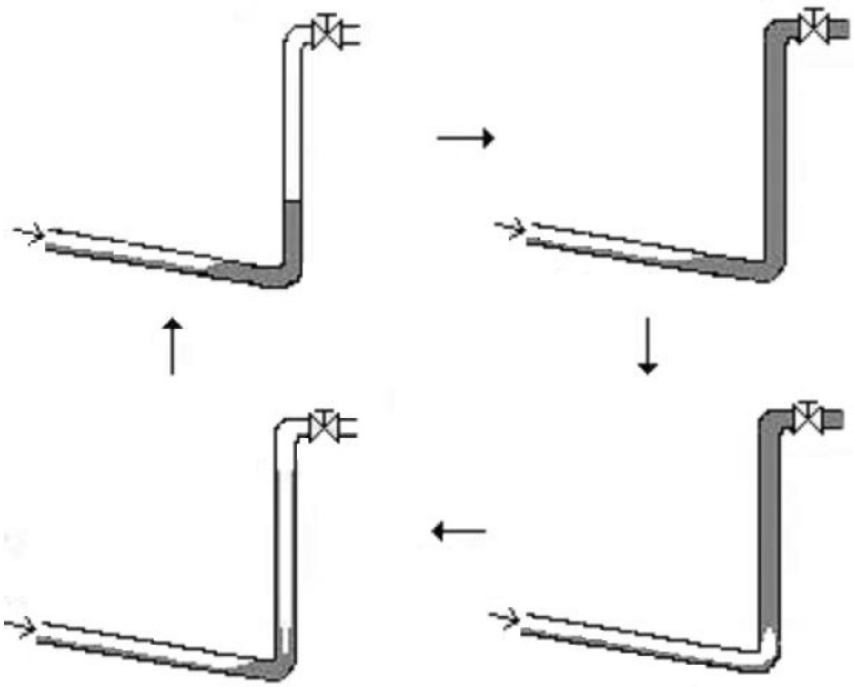

Figure 2.2: Graphic illustration of a slug cycle

left the riser, the velocity of the gas is no longer high enough to pull the liquid upwards. The liquid will start flowing back down the riser (step 4) and the accumulation of liquid starts again. A more detailed description of the severe slugging phenomenon can be found in for example Taitel (1986).

It is well known that riser slugging may be avoided by choking (decreasing the opening Z) of the valve at the riser top. To understand why this is the case, consider a pipeline-riser system in which the flow regime initially is non-oscillatory. A positive perturbation in the liquid holdup in the riser is then introduced. Initially, the increased weight will cause the liquid to ”fall down”. This will result in an increased pressure drop over the riser because 1) the upstream pipeline pressure increases both due to compression and less gas transport into the riser because of liquid blocking and 2) the pressure at the top of the riser decreases because of expansion of the gas. The increased pressure drop will increase the gas flow and push the liquid back up the riser, resulting in more liquid at the top of the riser than prior to the perturbation. Now, if the valve opening is larger than a certain critical value Z_{crit}, too much liquid will leave the system, resulting in a negative deviation in the liquid holdup that is larger than the original positive perturbation. Thus, we have an unstable situation where the oscillations grow, resulting in slug flow. For a valve opening less than the critical value Z_{crit}, the resulting decrease in the liquid holdup is smaller than the original perturbation, and we have a stable system that will return to its original, non-slugging state.

2.3 Case Description

In order to study the dominant dynamic behavior of a typical, yet simple riser slugging problem, the test case for severe slugging in OLGA is used. OLGA is a commercial multiphase simulator widely used in the oil industry. The nomenclature and geometry for the system are given in figure 2.3. The pipe diameter is 0.12 m. The feed into the system is nominally constant at 9 kg/s, with $W_L = 8.64$ kg/s (oil) and $W_G = 0.36$ kg/s (gas). The pressure after the choke valve (P_0) is nominally constant at 50 bar. This leaves the choke valve opening Z as the only degree of freedom in the system. The feed of oil and gas and the pressure P_0 are regarded as disturbances outside of our control.

In most real cases, the inflow is pressure dependent (W_L and W_G depends on P_I). This has some consequences on the results presented later in this chapter, and will be commented on when relevant. Real pipelines lie in hilly terrain which produce smaller terrain induced slugs, but these are assumed to be included in the disturbance description introduced later.

For the present case study, the critical value for the transition between a stable non-oscillatory flow regime and riser slugging is at a valve opening $Z_{crit} = 13\%$. This is illustrated by the OLGA simulations in figure 2.4 with valve openings of 10% (no slug), 20% (riser slugging) and 40% (riser slugging).

Simulations, such as those in figure 2.4, were used to generate the bifurcation diagram in figure 2.5, which illustrates the behavior of the system over the whole working range of the choke valve. For valve openings above 13% we have riser slugging and the two solid lines in figure 2.5 give the maximum and minimum pressure for the oscillations shown in figure 2.4. The dashed line represents the (desired) non-oscillatory flow regime, which is unstable without control. Since it is unstable, it is not normally observed in OLGA simulations, but we were able to compute these values by initializing the OLGA model to steady-state using the OLGA Steady State Processor. Thus, for choke valve openings above 13%, we have two solutions for each valve opening; one stable limit cycle and one unstable steady-state solution. For valve openings below 13%, the single solid line represents the stable non-oscillatory flow regime corresponding to the topmost simulation in figure 2.4.

2.4 Model Description

The primary goal of this chapter is to analyze the controllability properties of a system with riser slugging, and the type and complexity of the model we choose to use is affected by this goal. First, we need a model that can be linearized, as the analysis methods are based on linear models. This means that the internal states of the model should be readily available and that the model should be first-order continuous (at least around the operating points). The OLGA model is not suitable as the internal states are not available. Second, we will make simplifying assumptions that allows us to limit the complexity of the model.

Two types of one-dimensional models are commonly used to model multiphase flow; the *drift flux model*, with mass balances for each phase and a combined momentum balance, and the *two-fluid model*, with separate mass and momentum balances for each phase. For the drift flux type model, one also needs algebraic equations relating the velocities in the

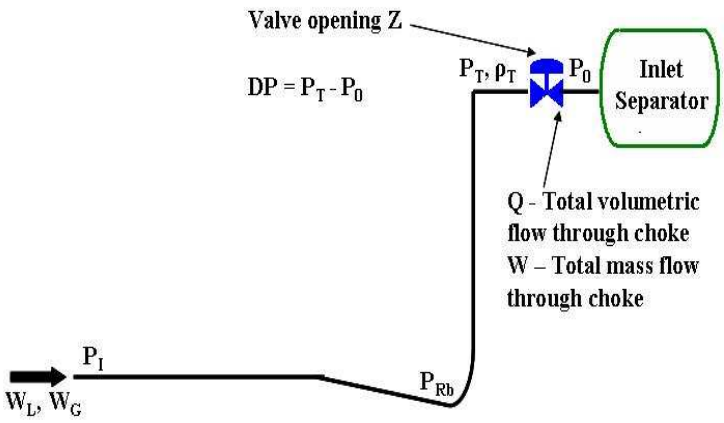

(a) Nomenclature

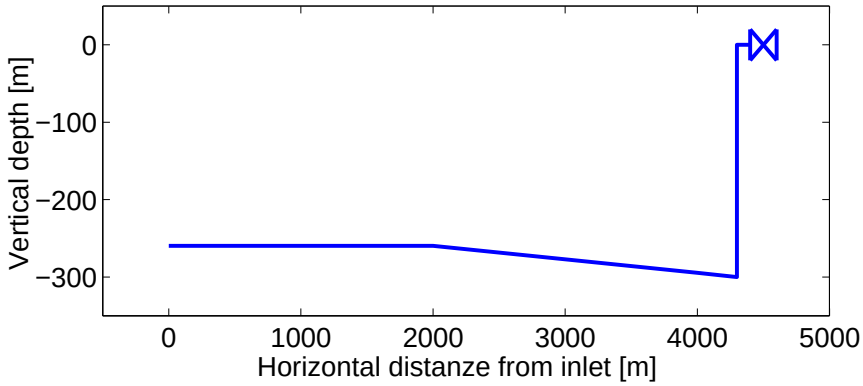

(b) Case Geometry

Figure 2.3: (a) Nomenclature used for the pipeline riser system and (b) System geometry

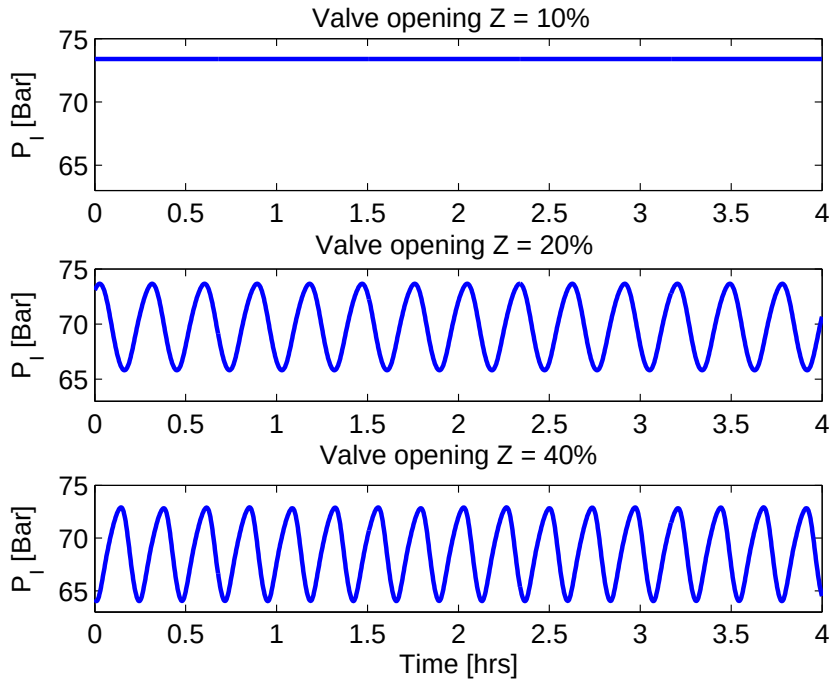

Figure 2.4: OLGA simulations for valve openings of 10, 20 and 40%

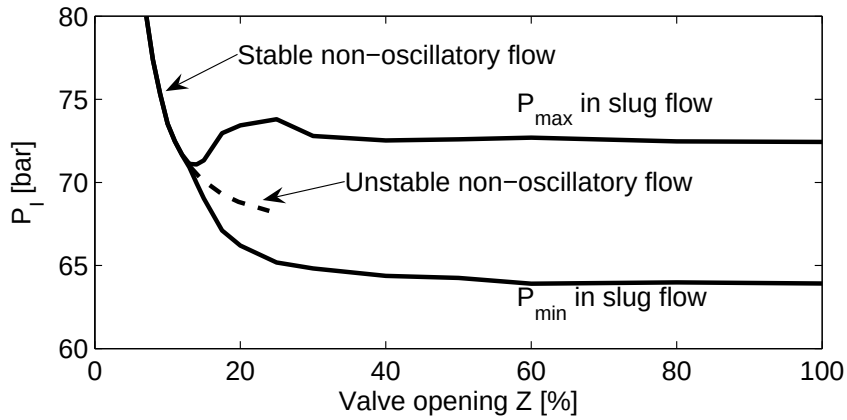

Figure 2.5: Bifurcation diagram for the case study, OLGA data

different phases. More details on the modeling of slug flow can be found in for example Bendiksen et al. (1985) and Taitel and Barnea (1990).

In this work we use a simplified two-fluid model, where the conservation equations for mass and momentum for the two phases are given by the following Partial Differential Equations (PDEs):

$$\frac{\partial}{\partial t}\left(\alpha_L \rho_L\right) + \frac{1}{A}\frac{\partial}{\partial x}\left(\alpha_L \rho_L u_L A\right) = 0 \tag{2.1}$$

$$\frac{\partial}{\partial t}\left(\alpha_G \rho_G\right) + \frac{1}{A}\frac{\partial}{\partial x}\left(\alpha_G \rho_G u_G A\right) = 0 \tag{2.2}$$

$$\frac{\partial}{\partial t}\left(\alpha_L \rho_L u_L\right) + \frac{1}{A}\frac{\partial}{\partial x}\left(\alpha_L \rho_L u_L^2 A\right) = -\alpha_L \frac{\partial P}{\partial x} + \alpha_L \rho_L g_x - \frac{S_{Lw}}{A}\tau_{Lw} + \frac{S_i}{A}\tau_i \tag{2.3}$$

$$\frac{\partial}{\partial t}\left(\alpha_G \rho_G u_G\right) + \frac{1}{A}\frac{\partial}{\partial x}\left(\alpha_G \rho_G u_G^2 A\right) = -\alpha_G \frac{\partial P}{\partial x} + \alpha_G \rho_G g_x - \frac{S_{Gw}}{A}\tau_{Gw} - \frac{S_i}{A}\tau_i \tag{2.4}$$

The notation and details regarding closure relations and model discretization etc. are given in appendix A. The model has four distributed dynamical states ($\alpha_L\rho_L$, $\alpha_G\rho_G$, $\alpha_L\rho_L u_L$ and $\alpha_G\rho_G u_G$), which together with the summation equation for the phase fractions $\alpha_L + \alpha_G = 1$ gives the phase fractions (α_L, α_G), gas density (ρ_G) and both velocities (u_L, u_G). We have assumed the following:

- Incompressible liquid with constant density ρ_L
- No pressure gradient over the pipeline cross-section, implying equal pressure in both phases at a given point in the pipeline
- No mass transfer between the phases
- No liquid droplet field in the gas
- Isothermal conditions
- Ideal gas equation of state, corrected with a constant compressibility factor.
- Flow out of the riser can be described by the choke valve model from Sachdeva et al. (1986), which is based on a no-slip assumption for the liquid and gas and assumes incompressible liquid and adiabatic gas expansion.

Horizontal and declined flow are fundamentally different from inclined flow due to the effect of gravity. Our model is based on stratified flow for the horizontal and declining pipe sections, and annular or bubbly flow for inclined pipe sections. The flow regime change from horizontal/declining pipe to inclining pipe does not introduce discontinuities, as this switch is only dependent on geometry.

It is assumed that the same algebraic relations between phase densities, velocities and friction are valid for all flow regimes, both horizontal and inclined. The expression for the wetted parameter is the only difference between the regimes. For bubble flow in inclined pipes, the wetted perimeter is computed based on an average bubble diameter. For annular

flow, the wetted perimeter is that of a gas core in a body of liquid. The transition between the two flow regimes for inclined flow is modeled using a sinusoidal weighting function ($sin(x)$, $0 \leq x \leq \pi$) and is assumed only to be a function of phase fraction ($x = f(\alpha_L)$).

The model is implemented in Matlab.

2.5 Model tuning and verification

The model described above is similar, but significantly simplified, compared to the one used in OLGA. For the purpose of this work, the OLGA model is assumed to be an accurate description of a real system, and data from the OLGA simulations are used to fit the parameters in the model (tune the model).

The level of tuning required for any mathematical model depends on the assumptions and simplifications made. In our case, we have assumed that the liquid density is constant. In fact, the density varies weakly with pressure, and we need to use a density that is representative for the problem we are studying. The same can be said about the equation of state; the ideal gas law is used for simplicity, and some tuning on the gas molecular weight and/or compressibility factor is needed as these change throughout the system. Other important tuning parameters are the proportionality constants in the friction correlations and the average bubble diameter for bubbly flow in the riser (for determining wetted perimeter in inter-phase friction).

Still, even with all these tuning factors, obtaining a good fit to the data for all valve openings is difficult. The system is distributed, and the effect of each tuning parameter is not always clear. We have focused on achieving a good qualitative fit to the data, as we are mainly interested in studying the general behavior of such a system. Also, we are mainly interested in studying the unstable stationary operating points rather than the stable, undesired slug flow. Thus, we want to fit the model to the stationary (unstable) operating line, the open-loop (uncontrolled) riser slugging data is of less importance.

The tuning was done by manually adjusting the model parameters using the bifurcation diagrams as tuning aids. The resulting fit is illustrated in figure 2.6, where the bold lines are the reference data (OLGA) and the thin lines are computed from the simple two-fluid model. We see that the fit for the stable non-oscillatory flow regime (at low valve openings) is excellent, whereas there are some deviations for the slug flow regime. Since the slug flow regime is undesirable, these deviations are, as mentioned above, of less importance for control purposes. Of more interest is the desired unstable non-oscillatory flow regime. We note that the fit is excellent for the riser top pressure (figure 2.6(b)), but that there is a small deviation of up to 1 bar for the inlet pressure in figure 2.6(a).

The deviation in pressure drop over the system is probably due to the assumption of no mass transfer between the phases and the related assumption of constant liquid density. If mass transfer were included, the lighter components in the oil would flash off as the pressure drops along the pipeline. This would increase both the gas fraction and the liquid density and thus affect the pressure drop over the pipeline.

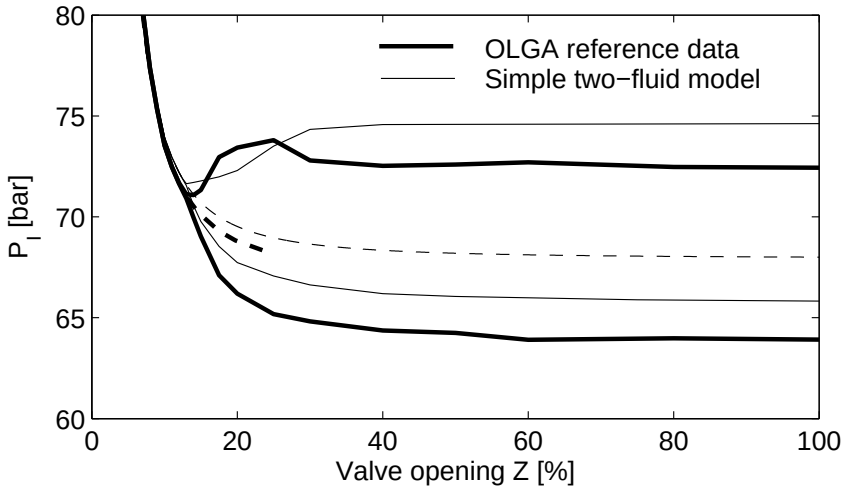

(a) Inlet Pressure

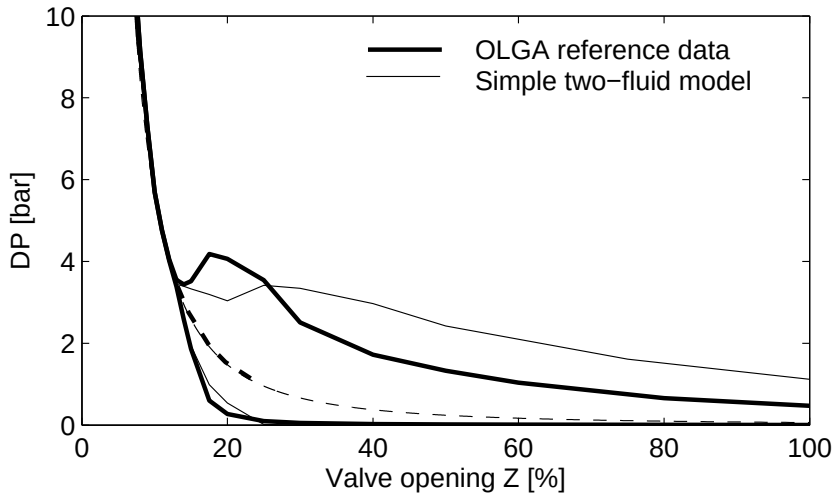

(b) Pressure drop over choke

Figure 2.6: Verification of tuned model for (a) Inlet pressure P_I and (b) Pressure drop over choke valve DP

2.6 Controllability analysis

The riser slugging case is interesting and challenging for control because it turns out to contain many conflicting controllability limitations. The riser slugging phenomena is oscillatory, and we find as expected that the unstable (RHP) poles p_i are complex. The most serious challenge for stabilizing control (avoiding riser slugging), is that there, for some measurement alternatives, also are unstable (RHP) zeros z located close to the unstable (RHP) poles p_i. Let us first illustrate some of the controllability problems by simulations before we review some control theory.

2.6.1 Introductory open-loop simulations

The main objective for anti-slug control is to stabilize the non-oscillatory flow regime using the valve position Z as a manipulated variable. In theory, for linear systems, any measurement where the instability is observable may be used. However, in practice input saturation (in magnitude or rate) or unstable zero dynamics (RHP-zeros) may prevent stabilization. To gain some insight into the latter, we show in figure 2.7 the simulated response to a step change in Z at $t = 0$ for four alternative measurements: Inlet pressure (P_I), Riser base pressure (P_{Rb}), pressure drop over topside choke valve (DP) and volumetric flow out of the riser (Q). The responses are both for the simple two-fluid model (thin lines) and OLGA (bold lines).

The valve position prior to the step is $Z = 10\%$, and a 2% step increase is applied, so this it at a point close to instability. The simulations show that the step change induces oscillations, but because we are at a stable operating point, these eventually die out. The oscillations for the OLGA simulation have a period of a 25 minutes, corresponding to a frequency of $p = 2\pi/(25 \cdot 60s) = 0.004s^{-1}$. The oscillations are a bit faster for the two-fluid model, with a period of about 17 minutes corresponding to a frequency $p = 0.006s^{-1}$.

For the three pressures, the main difference is for the initial response shown at the right. The P_{Rb}, there is an immediate decreasing initial response and we expect no problems with stabilization. For P_I, there is an effective delay of about 10 seconds, which will make stabilization a bit more difficult, but the time delay is probably not large enough to cause major problems. For DP there is also an effective delay of about 2 minutes with the two-fluid model and 4 minutes with OLGA, caused by inverse response. Finally, for the flow Q, the response is immediate, but we note that the steady-state gain is close to zero as Q eventually returns to its original value. This means that control of Q cannot be used to affect the steady-state behavior of the system. The small steady-state gain for Q is easily explained because the inflow to the system is given, and the outflow must at steady-state equal the inflow.

The inverse responses in the time domain for the measurement $y = DP$ correspond to RHP-zeros in the transfer function model. Also, the shape of the inverse response, with the initial response is in the ”right” direction followed by a correction in the ”wrong” direction, indicate a complex pair of RHP-zeros. The transfer functions can be used to derive more exact expressions for the deteriorating effect the RHP-zeros have on control performance. Such expressions are discussed next.

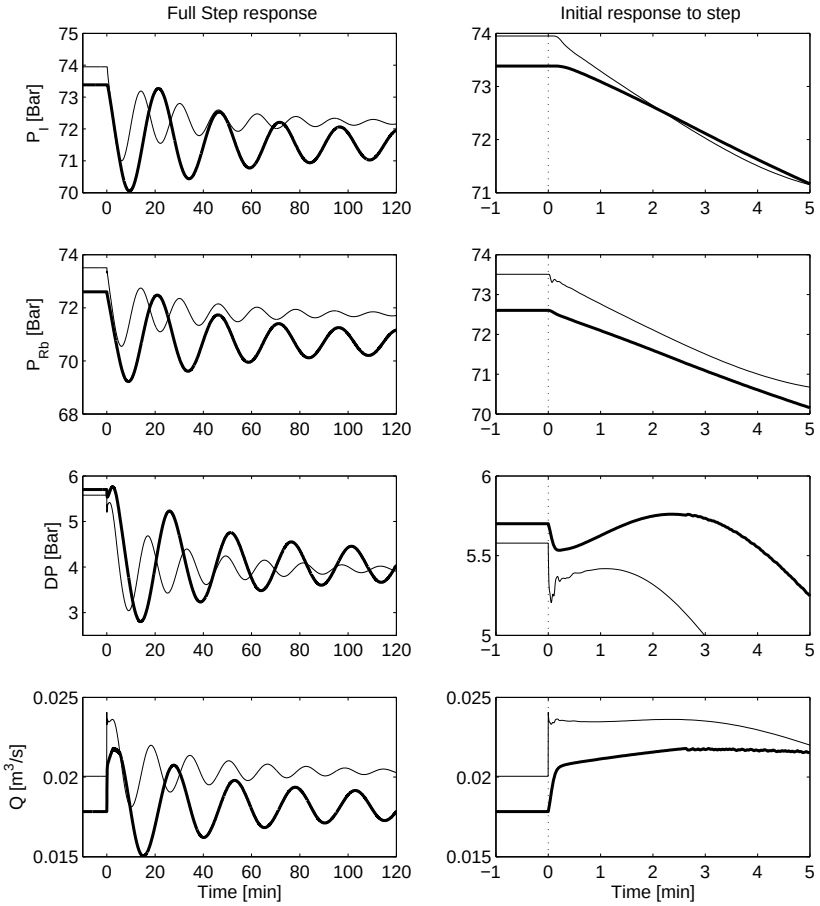

Figure 2.7: Open-loop responses with the simple two-fluid model (thin lines) and OLGA (bold lines) for a step in valve opening Z.

2.6.2 Controllability analysis: Theoretical Background

Transfer functions

Consider a process $y = G(s)u + G_d(s)d$ controlled by the controller $K(s)$ yielding the input to the plant $u = K(s)(r - y - n)$. The closed-loop response is:

$$y = Tr + SG_d d - Tn \tag{2.5}$$

where $S = (I + GK)^{-1}$ and $T = GK(I + GK)^{-1} = I - S$ are the sensitivity and complementary sensitivity function, respectively. The input to the plant is

$$u = KS(r - G_d d - n) \tag{2.6}$$

In addition to the closed-loop transfer functions in (2.5) and (2.6), the transfer function SG gives the effect of input disturbances on the output y (set $G_d = G$ in (2.6)). The transfer functions $S,\ T,\ KS$ and SG can also be interpreted as robustness to various kinds of uncertainty, where small magnitudes for the closed-loop transfer functions indicates good robustness properties. For example, S is the sensitivity toward inverse relative uncertainty, which is a good model of uncertainty in the pole locations (Skogestad and Postlethwaite, 1996).

Thus, by obtaining the lower bounds for the closed-loop transfer functions S, T, KS, SG, KSG_d and SG_d, we can get information regarding both achievable performance and possible robustness problems. We will consider bounds on the $\mathcal{H}_\infty$ norm, $\|M\|_\infty = \max_\omega |M(j\omega)|$, which is simply the peak value for the transfer function. The bounds presented below are all independent of the controller K, and are thus a property of the process itself. The bounds are, however, dependent on a systematic and correct scaling of the process, which will be addressed after the bounds has been introduced.

Lower bound on S and T

The lowest achievable peaks in sensitivity and complementary functions, denoted $M_{S,min}$ and $M_{T,min}$, are closely related to the distance between the unstable poles (p_i) and zeros (z_i). For SISO systems, Skogestad and Postlethwaite (1996) show that for any unstable (RHP) zero z;

$$\|S\|_\infty \geq M_{S,min} = \prod_{i=1}^{N_p} \frac{|z + \bar{p}_i|}{|z - p_i|} \tag{2.7}$$

Note that the bound approaches infinity as z approaches p_i.

For systems with only one unstable zero, the bound holds with equality. Chen (2000) shows that the bound in (2.7) also applies to $\|T\|_\infty$, and generalizes the bound to apply for MIMO systems with any number of unstable poles and zeros:

$$M_{S,min} = M_{T,min} = \sqrt{1 + \bar{\sigma}^2 \left(Q_p^{-1/2} Q_{zp}^T Q_z^{-1/2} \right)} \tag{2.8}$$

where the elements of the matrices Q_z, Q_p and Q_{zp} are given by:

$$[Q_z]_{ij} = \frac{y_{z,i}^H y_{z,j}}{z_i + \bar{z}_j}, \; [Q_p]_{ij} = \frac{y_{p,i}^H y_{p,j}}{\bar{p}_i + p_j}, \; [Q_{zp}]_{ij} = \frac{y_{z,i}^H y_{p,j}}{z_i - p_j} \tag{2.9}$$

The vectors $y_{z,i}$ and $y_{p,i}$ are the (unit) output direction vectors associated with the zero z_i and pole p_i, respectively. For SISO systems, these direction vectors all equal 1.

Time delays pose additional limitations. Chen (2000) show that the bound for $\|T\|_\infty$ is increased by a factor $|e^{p\theta}|$ for a single RHP-pole and by at least a factor $|e^{p_i\theta}|$ for multiple poles.

Lower bound on KS

The transfer function KS from measurement noise n to plant inputs u is at low frequencies closely related to the inverse of the process transfer function G. This can be seen by rewriting $KS = G^{-1}T$ (using $GKS = T$) and recalling that with integral action, $T(0) = I$. Unstable plants requires control and a connection between KS and G^{-1} is also found in the bound (Havre and Skogestad, 1997; Havre and Skogestad, 2001)

$$\|KS\|_\infty \geq |G_s(p)^{-1}| \tag{2.10}$$

where G_s is the stable version of G with the RHP-poles of G mirrored into the LHP. The bound is tight (with equality) for one real unstable pole p. For multiple and complex unstable poles p_i, Glover (1986) gives the tight bound

$$\|KS\|_\infty \geq 1/\underline{\sigma}_H\left(\mathcal{U}\left(G\right)\right) \tag{2.11}$$

where $\underline{\sigma}_H\left(\mathcal{U}\left(G\right)\right)$ is the smallest Hankel singular value of the antistable part of G.

Lower bound on SG and SG_d

Chen (2000) reports that for any unstable zero z in G;

$$\|SG\|_\infty \geq |G_{ms}(z)| \prod_{i=1}^{N_p} \frac{|z + \bar{p}_i|}{|z - p_i|} \tag{2.12}$$

$$\|SG_d\|_\infty \geq |G_{d,ms}(z)| \prod_{i=1}^{N_p} \frac{|z + \bar{p}_i|}{|z - p_i|} \tag{2.13}$$

where the subscript ms denotes the stable, minimum-phase version of the transfer function (both RHP-poles and RHP-zeros mirrored into the LHP). These bounds are only tight for one unstable zero z, but since they are valid for any RHP-zero z, they can also be applied for systems with multiple unstable zeros.

Lower bound on KSG_d

The stable, minimum phase part $G_{d,ms}$ of G_d can be regarded as a weight on KS. Thus, for any unstable pole p (Havre and Skogestad, 1997; Skogestad and Postlethwaite, 2005):

$$\|KSG_d\|_\infty = |G_s^{-1}(p)| \cdot |G_{d,ms}(p)| \tag{2.14}$$

The bound is only tight for one real unstable pole p. For multiple and complex unstable poles p_i, the following bound is tight (Skogestad and Postlethwaite, 2005):

$$\|KSG_d\|_\infty \geq 1/\underline{\sigma}_H \left(\mathcal{U}\left(G_{d,ms}^{-1}G\right)\right) \tag{2.15}$$

Pole vectors

For a plant $G(s)$ with state space realization ($A,\ B,\ C,\ D$), the output pole vector $y_{p,i}$ for a pole p_i is defined by (Havre and Skogestad, 2003)

$$y_{p,i} = Ct_i \tag{2.16}$$

where t_i is the right (normalized) eigenvector corresponding to p_i ($At_i = p_i t_i$). Havre and Skogestad (2003) finds, based on minimum input usage for stabilization, that the measurement corresponding to the largest element in the output pole vectors should be used for stabilizing control. Correspondingly, for input selection, the input that has the largest element in the input pole vector $u_{p,i} = B^H q_i$, where q_i is the left eigenvector of A ($q_i^H A = p_i q_i^H$), should be selected. One limitation on the use of pole vectors is that the relationship between the magnitude of the input usage and the magnitude of the pole vectors elements only holds for plants with a single unstable pole p. In our case, we have a pair of complex conjugate unstable poles p_i, but we shall see that the pole vectors still give some information about measurement selection.

Low frequency performance

Disturbance rejection is not strictly required for stabilizing control. However, to avoid the possible destabilizing effect of nonlinearity, the system should not "drift" too far away from its nominal operating point. To achieve low-frequency performance, the low-frequency gain must be sufficiently large. Specifically, for perfect low-frequency disturbance rejection, we must require $|G(j\omega)| \geq |G_d(j\omega)|$ at frequencies $\omega > \omega_d$ where $|G_d| > 1$.

2.6.3 Scaling

The models are scaled as outlined in Skogestad and Postlethwaite (1996), such that all signals in the system should be less than one in magnitude. This is both to include saturation effects and to be able to compare signals of different magnitude.

The outputs are scaled with the maximum allowed deviation given in tables 2.1 and 2.2. Nonlinear effects cause the process gain to vary with valve opening, and we find that the gain is smallest for large valve openings. Therefore, we scale the input with the maximum

allowed positive deviation in valve opening. For example, with a nominal valve opening of $Z = 30\%$, the input scaling is $D_u = 70\%$.

There are several different sources for uneven flow into the riser in a pipeline-riser system. First, the feed into the pipeline itself can vary, caused by upstream events (e.g changed production rate, routing of a different subset of wells into the pipeline or unstable wells). Second, hydrodynamic slugging, caused by the velocity difference between the liquid and the gas, can occur in the pipeline and give rise to uneven flow. Finally, terrain slugs, caused by accumulation of liquid in local low-points in the pipeline, can create small or medium-sized slugs in the pipeline. Flow variations into the pipeline are easily represented as weighted feed disturbances. To include the effect of hydrodynamic and terrain slugging in the controllability analysis without having to include the physical effects that cause these phenomena in the model, we assume that the effect of hydrodynamic and terrain induced slugging can be approximated as sinusoidal feed disturbances. Thus, we assume that the feed disturbances W_L and W_G are frequency-dependent. The disturbance weight

$$D = 0.2\frac{\left(\frac{2\pi}{180}s+1\right)\left(\frac{2\pi}{160}s+1\right)}{\left(\frac{2\pi}{90}s+1\right)\left(\frac{2\pi}{30}s+1\right)^2} \tag{2.17}$$

will give the disturbance distribution in figure 2.8. This disturbance weight allows for a 20% variation for the stationary value of the feed for each phase, and has a peak in the frequency range $0.03s^{-}1$ - $0.2s^{-1}$, corresponding to slug periods between 3 minutes and 30 seconds.

The downstream pressure P_0 is scaled to allowed for a frequency-independent variation of 1 bar.

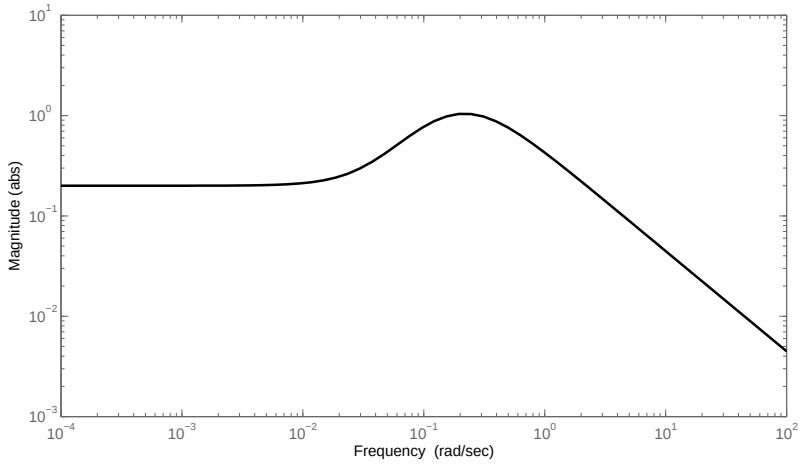

Figure 2.8: Disturbance weight to allow for hydrodynamic and terrain induced slugs in the feed pipeline

2.6.4 Stability - Poles

When the valve opening is increased, the stationary operating point moves along the single solid line in figure 2.6, through the bifurcation point at valve opening $Z_{crit} = 13\%$ and onwards along the dashed line for the unstable operating points. At the bifurcation point, there is a pair of complex poles (eigenvalues of the state matrix A of the linearized model) that cross into the right half plane, as seen from the root-locus plot in figure 2.9. This indicates that the bifurcation point is a Hopf bifurcation (Thompson and Stewart, 1986), which is also consistent with the shape of the bifurcation maps in figure 2.6.

Note that, as expected, the frequency of the oscillations ($p = 0.006s^{-1}$) observed for the step change from $Z = 10\%$ to $Z = 12\%$ in figure 2.7 correspond very closely to the imaginary parts of the poles in the figure 2.9.

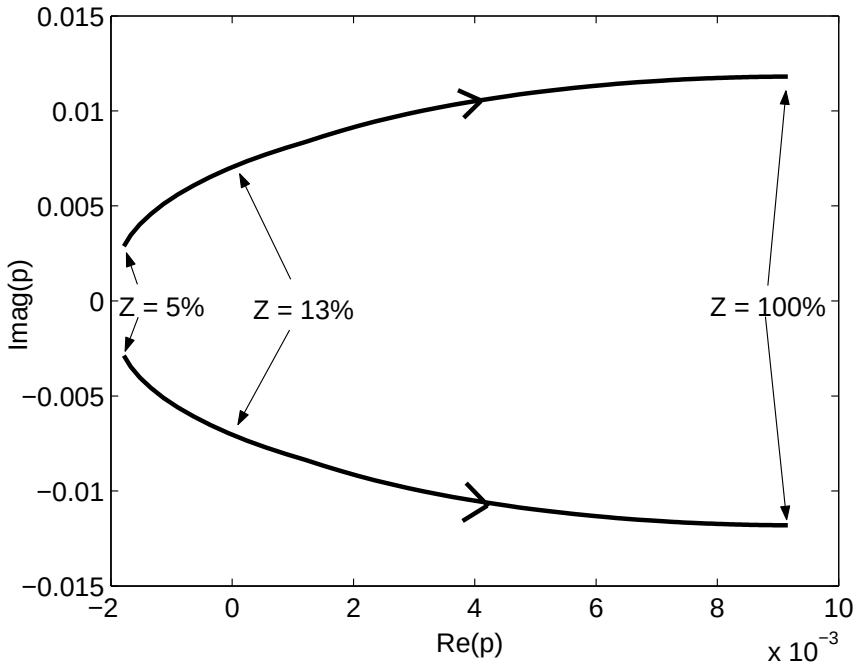

Figure 2.9: Open-loop root-locus plot with valve opening Z as independent parameter. Instability occurs at for $Z \geq 13\%$

2.6.5 Measurement evaluation

We will in the following study two different operating points, one at valve opening $Z = 17.5\%$, where the instability is fairly slow, and one at valve opening $Z = 30\%$, where the instability is faster and stabilization is more difficult. The process model G and disturbance model G_d is obtained from linearizing the discretized PDE model around these two operating points.

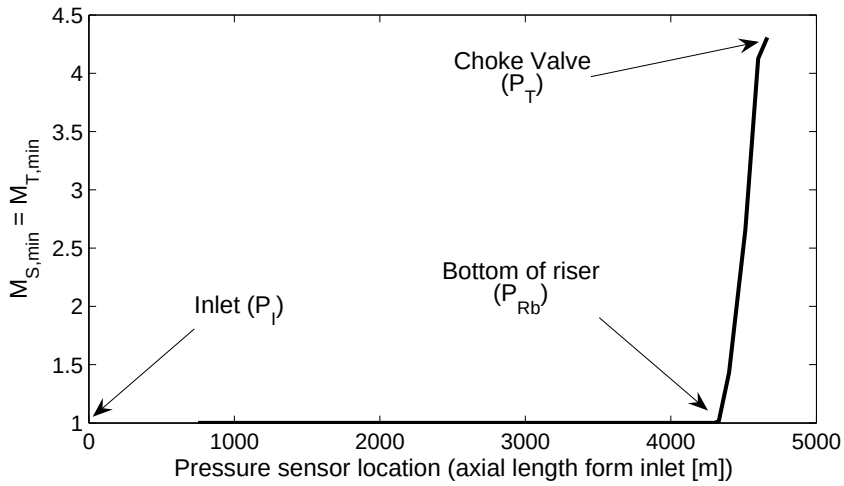

Figure 2.10: Minimum peaks on $|S|$ and $|T|$ (as given by the relative distance between RHP-poles p and RHP-zeros z) as function of pressure sensor location in pipeline

Pressure measurements are the most reliable measurements for stabilizing these systems. The location of the pressure sensor has a significant impact on the location of the RHP-zeros and hence on the controllability of the system. In figure 2.10, the minimal achievable peak for the sensitivity functions S and T, $M_{S,min} = M_{T,min}$ from (2.8) is plotted against pressure sensor location for the operating point with $Z = 30\%$. Figure 2.10 show that pressure measurements located in the horizontal or declining part of the pipeline (upstream of the riser), have no RHP-zeros that limit performance. However, as the pressure measurement is moved up the riser toward the choke valve, the fastest RHP-zero moves closer to the unstable pole, making stabilizing control more difficult.

Note that the effective time delay, which will increase as the pressure measurement is moved toward the pipeline inlet, is not included in figure 2.10. From the step responses in section 2.6.1, the effective time delay to the pipeline inlet is about 10 seconds, which will increase $M_{T,min}$ with a factor $|e^{|p_i|\theta}| = e^{0.011 \cdot 10} \approx 1.1$. Thus, the line for $M_{S,min} = M_{T,min}$ in figure 2.10 should slope slightly upwards toward the inlet, but the time delay is not large enough in this case to make a significant impact in this case.

For practical reasons, the pressure sensors are usually located at the pipeline inlet (P_I) and at the choke valve (P_T). For some pipelines, there is also a pressure measurement at the riser base (P_{Rb}). Since we assume constant pressure P_0 behind (downstream) the choke valve, the pressure drop ($DP = P_T - P_0$) over the choke and the pressure in front of the choke (P_T) are equivalent. In addition to these pressure measurements, we will include the density at the top of the riser (ρ_T), the mass flow through the choke (W) and the volumetric flow through the choke (Q) as measurement candidates for stabilizing control.

Table 2.1: Controllability data for the operating point $Z = 17.5\%$. Unstable poles at $p = 0.0014 \pm 0.0085i$. † denotes RHP-zeros that are not important for the control problem

						Minimum peaks[a]				
Measurement	Value	Scaling D_y	Smallest RHP-zero[b]	Pole vector[b]	$\|G(0)\|$[b]	$\|S\| = \|T\|$	$\|KS\|$	$\|SG\|$	$\|KSG_d\|$	$\|SG_d\|$
$P_I[bar]$	70	1	99†	0.36	18.9	1.0	0.03	0.0	0.06	0.0
$P_{Rb}[bar]$	69.5	1	1155†	0.37	19.0	1.0	0.03	0.0	0.06	0.0
$DP[bar]$	1.92	1	$0.01 \pm 0.01i$	0.21	17.6	1.6	0.04	17.1	0.08	0.95
$\rho_T[kg/m^3]$	432	50	0.016	0.28	1.5	1.4	0.03	28.6	0.07	1.60
$W[kg/s]$	9	1	-†	0.59	0	1	0.02	0	0.06	0
$Q[m^3/s]$	0.0208	0.002	-†	0.51	1.8	1	0.02	0	0.06	0

Table 2.2: Controllability data for the operating point $Z = 30\%$. Unstable poles at $p = 0.0045 \pm 0.0108i$. † denotes RHP-zeros that are not important for the control problem

						Minimum peaks[b]				
Measurement	Value	Scaling D_y	Smallest RHP-zero[a]	Pole vector[a]	$\|G(0)\|$[a]	$\|S\| = \|T\|$	$\|KS\|$	$\|SG\|$	$\|KSG_d\|$	$\|SG_d\|$
$P_I[bar]$	68.7	1	98.1†	0.30	3.3	1.0	0.30	0.0	0.35	0.005
$P_{Rb}[bar]$	68.2	1	1140†	0.31	3.3	1.0	0.28	0.0	0.33	0.004
$DP[bar]$	0.66	0.5	0.01±0.01i	0.17	6.1	4.3	0.62	16.8	0.97	5.5
$\rho_T[kg/m^3]$	427	50	0.015	0.27	2.6	0.18	0.64	14.6	0.55	4.7
$W[kg/s]$	9	1	-†	0.63	0	1	0.17	0	0.32	0
$Q[m^3/s]$	0.0211	0.002	-†	0.59	0.33	1	0.17	0	0.32	0.002

[a] Want these small
[b] Want these large

Tables 2.1 and 2.2 show the lower bounds on all the closed-loop transfer functions described in section 2.6.2 for all the measurement candidates and at both operating points. The location of the smallest unstable (RHP) zero and the pole vector elements, as well as the nominal value, stationary gain and scaling factor D_y (maximum allowed deviation) for each measurement candidate are also included in the tables. The following conclusions can be drawn from the tables:

- It is theoretically possible to stabilize the system with all the measurement candidates based since the input magnitude given by $\|KS\|_\infty$ and $\|KSG_d\|_\infty$ are less than unity for all measurement candidates.
- Upstream pressure measurements (P_I and P_{Rb}) are well suited for stabilizing control with a large steady-state gain and all peaks small.
- In practice, the pressure drop over the valve (DP) and density at the top of the riser (ρ_T) should not be used for stabilizing control because of the high peaks for $|S|$, $|T|$ (about 4) and $|SG|$ (about 20). The high peaks for these transfer function are caused by RHP-zeros z close to the RHP-poles p.
- Flow measurements at the pipeline outlet (W or Q) can be used for stabilizing control, also in practice. However, they both suffer from a close-to zero stationary gain ($|G(0)| = 0$ and 0.33, respectively), which means that good low-frequency (steady-state) performance is not possible. Note that the mass flow W has zero stationary gain because we assume that the feed rate is constant. For real systems, the feed rate is pressure dependent, and there would be a non-zero low-frequency gain, but it would probably still be too small to allow for low-frequency performance.
- The pole vectors give the same general conclusions as the closed-loop peaks, but since the link between pole vectors and measurement selection only holds for plants with a single unstable pole, the difference between the pole vector elements for the good and the bad control variables is not very large.

2.6.6 Controllability analysis of flow control ($y = Q$)

From table 2.2, the potential problem with flow control ($y = Q$) is a low steady-state gain. To confirm this, we show in figure 2.11 the Bode magnitude plot of the linear scaled process model $G(s)$ obtained at the operating point $Z = 30\%$, together with the models $G_{d1-3}(s)$ for the disturbances. The disturbance gain for the flow disturbances are high for low frequencies and drops off sharply above about $\omega = 0.2$. Above $\omega = 0.2$, flow disturbances are effectively dampened through the pipeline. The downstream pressure disturbance P_0 does not pose a problem for control. Note that the high-frequency gain for this disturbance is unrealistic, and stems from the fact that we used a constant scaling over all frequencies.

Thus, if the volumetric flow ($y = Q$) is chosen as the primary controlled variable, the controller will not be able to suppress low-frequency disturbances because the disturbance gain is higher that the process gain, $|G_d| > |G|$. This may cause a disturbance to drive the operation into a point where the controller no longer manages to stabilize the process. This

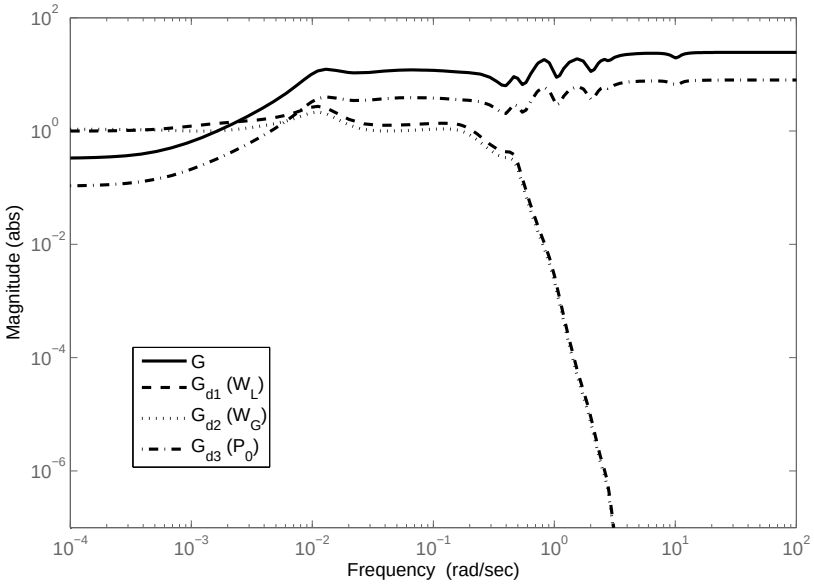

Figure 2.11: Frequency dependent gain for $y = Q$ at operating point $Z = 30\%$

implies that this measurement is best suited to use in an inner loop in a cascade controller, rather than for independent stabilizing control.

2.6.7 Controllability analysis of upstream pressure control ($y = P_I$ or $y = P_{Rb}$)

From tables 2.1 and 2.2, the upstream pressure measurements P_I and P_{Rb} both seem to be very promising candidates for control. In figure 2.12, we show the Bode magnitude plot of the linear scaled process model $G(s)$ for the inlet pressure $y = P_I$, obtained at the operating point $Z = 30\%$, together with the models $G_{d1-3}(s)$ for the disturbances. The corresponding Bode plot for the riser base pressure ($y = P_{Rb}$) is almost identical. The process gain is higher that the disturbances, $|G| > |G_d|$, for frequencies up to about $\omega = 0.15$. Above this frequency, the disturbance gain is lower than unity, and disturbance rejection is not strictly needed. However, we will see in the next section that the peak in the disturbance magnitude at $\omega \approx 0.2$ can, even if it is below 1, cause oscillatory flow out of the system and excessive valve movement for the stabilized system.

The analysis has so far not considered the major difference between the measurements P_I and P_{Rb}, which is the effective time delay due to pressure wave propagation in the pipeline. The simulations (both with OLGA and with the simple two-fluid model) in section 2.6 showed that there are virtually no time delay through the riser to the riser base measurement P_{Rb}, whereas the pressure wave takes about 10 seconds to propagate back to the measurement P_I. This imposes an upper bound on the closed-loop bandwidth of the system, as we need the crossover frequency ω_c to be less than the inverse of the time delay θ, $\omega_c < 1/\theta$. On

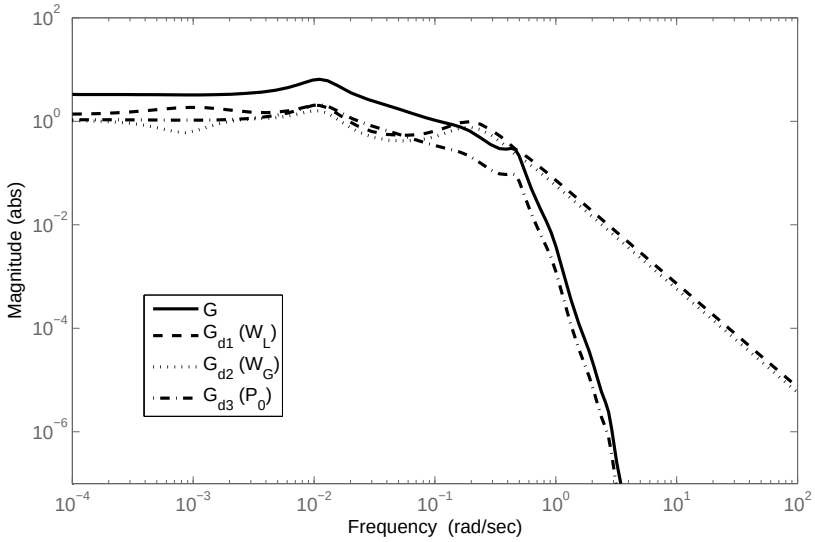

Figure 2.12: Frequency dependent gain for $y = P_I$ at operating point $Z = 30\%$

the other hand, the instability requires a bandwidth of approximately $\omega \geq |p|$ for complex unstable poles (Skogestad and Postlethwaite, 1996). With $|p| \approx 0.01$, this means that we for this operating point would have to have a closed-loop crossover frequency in the range $0.015 < \omega_c < 0.1$ when using $y = P_I$. For even longer pipelines than the one studied in this example, the time delay may be to high for the inlet pressure to be used for stabilizing control.

Thus, the analysis shows that the riser base pressure P_{Rb} and the inlet pressure P_{Rb} are good candidates for stabilizing control of these systems. We should be able to design a controller that stabilize the system with little input usage, that is able to effectively suppress (low-frequency) disturbances, and that has good setpoint tracking properties. Our main concern would be to suppress flow disturbances in the medium-to-high frequency range (flow disturbances with $\omega \approx 0.2$, meaning waves and/or hydrodynamic slugging with a period of about 30 seconds).

2.6.8 Additional remarks

We have so far mainly discussed single input-single output (SISO) control, but from the above discussion, the measurements have advantages in different frequency ranges. An upstream pressure measurement (P_I or P_{Rb}) has excellent low-frequency properties, while a measurement of the flow through the choke valve (Q or W) has good high-frequency properties. Combining these two measurements in a cascade controller or a similar control scheme that can utilize the benefits of both the measurement candidates would probably be a good way to approach the problem. Such a scheme has indeed already been reported by Skofteland and Godhavn (2003) and Godhavn, Mehrdad and Fuchs (2005). However, analysis of such systems is outside the scope of this chapter, and we will return to this in chapter 5 and

6.

It should also be mentioned that the operating point at $Z = 30\%$, used in the above analysis, is a fairly aggressive operating point with relatively fast instability and low process gain. If we were to perform the same analysis at the more conservative operating point ($Z = 17.5\%$), the controllability of the system would be significantly improved to a relatively minor cost in terms of pressure drop.

2.7 Simulations

Since direct design of model-based optimal controllers are complicated due to the complexity of the model, simple PI-controllers are used to illustrate and confirm the results from the controllability analysis in section 2.6. The simulations use the simple two-fluid model described in section 2.4. One reason for not using the OLGA model is that it is difficult with OLGA to impose the type of disturbances we want to consider. In chapters 5 and 6, where the focus will be more on controller design and less on controllability analysis, we will test our controllers on the reference systems against which they were tuned.

2.7.1 Stabilizing pressure control ($y = P_I$)

A simple feedback PI controller with controller gain $K_c = -0.3bar^{-1}$ and integral time $\tau_I = 500s$ stabilizes the system and give a crossover frequency of $\omega_c = 0.033s^{-1}$ for the operating point with $Z = 30\%$. However, nonlinear effects make it difficult to stabilize the process directly at this operating point from initial severe slugging behavior. An easy solution to this problem is to initially stabilize the process at a less aggressive operating point and then change the pressure setpoint gradually to get to the desired operation point.

In figure 2.13, the process is started up without control with a constant valve opening of $Z = 30\%$. At $t = 30\ min$, the controller is turned on with a setpoint of 70 bar and we see that the PI controller stabilizes the system. At $t = 120\ min$ the setpoint is changed to the desired value of 68.7 bar. We have attempted to represent the real-life hydrodynamic slugging at the inlet by applying sinusoidal feed signals in counter-phase for the gas and liquid feed. The amplitude of the oscillations were $\pm 100\%$ of its nominal value, and the frequency were $0.2rad/s$. The controller manages to keep the process stable even with these large disturbances, but the valve movement and flow oscillations at the outlet might be a problem.

2.7.2 Stabilizing flow control ($y = Q$)

To stabilize the process by controlling volumetric flow Q, we use a simple feedback PI controller with gain $K_c = 80m^{-3}s$ and integral time $\tau_I = 500s$. We added a lag filter with two poles at $\omega = 0.5s^{-1}$ to the controller to avoid sensitivity to noise. The crossover frequency for this system is $\omega_c = 0.28s^{-1}$. The setpoint for the flow is reached quickly, and the disturbance rejection is far better than the above case with pressure control. However, the low-frequency (stationary) behavior of the system is very sluggish, as expected from

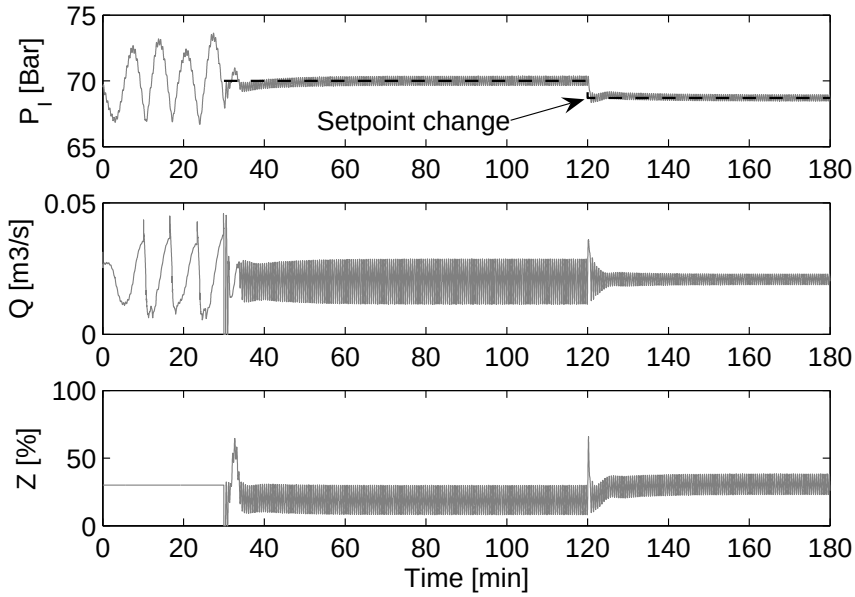

Figure 2.13: Simulation of stabilizing pressure control ($y = P_I$). Controller turned on at t=30 min. Setpoint change at t=120 min.

the controllability analysis. This is illustrated by the slow return of the pressure (P_I) to its steady-state. This could at least partly be remedied by an outer loop, but the response time would depend on the input to the outer loop.

The poor low-frequency response is further illustrated by applying a 10% reduction in the liquid feed rate. As shown in figure 2.15, the system under flow control goes unstable because the control system cannot suppress the disturbance. This moves the system away from its nominal operating point and into an operating region where the controller no longer can stabilize the system. The pressure control system has no problems in dealing with the step in the liquid feed rate.

2.8 Comments on model complexity

The PDE-model used in this chapter is discretized in space to transform it into a system of ODE's that is needed for conventional controllability analysis and controller design. The drawback of this model structure is that the model order (state dimension) of the resulting system of ODE's is high, and the direct numerical optimization needed for design of (optimal) model based controllers gets complicated. Additionally, due to high model order, any controller based on a systematic design procedure, such as LQG control, will have a high number of states. This may be partly remedied by model reduction, but other solutions may also be conceivable.

The Bode diagram for the linear process model obtained around the operating point $Z = 30\%$ with $y = P_I$ as measurement is given in figure 2.16. Both the phase and the

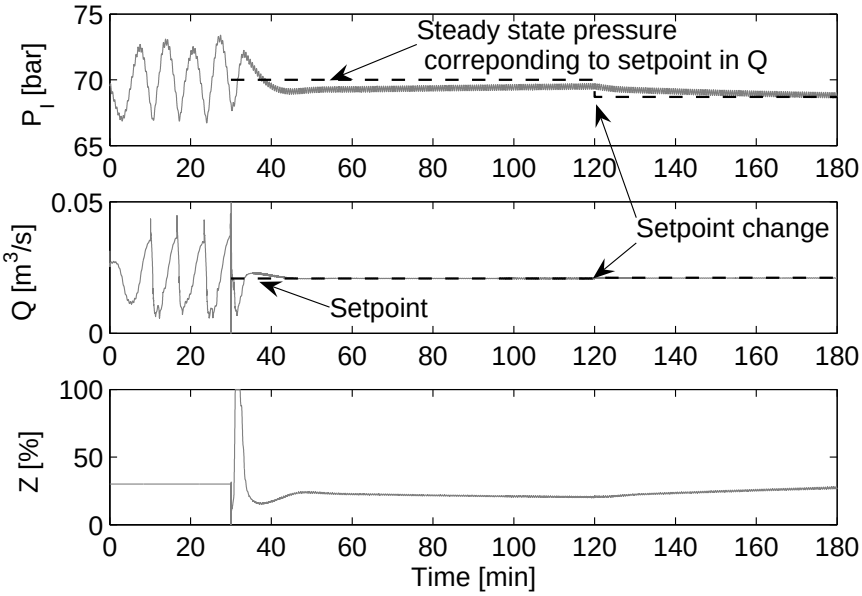

Figure 2.14: Simulation of stabilizing flow control (y=Q). Controller turned on at t=30 min. Setpoint change at t=120 min.

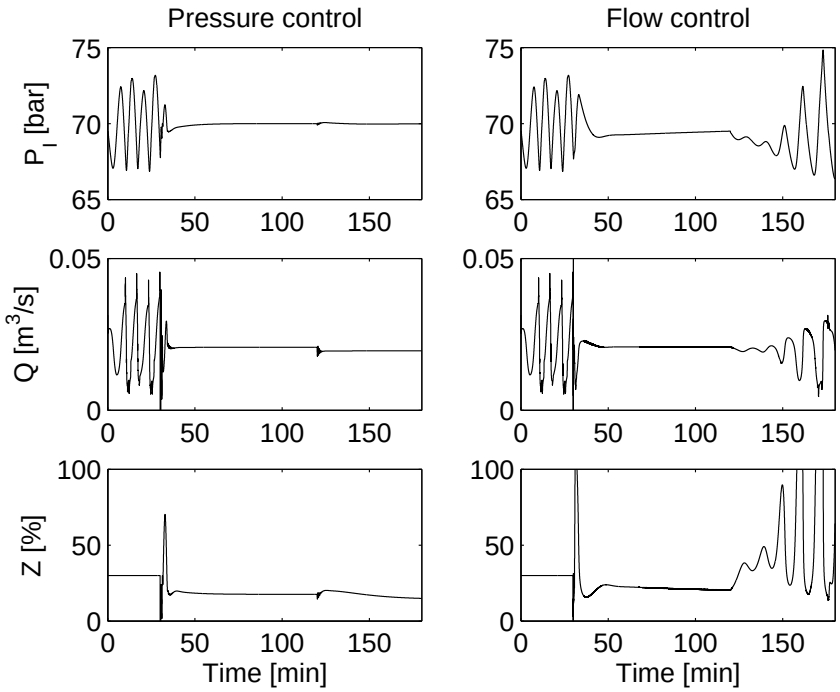

Figure 2.15: Simulation of step in liquid feed at t=120 min illustrating low-frequency disturbance rejection problems with flow control

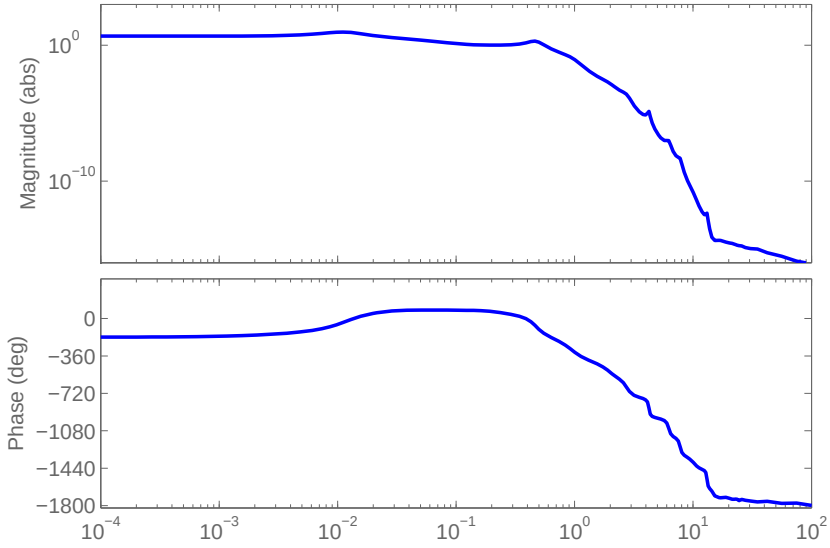

Figure 2.16: Bode diagram for process model $G(s)$, $y = P_I$ at $Z = 30\%$

magnitude are relatively smooth, and resemble a significantly simpler model than the one used in this work. This leads one to suspect that the underlying mechanics of this process can be described using a greatly simplified model. This suspicion is further strengthened by physical arguments. The severe slugging is mainly a process driven by the competing effects of the pressure in the upstream (horizontal/declining) part of the pipeline and the weight of the liquid in the riser. Since both pressure and gravity are bulk quantities, we should be able to describe the process using greatly simplified model based on bulk quantities rather than the distributed model used in this chapter. Such a simplified model will be introduced in chapter 3.

2.9 Conclusions

We have shown that riser slugging in pipelines can be stabilized with simple control systems, but that the type and location of the measured input to the controller is critical. Of the possible candidates studied in this work, only an upstream (inlet or riser base) pressure measurement and a flow measurement at the outlet are viable candidates for stabilizing control.

Use of an upstream pressure measurement works well for stabilization, but is less suited for suppressing high-frequency flow disturbances such as small hydrodynamic slugs that might be formed in the pipeline. It might also be a problem using the inlet pressure as a primary control variable for long pipelines due to the time delay associated with pressure wave propagation.

Use of an outlet flow measurement is effective for suppressing high-frequency flow dis-

turbances. However, the low-frequency disturbance rejection and setpoint tracking properties are poor, and this makes a stabilizing controller based on a topside flow measurement a viable option only if it is used in combination with another measurement (for example cascade or SIMO control).

The analysis of the properties of this system reveals that the underlying mechanics of the system probably can be described by a simpler model than the PDE-based model used in this work.

2.10 Acknowledgments

Thanks to Vidar Alstad, who participated in the development and implementation of the simplified two-fluid model used in this chapter.

Chapter 3

A low-dimensional dynamic model of severe slugging for control design and analysis

Espen Storkaas and Sigurd Skogestad

Based on a paper submitted to SPE Journal

Abstract

A novel simplified dynamic model of a pipeline-riser system at riser slugging conditions is introduced. The model covers the stable limit cycle known as riser slugging, and even more importantly for control purposes, predicts the presence of the unstable but preferred stationary flow regime that exists at the same boundary conditions.

The model has only three dynamic states, namely the holdups of gas and liquid in the riser and the holdup of gas in the upstream pipeline. The most important adjustable parameters are the ”valve constant” for the flow of gas into the riser and two parameters describing the fluid distribution in the riser.

The model has been fitted to data both from an OLGA test case and experiments. We have in all cases achieved good agreement with the reference data. The model has been further verified by showing that its controllability predictions are almost identical to those of a more detailed two-fluid model based on partial differential equations.

3.1 Introduction

To design efficient control systems, it is advantageous to have a good model of the process. Here, the word ”good” must be seen in context with how the model is used. For control purposes, it is important to concentrate on the physical phenomena that are significant at the relevant timescales for control. This allows us to use simpler models for control purposes than for more detailed simulations.

In chapter 2, a PDE-based two-fluid model was used to show that there existed an unstable non-oscillatory flow regime at the same boundary conditions as riser slugging in pipeline-riser systems, and that simple control systems could be used to stabilize this unstable operating point. It was also found that the model was unnecessarily complex for performing controllability analysis and controller design for a pipeline-riser system. Based on the frequency response for the linearized two-fluid model, it was concluded that a simplified model could be used to describe the process.

The objective of a control system design to avoid riser slugging is to stabilize the unstable operating point and by that avoiding riser slugging. The relevant timescale for control is then the time it takes for the instability (riser slug formation) to evolve. Recall from chapter 2 that the unstable poles for an industrial-scale system had a frequency of about 0.005-0.01s^{-1}, corresponding to about 100-200 seconds. This means that the relevant timescale for stabilizing the flow in such pipeline-riser systems is on the order of a few minutes. Based on that timescale, physical phenomena whose dominant dynamical behavior is in the order of a few seconds in industrial-sized systems can be regarded as instantaneous. Note that this does not limit the models applicability for smaller, lab-scale systems since the timescales for both the control problem and the relevant physical phenomena are relative to the size of the system. Thus, the timescale of the riser slugging problem allows us to use a simple ”bulk” model of the distributed system with only three states.

We did not find any published simplified dynamic models of riser slugging that were suitable for control purposes. A related phenomena is instability in gas lift systems, and our starting point was simplified models for this (Jansen et al., 1999; Eikrem et al., 2004). However, direct extension of these models was not successful, and we had to include new mechanisms for riser inlet blocking and ”entrainment” in the riser.

After developing the simplified model, we proceed to show that the model predicts system properties relevant to control which are very similar to those found using the more complicated distributed model used in chapter 2.

3.2 Model Description

The conventional multiphase flow models (e.g. the two-fluid model used in chapter 2) use distributed conservation equations and are developed to cover the behavior of two-phase flow in pipelines over a wide range of pipe geometries, flow regimes and boundary condition. We are looking for a simple model that predicts the following important characteristics of the riser slugging system (in order of importance):

1. the presence of the (desired) unstable stationary solution (flow regime) at the same

boundary conditions as those corresponding to riser slugging

2. the dynamic behavior of the unstable points (i.e. the nature of the transition from smooth flow to riser slugging)

3. the stability of the flow regimes as function of choke valve opening

4. the amplitude/frequency of the oscillations of fully developed riser slugging

The order of the items above show that we for control purposes are more interested in the desired (open-loop unstable) flow regime than the naturally occurring (open-loop stable) riser slugging. This is because the purpose of the model is to be a tool to help us avoid the riser slugging and by that ensure smooth operation. A parallel to this can be found in everyday life; if you are teaching someone to ride a bike, you are teaching them how the bike behaves when they have mastered the balancing act of riding the bike (the desired unstable operating point), not how it behaves when it lies on the ground (the undesired slug flow).

3.2.1 Assumptions

The model is based on the setup depicted in figure 3.1. The main assumptions are:

A1 Neglected liquid dynamics in the upstream feed pipeline, that is, constant liquid velocity in this section.

A2 Constant gas volume V_{G1} (but possible varying mass of gas) in the feed pipeline. This follows from assumption A1 if we also neglect the liquid volume variations due to variations in the liquid level h_1 at the low-point.

A3 Only one dynamical state (m_L) for liquid holdup in the riser section. This state includes both the liquid in the riser and in the low-point section (with level h_1)

A4 Two dynamical states for gas holdup (m_{G1} and m_{G2}), occupying the volumes V_{G1} and V_{G2}, respectively. The gas volumes are ”connected” by a pressure-flow relationship in the low-point.

A5 Ideal gas behavior

A6 Stationary pressure balance over the riser (between pressures P_1 and P_2)

A7 Simplified valve equation for gas and liquid mixture leaving the system at the top of the riser

A8 Constant temperature

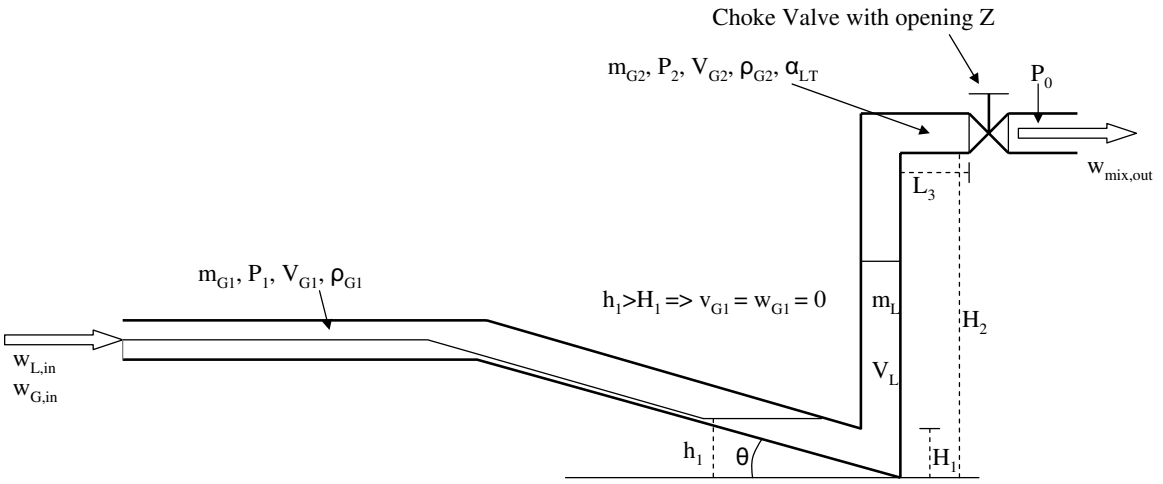

(a) Simplified representation of riser slugging

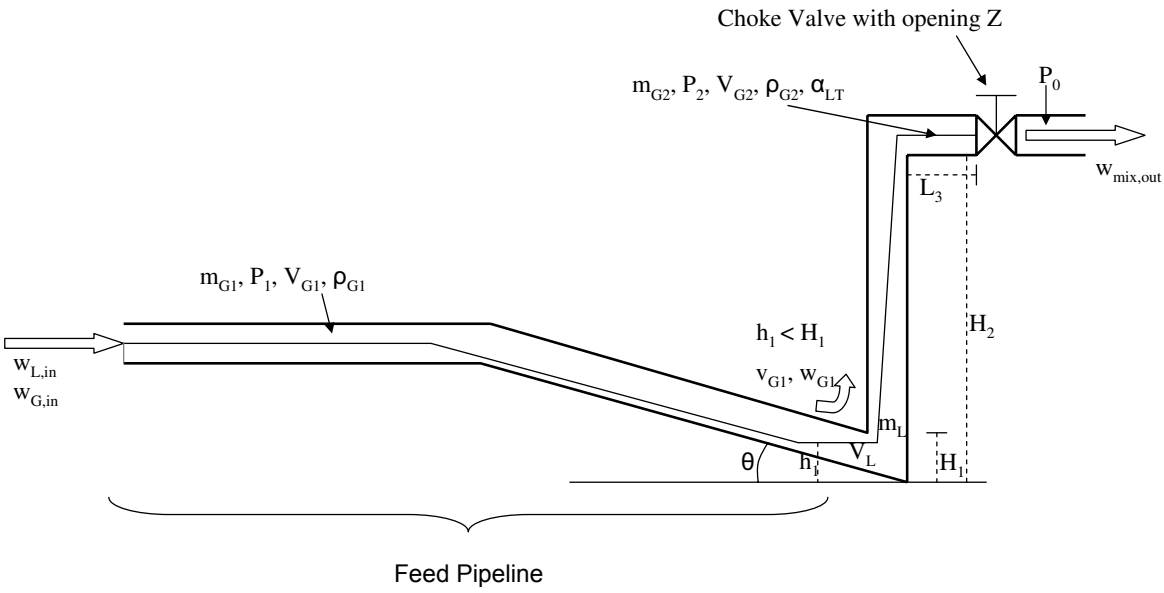

(b) Simplified representation of desired flow regime

Figure 3.1: Schematic representation of model parameters

3.2.2 Model fundamentals

The model has three dynamical states, as stated by assumptions A3 and A4:

- mass of liquid m_L in the riser and around the low-point
- mass of gas m_{G1} in the feed section
- mass of gas m_{G2} in the riser

The corresponding mass conservation equations are

$$\frac{\partial}{\partial t} m_L = w_{L,in} - w_{L,out} \tag{3.1}$$

$$\frac{\partial}{\partial t} m_{G1} = w_{G,in} - w_{G1} \tag{3.2}$$

$$\frac{\partial}{\partial t} m_{G2} = w_{G1} - w_{G,out} \tag{3.3}$$

Based on assumptions A1 - A8 and figure 3.1, the computation of most of the system properties such as pressures, densities and phase fractions are then straightforward.

Some comments:

- The stationary pressure balance over the riser (Assumption A6) is assumed to be given by
$$P_1 - P_2 = \bar{\rho} g H_2 - \rho_L g h_1 \tag{3.4}$$
Here $\bar{\rho}$ is the average mixture density in the riser. The use of a stationary pressure balance is justified because the pressure dynamics are significantly faster than the time scales in the control problem. For long pipelines, it might be necessary to add some dynamics (i.e. time delay) between the pipeline pressure (P_1) and the measured pressure if the pressure sensor is located far from the riser.

- The boundary condition at the inlet (inflow $w_{G,in}$ and $w_{L,in}$) can either be constant or pressure dependent.

- A simplified valve equation for incompressible flow is used to describe the flow through the choke valve,
$$m_{mix,out} = K_1 z \sqrt{\rho_T \left(P_2 - P_0\right)} \tag{3.5}$$
If a more accurate description of the flow out of the system is needed, the Sachdeva model (Sachdeva et al., 1986) can be used.

- The most critical part of the model is the phase distribution and phase velocities in the riser. The gas velocity is based on an assumption of purely frictional pressure drop over the low-point and the phase distribution is based on an entrainment model. This is discussed in more detail below.

The entire model is given in detail in Appendix B. A Matlab version of the model is available on the web (Storkaas, 2003).

3.2.3 Relationship between gas flow into riser and pressure drop

When the liquid is blocking the low point ($h_1 > H_1$ in figure 3.1(a)), the gas flow w_{G1} is zero.

$$w_{G1} = 0, \quad h_1 \geq H_1 \tag{3.6}$$

When the liquid is not blocking the low point ($h_1 < H_1$ in figure 3.1(b)), the gas will flow from V_{G1} to V_{G2} with a mass rate $w_{G1}[kg/s]$. From physical insight, the two most important parameters determining the gas rate are the pressure drop over the low-point and the free area given by the relative liquid level ($(H_1 - h_1)/H_1$) at the low-point. This suggests that the gas transport could be described by a valve equation, where the pressure drop is driving the gas through a "valve" with opening $(H_1 - h_1)/H_1$. Based on trial and error, we propose to use the following "valve equation":

$$w_{G1} = K_2 f(h_1) \sqrt{\rho_{G1}(P_1 - P_2 - \rho_L g \alpha_L H_2)}, \quad h_1 < H_1 \tag{3.7}$$

where $f(h_1) = \hat{A}(H_1 - h_1)/H_1$ and $\hat{A}$ is the gas flow cross-section at the low-point. Note that $f(h_1) = \hat{A}(H_1 - h_1)/H_1$ is approximately quadratic in the "opening" $(H_1 - h_1)/H_1$.

Separating out the gas velocity with $w_{G1} = v_{G1}\rho_{G1}\hat{A}$ yields

$$v_{G1} = \begin{cases} K_2 \frac{H_1 - h_1}{H_1} \sqrt{\frac{P_1 - P_2 - \rho_L g \alpha_L H_2}{\rho_{G1}}} & h_1 < H_1 \\ 0 & h_1 \geq H_1 \end{cases} \tag{3.8}$$

3.2.4 Entrainment equation

The final important element of the model is the fluid distribution in the riser. This distribution can be represented in several ways. One approach is to use a slip relation to relate the liquid velocity to the gas velocity and use the velocities to compute the distribution. This is similar to the approach used in a drift flux model (Zuber and Findlay, 1965). We made several attempts to derive a model based on this approach, but were not successful.

Another approach is to model directly the volume fraction of liquid (α_{LT}) in the stream exiting the riser. We found that this approach was better suited for our purposes. The liquid fraction will lie between two extremes:

1. When the liquid blocks the flow such that there is no gas flowing through the riser ($v_{G1} = 0$), we have $\alpha_{LT} = \alpha^*_{LT}$. In most cases we will then have only gas exiting the riser (see figure 3.1(a)), and $\alpha^*_{LT} = 0$. However, eventually the entering liquid may cause the liquid to fill up the riser and α^*_{LT} will exceed zero. For more details, see appendix B.

2. When the gas velocity is very high there will be no slip between the phases, $\alpha_{LT} = \alpha_L$, where α_L is average liquid fraction in the riser.

The transition between these two extremes should be smooth. We assume that the transition depends on a parameter q as depicted graphically in figure 3.2 and represented by the

entrainment equation

$$\alpha_{LT} = \alpha^*_{LT} + \frac{q^n}{1+q^n}\left(\alpha_L - \alpha^*_{LT}\right) \tag{3.9}$$

The parameter n is used to tune the slope of the transition, as illustrated in figure 3.2.

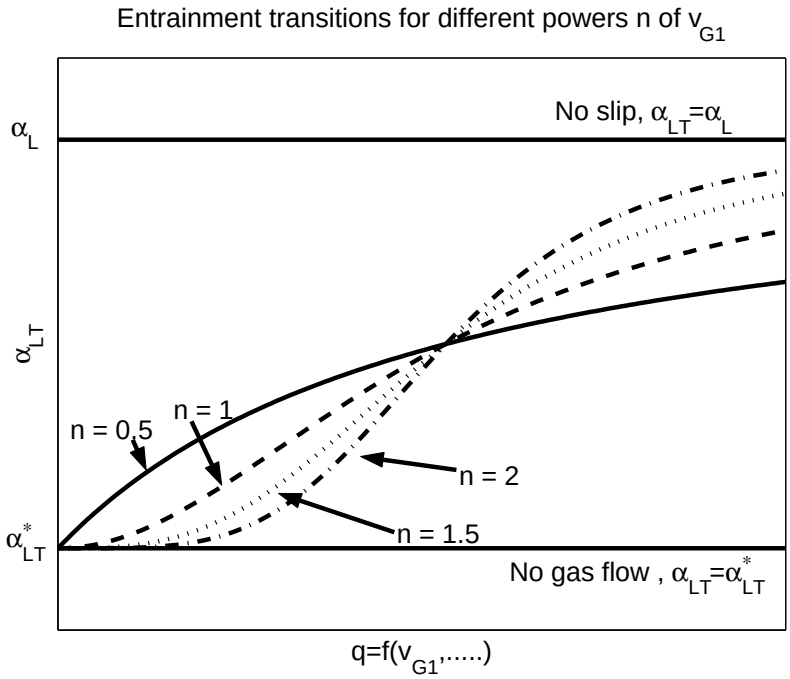

Figure 3.2: Transition between no and full entrainment

The final parameter q in (3.9) must depend on the gas velocity in the system. To derive this relationship, we note that the entrainment of liquid by the gas in the riser is somewhat similar to flooding in gas-liquid contacting devices such as distillation columns. The flooding velocity is equal to the terminal velocity for a falling liquid drop and is given by

$$v_f = k_f\sqrt{\frac{\rho_L - \rho_G}{\rho_G}} \tag{3.10}$$

This expression only gives a yes/no answer to whether it is flooding ($v_G > v_f$) or not ($v_G < v_f$). To get a smooth transition, we use the square of the ratio of the internal gas velocity v_{G1} to the flooding velocity v_f. Thus, $q = k\left(\frac{v_{G1}}{v_f}\right)^2$ and introducing v_f from (3.10) gives

$$q = \frac{K_3\rho_{G1}v^2_{G1}}{\rho_L - \rho_{G1}} \tag{3.11}$$

where $K_3 = k/k_f^2$. Equation (3.11) combined with (3.9) produces the transition depicted in figure 3.2. The tuning parameter K_3 will shift the transition along the horizontal axis.

3.3 Tuning Procedure

The simplified three-state model contains four empirical parameters that can be used to tune the model. These are: K_1 in the choke valve equation (3.5), K_2 in the expression for internal gas velocity (3.8) and K_3 and n in the entrainment model ((3.9) and (3.11)). In addition, some of the physical parameters that are assumed constant in the model are varying in the real system, and the values for these parameters can also be adjusted to improve the fit to the reference data. These physical parameters include the average molecular weight of the gas, M_G, and the upstream gas volume, V_{G1}.

The tuning of the model will depend on the available data. Field data for the real system is obviously the best alternative, but sufficient data is rarely available for industrial systems, especially for riser slugging. An alternative approach is to obtain data from a more detailed model, for example a commercial multiphase simulator such as OLGA, that is tuned to give a reasonably accurate description of the system. This approach can provide reference data over a wide range of operating conditions and valve openings without the prohibiting costs associated with field test.

The analysis of a riser slugging system in chapter 2 shows that the system goes through a Hopf bifurcation at the transition from the stable flow regime to riser slugging. Here the system must have a pair of purely complex eigenvalues (poles). This fact restricts the solution space for the stationary solution (the zero solution of (3.1), (3.2) and (3.3)) at the bifurcation point.

Our tuning strategy is to identify the bifurcation point from the reference data and use two measurements (for example the upstream pressure P_1 and the topside pressure P_2) to fix two degrees of freedom in the stationary solution of the model. K_2 and h_1 are strongly correlated through (3.7), and since the stationary value of h_1 is bounded in the interval $0 < h_1 < H_1$, it is easier to assign a value to h_1 than to K_2 when tuning the model. Thus, fixing h_1 and iterating on the value for n to obtain purely complex eigenvalues allows us to find K_1, K_2 and K_3 from the stationary solution of the model. Finally, the value used for h_1 and possibly the physical properties M_G and V_{G1} can be adjusted to to get an acceptable fit of pressure levels, amplitudes, and frequencies for other valve openings.

Note that since the pipeline leading into the riser is treated as one control volume, we cannot model variations in pressures etc. along the pipeline. This means that we can only tune the model to data from a specified point in the feed pipeline.

3.4 Model verification

For verification, the model is fitted to experimental data from a medium scale loop (15 m riser) and to the OLGA test case (300 m riser) used in chapter 2. Sivertsen and Skogestad (2005) have also fitted the model to experimental data from a miniloop (1 m riser) with good results.

Table 3.1: Parameters identified to fit experimental Tiller data

Parameter	Value	Unit
K_1 in choke valve equation	0.0014	m^{-2}
K_2 in the expression for internal gas velocity (3.8)	2.81	-
K_3 in the entrainment model (3.11)	16.7	s^2/m^2
n in the entrainment model (3.9)	1.75	-
Upstream gas volume V_{G1}	0.80	m^3
Molecular weight gas M_G	146.1	$kg/kmole$

3.4.1 Experimental Tiller data

The experimental data were obtained from recent experiments performed by Statoil at a medium scale loop at the SINTEF Petroleum Research Multiphase Flow Laboratory at Tiller outside Trondheim, Norway. The loop consists of a 200 meters long slightly declining feed pipeline entering a 15 meters high vertical riser with a control valve located at the top. The fluids used are SF_6 for the gas and Exxsol D80 (a heavy hydrocarbon) for the liquid. After the riser the mixture enters a gas-liquid separator with an average pressure of 2 bar. The inflow into the feed pipeline is pressure dependent. More information on these experiments can be found in Skofteland and Godhavn (2003), Fard et al. (2003) and Godhavn, Mehrdad and Fuchs (2005).

The experimental data consist of four data points for non-oscillatory flow, where one is for stable flow, one is the bifurcation point and the last two point are for stabilized (open-loop unstable) operation. In addition, data for riser slugging with 100% open choke valve are available. The experimental data are represented by the dots in figure 3.3, where the two dots at $Z = 100\%$ represent the maximum and minimum pressure in the slug cycle.

As seen in figure 3.3, we were able to obtain a very good fit with our simplified model to the experimental results using the tuning procedure described in section 3.3. The model parameters from the tuning are given in table 3.1. More importantly, the controllers designed based on the simplified model reproduced the stability results confirmed experimentally. In fact, the optimized controller tunings found using the model matched the ones found to be optimal from the experimental work.

Note that this is the only case studied in this thesis where the feed flow is pressure dependent. However, the inflow mechanism seems to have little influence on the controllability. An analysis of the model gives the same general controllability findings and local (linear) behavior as for the simulated OLGA test case with constant inflow studied chapter 2. The only major difference is that, as expected, the low-frequency gain associated with flow measurements at the outlet is larger when the inflow is pressure dependent. However, the low-frequency gain is still low, so the controllability problem remains.

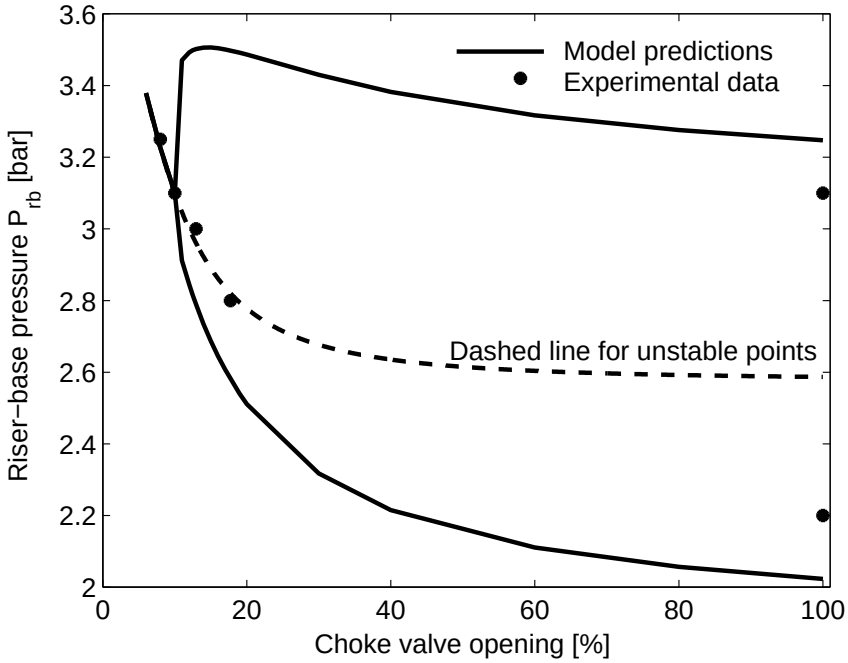

Figure 3.3: Bifurcation diagram for the Tiller experimental data

3.4.2 Simulated OLGA test case

The test case for riser slugging OLGA, also studied in chapter 2, is used as a second verification case. The case geometry and nomenclature is shown in figure 2.3 (page 14). The relationship between the nomenclature used in the model (figure 3.1) and the nomenclature used for the physical system depicted in figure 2.3(a) are given in table 3.2.

Model Tuning

The model was tuned as outlined in section 3.3 and resulted in the parameters given in table 3.3. The reference data was from OLGA simulations consisted of data both for riser slugging and for the stable and unstable regions of the stationary flow regime. The unstable stationary

Table 3.2: Nomenclature for physical system and model. * Only one of these pressures can be described by the model.

Description	Physical system (figure 2.3(a))	Model (figure 3.1)
Topside pressure	P_T	P_2
Topside density	ρ_T	ρ_2
Riser-base pressure *	P_{Rb}	P_1
Inlet pressure *	P_I	P_1

Table 3.3: Parameters identified to fit the simulated OLGA data

Parameter	Value	Unit
K_1 in choke valve equation	0.0054	m^{-2}
K_2 in the expression for internal gas velocity (3.8)	6.84	-
K_3 in the entrainment model (3.11)	0.11	s^2/m^2
n in the entrainment model (3.9)	2.3	-
Upstream gas volume V_{G1}	12.64	m^3
Molecular weight gas M_G	20.6	$kg/kmole$

operation points were obtained using the OLGA Steady State Processor. The bifurcation point were identified to be at a valve opening of $Z = 13\%$, and the corresponding values for the inlet pressure P_I and pressure drop over the valve DP were used to obtain a first tuning of the model.

Comparison with OLGA reference data and two-fluid model

In figure 3.4, the bifurcation diagrams for the inlet pressure P_I and the topside pressure P_T predicted by the simplified 3-state model are compared to the OLGA reference data and to the data from the PDE-based two-fluid model used in chapter 2. For each model, the solid lines represent operation with constant valve opening (without control). Riser slugging is represented by two solid lines, and the system is oscillating between the maximum and minimum pressure levels indicated in the bifurcation diagrams. The dashed lines indicate the unstable stationary flow regime.

Figure 3.4 shows that the simplified model gives an excellent fit to the OLGA reference data for the desired, non-oscillatory flow regime. The amplitude of the riser slugging is also predicted with good accuracy. Figure 3.4(a) shows that the simplified model actually gives the correct pressure drop over the pipeline-riser system, whereas the more complicated PDE-based model predicted the pressure drop to be about 5% too high. The pressure drop over the choke valve in figure 3.4(b) fits the reference data for the stationary flow regime for both models while there are some minor deviations for the riser slugging regime.

The slug frequency is not included in the bifurcation diagram, but simulations show that the simplified three-state model predicts a slug frequency that, compared to the OLGA simulations, is about 10-20% too high for low-to-medium range valve openings and up to about 50% too high for large valve openings. The higher frequency probably comes from neglecting the liquid dynamics in the feed section. This is not surprising since we have in this case tuned to achieve a good fit for the amplitude, and when the upstream gas volume is fixed, we cannot fit both frequency and amplitude simultaneously.

3.5 Control properties of model

To further verify the model, we first investigate the open-loop step responses for the OLGA test case for the 3-state model and compare these with the two fluid model from chapter 2

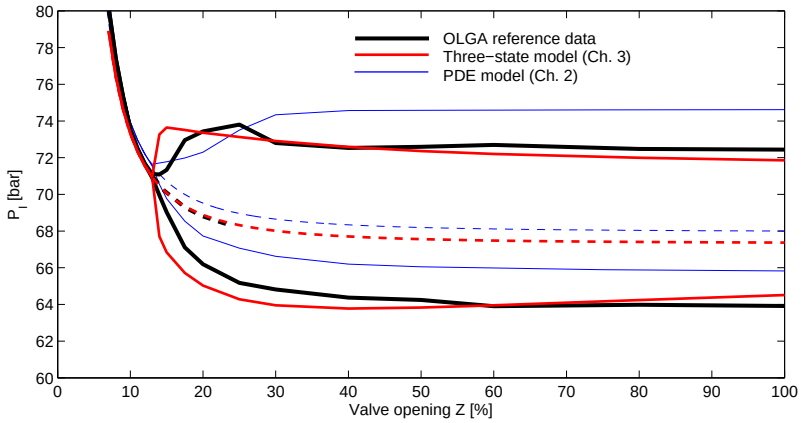

(a) Inlet Pressure

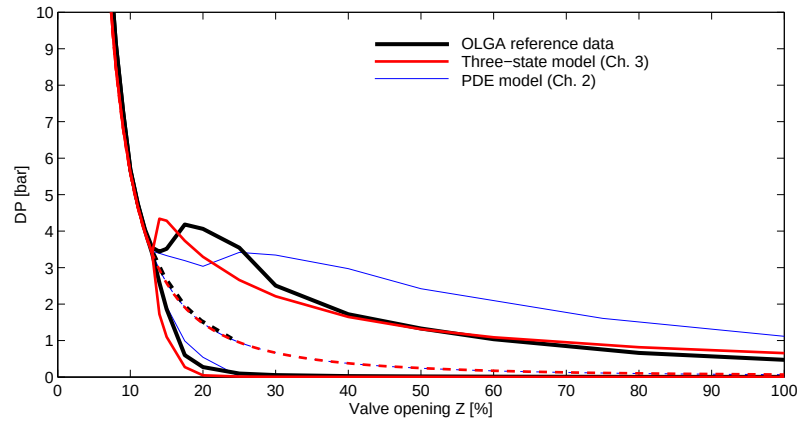

(b) Pressure drop over choke

Figure 3.4: Bifurcation diagrams for the simulated OLGA case (a) Inlet pressure P_I, (b) Pressure drop over choke valve DP

and with OLGA. We then compare the local (linear) behavior and the controllability results for the simplified model and two-fluid model at a valve opening of $Z = 30\%$. We generally find an excellent agreement with the significantly more complicated models, which is based in quite different modeling assumptions. This further shows that the simple 3-state model is excellent for control purposes.

3.5.1 Open-loop step response

Figure 3.5 shows the simulated step response to a step from $Z = 10\%$ to $Z = 12\%$ at t=0 for the simple 3-state model, the two-fluid model used in chapter 2 and OLGA. The same step response (without the 3-state model) was used in section 2.6.1 to gain some insight into the dynamic behavior of the different measurement alternatives.

We observe the following for the 3-state model:

- The oscillations have a frequency that is similar to OLGA, which indicates that the imaginary parts of the poles responsible for the oscillatory behavior have almost the same magnitude.
- An effective time delay of about 10s is missing in the response for $y = P_I$
- The effective time delay in $y = DP$, which is caused by unstable (RHP) zero dynamics, is 1-2 minutes. This is similar to the two-fluid model, but shorter than in OLGA. Also, the inverse response in the 3-state model has a shape that is consistent with real RHP-zeros, whereas the other two responses are indicative of complex RHP-zeros.
- The response for $y = Q$ is very similar to the two other models.

3.5.2 Frequency response comparison

Figure 3.6(a) shows the Bode plot with the valve opening Z as input and the inlet pressure P_I as output for the simplified model (solid lines) and the two-fluid model from chapter 2 (dashed lines). Recall that P_I was identified in chapter 2 as a good candidate for stabilizing control.

The step responses in the previous section show that a time delay of about 10 seconds is missing in the simplified 3-state model. The time delay is due to pressure wave propagation through the pipeline. Time delay manifests itself in a Bode plot as a drop in the phase and is evident in the lower part of figure 3.6(a). For a time delay of about $\theta = 10\ s$, the phase should theoretically drop about $57°$ at $\omega = 1/\theta = 0.1$ and drop sharply after this. This is consistent with the phase behavior of the two-fluid model. Note that this delay may easily be added to the simplified model to improve its behavior.

Another difference is a drop in the process gain (magnitude) for high frequencies in the two-fluid model. This drop in gain is a dampening effect that occurs due to the dynamics in the feed line which is not included in the simplified model. However, this damping occurs at higher frequencies than the desired bandwidth of the control problem, and the model deviation is therefore not important.

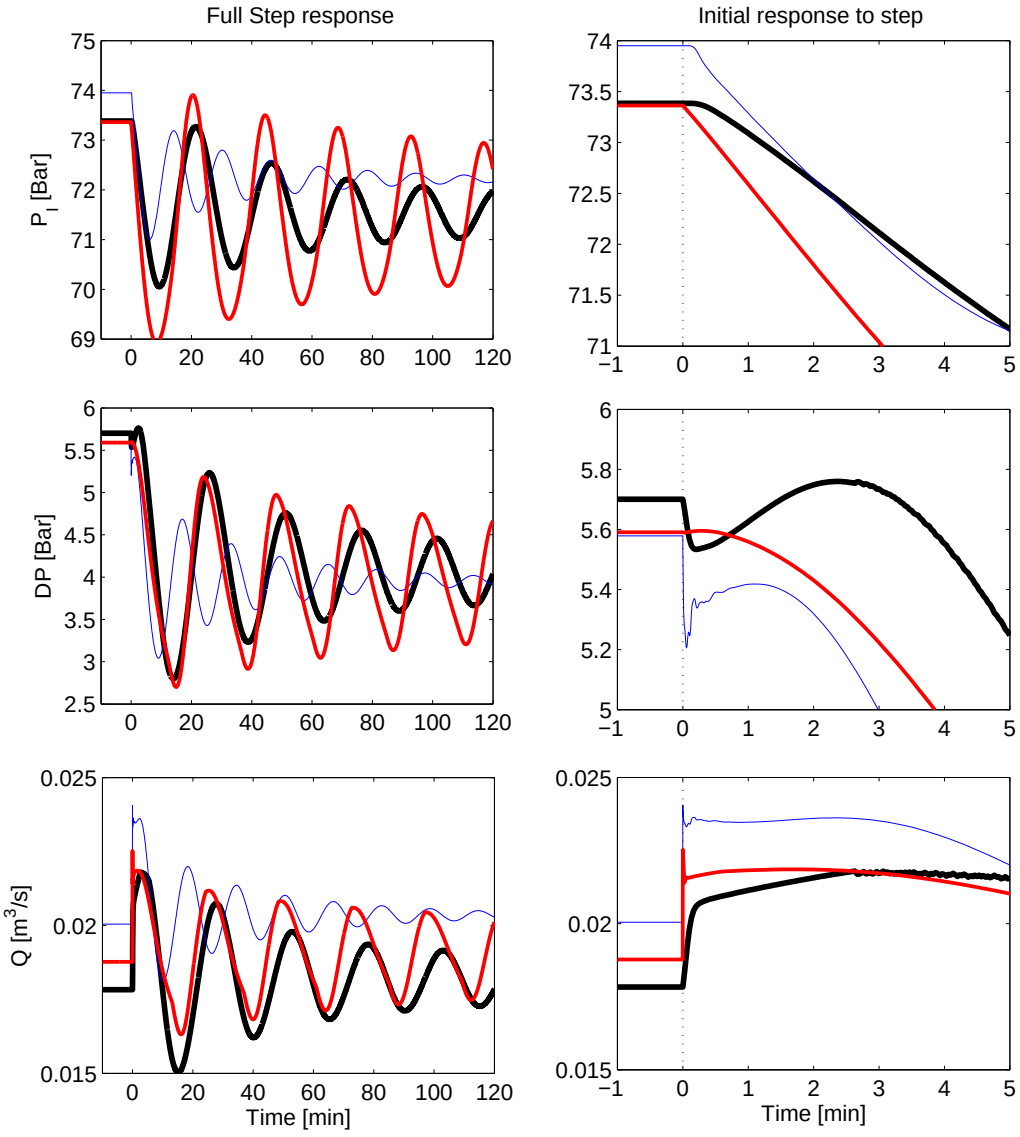

Figure 3.5: Open-loop step response with simple 3-state model (normal lines), two-fluid model (thin lines) and OLGA (thick lines).

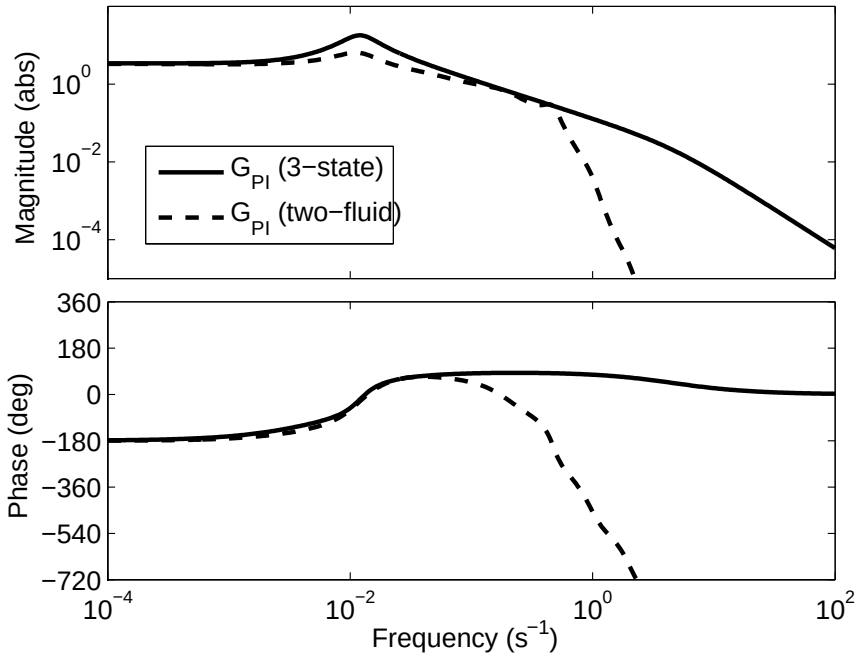

(a) Response from $u = Z$ to $y = P_I$

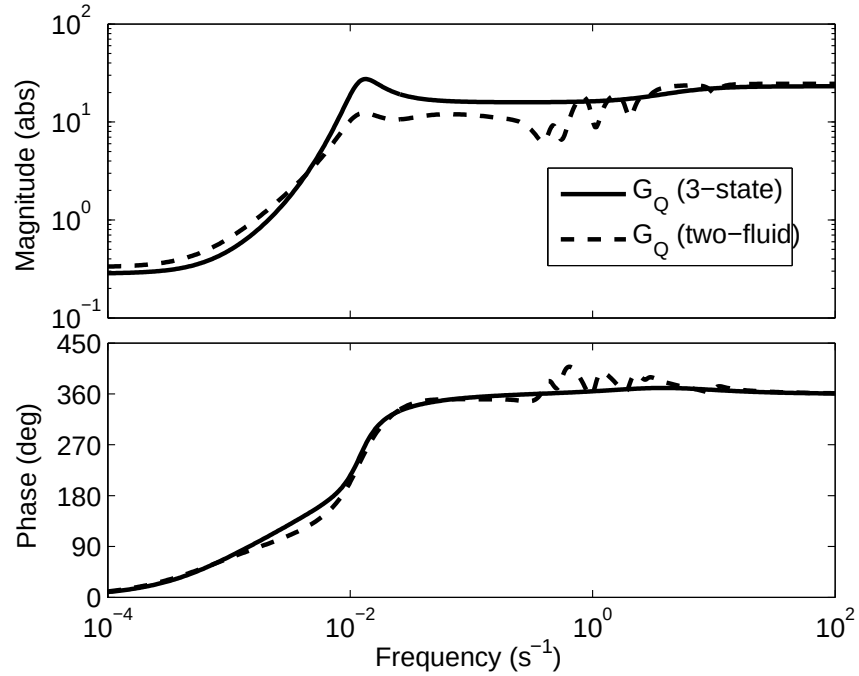

(b) Response from $u = Z$ to $y = Q$

Figure 3.6: Comparison of frequency responses for simplified (solid) and two-fluid model (dashed).

A third difference is that the simplified model has a higher gain in the frequency range around the instability. The reason for this is not clear, and we make no claim as to which model gives the right representation of the gain. However, we will show later in the thesis that effective and robust controllers can be designed based on the 3-state model, which serves as a strong indication that the gain representation is reasonably correct.

Figure 3.6(b) shows the Bode plot with the valve opening Z as input and the volumetric flow through the choke valve Q as output. The differences are small, except for a higher gain around the frequency of the instability.

Figure 3.7 shows the corresponding responses for disturbances in liquid feed (W_L), gas feed (W_G) and downstream pressure (P_0). As above, the deviations between the simplified model and the two-fluid model can be explained by the difference in feed-line dynamics.

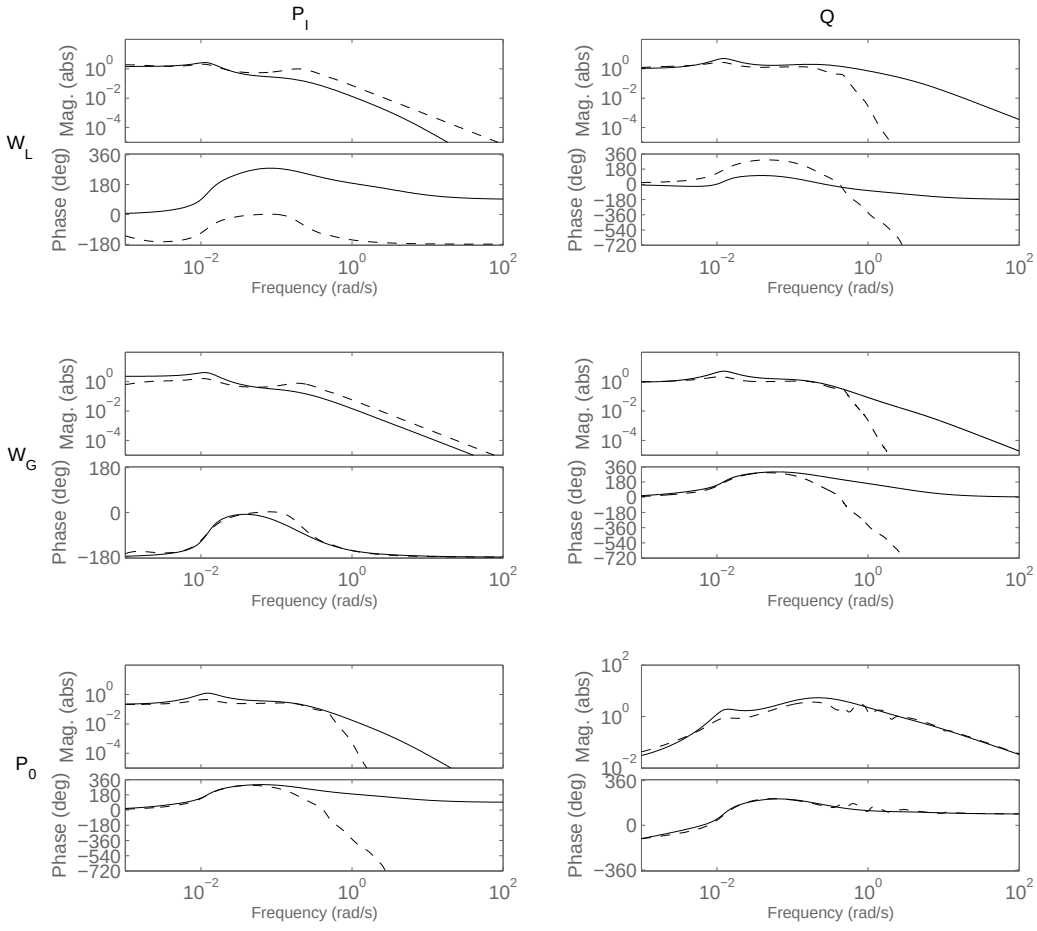

Figure 3.7: Comparison of disturbance frequency responses for 3-state (solid) and two-fluid model (dashed). Left column: $y = P_I$, right column: $y = Q$. First row: $d_1 = W_L$, second row: $d_2 = W_G$, third row: $d_3 = P_0$.

3.5.3 Controllability analysis

In chapter 2, the lower bounds on the transfer functions S, T, KS, SG, KSG_d and SG_d were computed based on the two-fluid model. The lower bounds serve both as measures of the achievable performance (e.g. the lower bound on KSG_d give the minimum input usage due to disturbances) and a as robustness indicators (e.g. SG is a measure of the sensitivity toward inverse additive uncertainty). Values significantly higher than unity for any of the lower bounds on the closed loop transfer functions are indications of controllability problems. The pole vectors were also computed as a tool for measurement selection

Chapter 2 considered the input pressure P_I, the riser-base pressure P_{rb}, the pressure drop over the choke valve DP, the density in the top of the riser ρ_T, the mass flow rate through the choke valve W and the volumetric flow rate through the choke valve Q as measurement candidates for stabilizing control of the pipeline-riser system. The controllability analysis concluded that the inlet or riser-base pressure were the best measurement candidates. The flow-rate Q and W were also found to be good candidates, but only in an inner loop in a cascade controller due to poor properties at low frequencies.

We here compare the models by computing the same bounds for the simple 3-state model, except that we omit the riser-base pressure P_{Rb} from the analysis since in the simplified model, $P_{Rb} \approx P_I$.

Tables 3.4 and 3.5 summarize the controllability results for the two models at $Z = 17.5\%$ and $Z = 30\%$, respectively. The bounds on the closed loop transfer functions and the pole vectors are computed as described in chapter 2. Although there are some differences between the two models, the conclusion is as before; we should preferably control the inlet pressure P_I, and if that measurement is not available, we should use the volumetric flow Q or the mass flow W in an inner loop in a cascade controller.

One trend is that the value for $\min_K \|KS\|_\infty$ (that is, the minimum peak for $|KS|$) is lower for the simplified model than for the PDE-based two-fluid model. This is consistent with the difference in peak gains observed form the Bode plots.

For the measurement alternatives DP and ρ_T, which both have unstable zeros, the value for $M_{S,min} = M_{T,min}$ are lower for the simplified model than for the PDE-based model from chapter 2. The reason is the difference in the location of the unstable zeros, which are also given in the tables. For $y = DP$, the simplified model has real unstable zeros, whereas the PDE model has a pair of complex unstable zeros that lie closer to the complex pair of unstable poles. This is consistent with the shape of the inverse responses in figure 3.5.

Table 3.4: Controllability data for the operating point $Z = 17.5\%$. Unstable poles at $p = 0.0007 \pm 0.0073i$ for simplified model and at $p = 0.0014 \pm 0.0085i$ for PDE-based model.

						Minimum peaks[a]				
Measurement	Value	Scaling	Smallest RHP-zero[b]	Pole vector[b]	$\|G(0)\|^b$	$\|S\| = \|T\|$	$\|KS\|$	$\|SG\|$	$\|KSG_d\|$	$\|SG_d\|$
$P_I[bar]$ (3-state)	69.35	1	-	0.49	19	1	0.01	0	0.06	0
$P_I[bar]$ (PDE)	70	1	99	0.36	18.9	1.0	0.03	0.0	0.06	0.0
$DP[bar]$ (3-state)	1.91	1	0.018	0.21	17.7	1.1	0.02	5.9	0.06	1.37
$DP[bar]$ (PDE)	1.92	1	0.01±0.01i	0.21	17.6	1.6	0.04	17.1	0.08	0.95
$\rho_T[kg/m^3]$ (3-state)	464	50	0.0045	0.35	1.4	1.2	0.01	27.4	0.06	2.25
$\rho_T[kg/m^3]$ (PDE)	432	50	0.016	0.28	1.5	1.4	0.03	28.6	0.07	1.60
$W[kg/s]$ (3-state)	9	1	-	0.64	0	1	0.01	0	0.06	0
$W[kg/s]$ (PDE)	9	1	-	0.59	0	1	0.02	0	0.06	0
$Q[m^3/s]$ (3-state)	0.0194	0.002	-	0.42	1.5	1	0.01	0	0.06	0
$Q[m^3/s]$ (PDE)	0.0208	0.002	-	0.51	1.8	1	0.02	0	0.06	0

Table 3.5: Controllability data for the operating point $Z = 30\%$. Unstable poles at $p = 0.0038 \pm 0.0115i$ for simplifeid model and at $p = 0.0045 \pm 0.0108i$ for PDE-based model.

						Minimum peaks				
Measurement	Value	Scaling	Smallest RHP-zero[b]	Pole vector[b]	$\|G(0)^b\|$	$\|S\| = \|T\|$	$\|KS\|$	$\|SG\|$	$\|KSG_d\|$	$\|SG_d\|$
$P_I[bar]$ (3-state)	68	1	-	0.32	3.4	1	0.11	0	0.31	0
$P_I[bar]$ (PDE)	68.7	1	98.1	0.30	3.3	1.0	0.30	0.0	0.35	0.005
$DP[bar]$ (3-state)	0.68	0.5	0.016	0.17	6.3	1.9	0.25	15.1	0.31	5.8
$DP[bar]$ (PDE)	0.66	0.5	0.01±0.01i	0.17	6.1	4.3	0.62	16.8	0.97	5.5
$\rho_T[kg/m^3]$ (3-state)	459	50	0.0045	0.34	0.26	1.5	0.13	4.4	0.38	2.0
$\rho_T[kg/m^3]$ (PDE)	427	50	0.015	0.27	0.27	2.6	0.64	14.6	0.55	4.7
$W[kg/s]$ (3-state)	9	1	-	0.73	0	1	0.06	0	0.31	0
$W[kg/s]$ (PDE)	9	1	-	0.63	0	1	0.17	0	0.32	0
$Q[m^3/s]$ (3-state)	0.0196	0.002	-	0.47	0.28	1	0.09	0	0.31	0
$Q[m^3/s]$ (PDE)	0.0211	0.002	-	0.59	0.33	1	0.17	0	0.32	0.002

[a] Want these small
[b] Want these large

3.6 Conclusions

We have developed a simplified model of riser slugging suitable for controller design and analysis. The model has three states and is based on 'phenomenological' modeling, where we identify the major characteristics of the system at hand and develop a model that incorporates these characteristics. The major characteristics of the riser slugging systems are the stability of the flow as a function of choke valve position, the nature of the transition to instability (Hopf bifurcation), the presence of an unstable steady-state solution and the amplitude of the oscillations. It should be stressed that it is more important for the model to describe the (desired) steady state flow regime than than the (undesired) slug behavior.

We have fitted the model to data both from an OLGA test case and from medium-scale experiments. We have in both cases achieved good agreement with the data. It is our experience that the simplified model is easier to fit to experimental data than the more complicated PDE-based two-fluid models that are based on a more "rigorous" representation of the true system. A controllability analysis shows the same results for a PDE-based two-fluid model and the simplified model, adding additional verification to the simplified model. The model has also been used for controller design (chapters 5 and 6) with good results.

The model is available on the web (Storkaas, 2003).

3.7 Achnowledgments

Thanks to John-Morten Godhavn and the Statoil research center for providing the experimental data used in section 3.4.1 to verify the simplified 3-state model.

Chapter 4

Implication of input rate limitations on controllability and controller design

Espen Storkaas and Sigurd Skogestad

Manuscript in preparation

Abstract

The conventional process controllability analysis on input usage has focused almost exclusively on signal magnitudes. However, input rate can in many cases be more important, especially when large valves are used for stabilizing control and/or for suppression of (relatively) fast disturbances.

This chapter will introduce simple expressions for computing the minimum input movement rate required for control of both stable and unstable systems. The input rates can be included in a frequency-dependent bound on the input u. The bound can be used for controllability analysis and also for controller design.

4.1 Introduction

Prior to designing a control system, there is a number of questions that should be asked; How well can the process be controlled? What control structure should be used? How might the process be changed to improve control? These questions can be answered by a controllability analysis (Skogestad and Postlethwaite, 1996) performed on the process prior to the actual controller design. For example, design parameters like the valve size (e.g. CV value) that would ensure a controllable system can be determined by such an analysis.

In order to interpret the results from the controllability analysis, it is recommended that the process models are scaled such that the signals have similar magnitude. The models are usually scaled such that the inputs and outputs are less than one in magnitude. For example, $u = 1$ may imply that a valve is fully open and $u = -1$ that a valve is fully closed. However, if input movement rate is limited, then this should be taken into account when scaling the process.

The significance of the input movement rate is highly case-dependent. Small valves with low pressure drop are usually fast-acting, and when such valves are used to control slow processes, the input rate is will probably not affect the control problem. On the other hand, the movement rate of large valves may be in the same frequency range as the desired bandwidth for the process. In these cases, the effect of the input movement rate may be crucial.

The objective of this chapter is two-fold. 1) Find the minimum input movement rate necessary to achieve the design targets for the control system and then 2) design control systems that explicitly takes the limited input movement rate into account. The effect of a limited input movement rate is especially important for stabilizing controllers for unstable systems where input saturation can destroy the stabilizing feedback effect of the control system and thus cause instability.

Notation

We base the analysis on sinusoidal input (and output) signals where $u(t)$ is a sinusoidal signal with frequency ω and frequency-dependent magnitude $|u_0(\omega)|$, $u(t) = |u_0(\omega)|sin\omega t$. The process gain $|G(j\omega)|$ gives the frequency-dependent amplification of a sinusoidal input signal $u(t)$ resulting in a output signal $y(t)$ with magnitude $|y_0(\omega)| = |G(j\omega)||u_0(\omega)|$.

4.2 Control limitations imposed by input magnitude constraints

The inputs are assumed to be limited by hard (magnitude) constraints of the kind $u_{min} \leq u \leq u_{max}$. Then, without considering input movement rate limitations, the process would normally be scaled with the maximum allowable input change, $G(s) = \hat{G}(s)D_u$, where $\hat{G}(s)$ is the unscaled process transfer function and $D_u = min(|u_{min} - u_{nom}|, |u_{max} - u_{nom}|)$ where u_{nom} is the nominal input magnitude. Taking the minimum allows for possible asymmetry in the input range. It is assumed in the remainder of this chapter that the models are scaled to

take into the account the magnitude constraint on the inputs. Thus, to avoid input magnitude saturation we will require

$$|u_0(\omega)| < 1 \tag{4.1}$$

4.3 Effect of input rate limitations on input magnitude

When the input movement rate is limited, it is not possible to implement sinusoids with unit amplitude at higher frequencies. This is illustrated in figure 4.1, where a sinusoidal signal $u(t)$ with unit amplitude is sent through a rate limiter which limits the slope of the signal ($|\frac{du}{dt}|$) to be less that a value $\dot{u}_{max}$, $|\frac{du}{dt}| \leq \dot{u}_{max}$. We see that input signals $u(t)$ with frequencies equal to or lower than $\omega = \dot{u}_{max}$ is unaffected by the rate limitations, whereas rate saturation of signals with higher frequencies lead to distorted output signals.

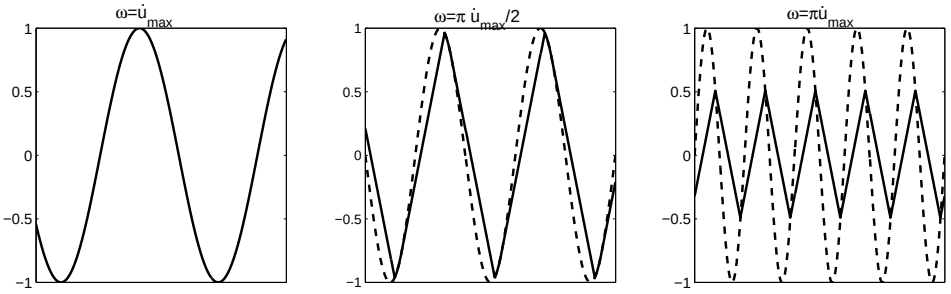

Figure 4.1: Illustration of rate limitation. Dashed line is sinusoidal input, solid is output

The effect of the rate limitation in figure 4.1 is easy to explain. The slope of a sinusoidal signal $u(t) = |u_0(\omega)|sin\omega t$ is $\frac{du}{dt} = |u_0(\omega)|\omega\cos\omega t$ and has $|u_0(\omega)|\omega$ as its maximal value. The rate limiter will not affect the sinusoidal signal $u(t)$ if $\left|\frac{du}{dt}\right| \leq \dot{u}_{max}$ or, equivalently, $|u_0(\omega)|\omega \leq \dot{u}_{max}$. This gives the input magnitude limitation due to the rate limitation:

$$|u_0(\omega)| \leq \frac{\dot{u}_{max}}{\omega} \tag{4.2}$$

Combining the limitations from input magnitude (4.1) and rate (4.2) yields

$$|u_0(\omega)| \leq min\left(\frac{\dot{u}_{max}}{\omega}, 1\right) \tag{4.3}$$

The maximum input magnitude in (4.3) is shown graphically in figure 4.2 as a function of frequency.

Instead of maximum rate $\dot{u}_{max}$ on the input movement, we may specify the opening time T_I. If the inputs has been scaled in the range [-1, 1] as just outlined, then the time to go from a closed ($u = -1$) to an open ($u = 1$) valve with an input rate $\dot{u}_{max}$ is

$$T_I = \frac{2}{\dot{u}_{max}} \tag{4.4}$$

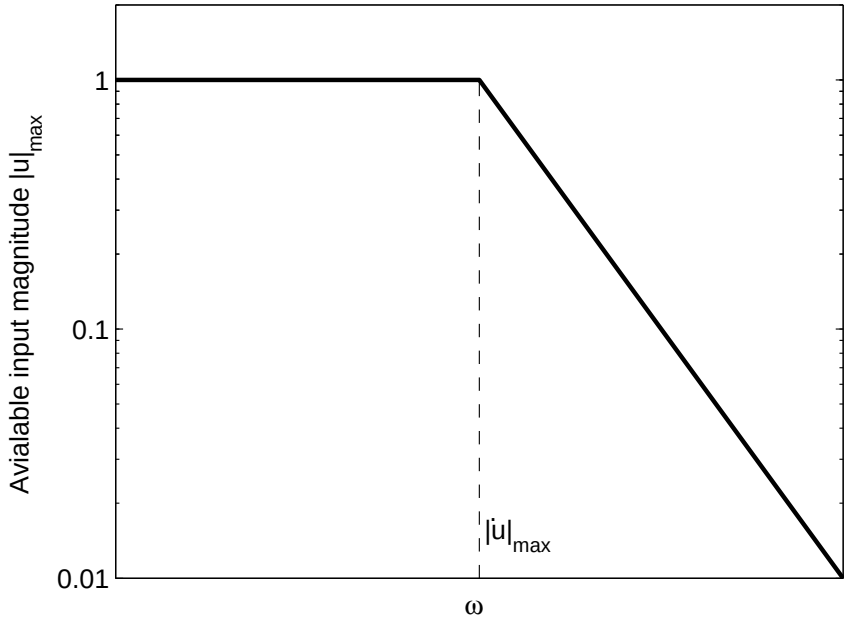

Figure 4.2: Graphical illustration of available input magnitude

4.4 Required input rates for stabilizing control

Saturation, whether it is caused by input magnitude or rate, is usually most critical for a control system designed to stabilize an unstable plant. Feedback is needed, and stabilizing control relies on constantly making small changes to the process inputs to keep the system stable. If the input saturates, then the process is effectively "open loop" and the stabilizing effect is lost (at least until the input comes out of saturation). Thus, for unstable plants, it is important to avoid that disturbances or noise drive the input into saturation. For an everyday example of this, imagine balancing a stick in the palm of your hand. This is normally quite easy to do (at least with a reasonably long stick), but imagine not being allowed to move your hand to the right? If the stick starts tilting to the right, you will clearly no longer be able to keep the stick upright.

For a process $G(s)$ and disturbance model $G_d(s)$ ($y = Gu + G_d d$), the closed loop transfer function from disturbance d to plant input u is KSG_d and we have in terms of the magnitude

$$|u_0(\omega)| = |KSG_d(j\omega)| \cdot |d_0(\omega)| \tag{4.5}$$

For an unstable plant we need feedback and there exists a lower bound on $\|KSG_d\|_\infty$ for any controller K. With a sinusoidal disturbance of magnitude $|d_0(\omega) = 1$ ($d(t) = \sin \omega t$), we have for any unstable pole p (Havre and Skogestad, 1997; Skogestad and Postlethwaite, 2005),

$$\max_\omega |u_0(\omega)| = \|KSG_d(s)\|_\infty \geq \left|G_s(p)^{-1} G_{d,ms}(p)\right| \tag{4.6}$$

Here, the subscript s denotes the "stable version" of the transfer function (the RHP-poles mirrored into the LHP) and the subscript ms denotes the "minimum-phase, stable version" (both RHP poles and zeros mirrored into the LHP).

In terms of Laplace transforms, $\mathcal{L}\left(\frac{du}{dt}\right) = su(s)$. Thus, the corresponding bound on the input rate $|du/dt|$ due to sinusoidal disturbances of magnitude 1 is

$$\max_{\omega} \left|\frac{du}{dt}\right| = \|sKSG_d(s)\|_\infty \geq \left|pG_s(p)^{-1}G_{d,ms}(p)\right| \tag{4.7}$$

Equation (4.6) combined with the the magnitude limitation $|u| \leq 1$ yields the criteria for stabilizing control without input magnitude saturation:

$$\left|G_s(p)^{-1}G_{d,ms}(p)\right| \leq 1 \tag{4.8}$$

Correspondingly, equation 4.7 combined with the rate saturation demand $|\frac{du}{dt}| \leq \dot{u}_{max}$ yields the criteria for stabilizing control with input rate limitations:

$$\left|pG_s(p)^{-1}G_{d,ms}(p)\right| \leq \dot{u}_{max} \tag{4.9}$$

The bounds in (4.6) and (4.7) are only tight for plants with a single unstable pole p. For the general case, with multiple unstable poles or MIMO, the following conditions are exact (Skogestad and Postlethwaite, 2005):

$$\underline{\sigma}_H^{-1}\left(\mathcal{U}\left(G_{d,ms}^{-1}G\right)\right) \leq 1 \tag{4.10}$$

$$\underline{\sigma}_H^{-1}\left(\mathcal{U}\left(s^{-1}G_{d,ms}^{-1}G\right)\right) \leq \dot{u}_{max} \tag{4.11}$$

where $\underline{\sigma}_H\left(\mathcal{U}\left(X\right)\right)$ is the smallest Hankel singular value of the antistable part of the argument X.

The same expressions can be used to describe the effect of noise by replacing G_d with N, where N is the noise model. For combined noise and disturbance rejection, we may replace G_d by $[G_d \quad N]^T$.

Example 4.1 *Consider the unstable process* $G(s) = \frac{20(s+1)}{(10s+1)(2s-1)}$ *with disturbance model* $G_d(s) = \frac{10}{(10s+1)(s+1)}$. *Since* $|G_s(p)^{-1}G_{d,ms}(p)| = \frac{(2\cdot 0.5+1)}{2(0.5+1)^2} = 0.44 \leq 1$, *it is possible to stabilize the process without saturating the input if the input rate satisfies* $\dot{u}_{max} \geq p|G_s(p)^{-1}G_{d,ms}(p)| = 0.22\ sec^{-1}$. *This corresponds to an opening time of less than* $T_I = 2/0.22 = 9\ sec$. *Since* $G(s)$ *contains only one unstable pole, (4.8) and (4.9) are equivalent to (4.10) and (4.11) for this example.*

4.5 Required input rate for performance

We do not only require stability, for control performance we want the control error e small. We will here consider the required input usage for perfect control ($e = 0$). Note that, for unstable systems, the performance requirements derived in this section come in addition to the requirements for stability derived in the previous section.

For perfect control ($e = y - Rr = 0$) of the plant $y = Gu + G_d d$, the plant input must be

$$u = G^{-1}Rr - G^{-1}G_d d \tag{4.12}$$

Thus, for perfect rejection of a sinusoidal disturbance with amplitude $|d_0(\omega)| = 1$, we need $|u_0(\omega)| = |G^{-1}G_d|$. Perfect disturbance rejection is a reasonable assumption at low frequencies if we require low-frequency performance. However, perfect disturbance rejection is unrealistic at high frequencies. If we assume that it is acceptable to have control error $|e| < 1$ at high frequencies, then we do not need control at frequencies above ω_d where $|G_d|$ drops below 1. To be able to achieve perfect control and satisfy the input limitations in (4.3) we must then require

$$\left|G\left(j\omega\right)^{-1} G_d\left(j\omega\right)\right| \leq \min\left(\frac{\dot{u}_{max}}{\omega}, 1\right) \quad \forall\, \omega \leq \omega_d \tag{4.13}$$

or equivalently, in terms of individual bounds,

$$\max_{\omega \leq \omega_d} \left|G\left(j\omega\right)^{-1} G_d\left(j\omega\right)\right| \leq 1 \tag{4.14}$$

$$\max_{\omega \leq \omega_d} \left|\omega G\left(j\omega\right)^{-1} G_d\left(j\omega\right)\right| \leq \dot{u}_{max} \tag{4.15}$$

The corresponding requirements for perfect reference tracking can be found by replacing G_d by R in (4.14) and (4.15).

Perfect control can never be realized in practice, but the input usage is usually close to what is needed in practice, as is also shown later in this chapter. More exact requirements can easily be derived for acceptable control ($|e| \leq 1$), but the resulting bounds were not found to be useful in our case. For an unstable system, the requirements for perfect control will be stricter than the requirements for stabilization for process where disturbance rejection is needed for frequencies around the instability ($G_{d,ms}(p) > 1$). For processes where the disturbance gain is low around the instability ($G_{d,ms}(p) < 1$), the requirements for stabilization (i.e. (4.9)) will usually be stricter.

Example 4.2 *The required input rate for performance for the process from example 4.1* $\left(G(s) = \frac{20(s+1)}{(10s+1)(2s-1)},\ G_d = \frac{10}{(10s+1)(s+1)},\ \omega_d = 0.78\right)$ *with the reference model* $R = \frac{2}{(10s+1)^2}$ *(*$\omega_r = 0.1$*) are*

- *for perfect disturbance rejection:* $\dot{u}_{max} = 0.45\ sec.^{-1}$*, corresponding to a opening time of* $T_I = 4.4\ sec.$
- *for perfect command tracking:* $\dot{u}_{max} = 0.0072\ sec.^{-1}$*, corresponding to a opening time of* $T_I = 278\ sec.$

Thus, in this case, the requirement for perfect disturbance rejection is stricter than the requirement for stabilization.

4.6 Controller design with input rate limitations

Designing controllers that satisfy the upper bounds on input rate derived above requires a systematic design procedure, especially if the available input rate is close to the theoretical minimum. To minimize the input magnitude for a process with disturbances, the transfer function KSG_d should be minimized. Frequency-varying bounds on the input, such as (4.3) can be included by introducing a weight $W_u(s)$, $|u| < |W_u^{-1}(s)|$. The transfer function to be minimized becomes $W_u KSG_d$.

4.6.1 Input weight for controller design

For controller design, the bound in (4.3) can not be used as a weight W_u since it has a infinite-dimensional realization due to the break point at $\omega = \dot{u}_{max}$. Thus, a lower-order approximation has to be used, and we use a first order lag-filter approximation

$$min\left(\left|\frac{\dot{u}_{max}}{\omega}\right|, 1\right) \approx \left|\frac{1}{\frac{j\omega}{\dot{u}_{max}} + 1}\right|$$

which gives

$$W_u(s) = \dot{u}_{max}^{-1} s + 1 \tag{4.16}$$

The difference between the exact bound in (4.3) and the weight W_u^{-1} is illustrated in figure 4.3. Note that the approximation is conservative, in that the bound implied by the weight W_u is tighter than the actual bound.

Requiring $|u| \leq W_u^{-1}$, with W_u described by (4.16), results in the following bounds on the input rate:
Stabilization:

$$\dot{u}_{max} \geq |p| \left(\left|G_s(p)\, G_{d,ms}(p)^{-1}\right| - 1\right)^{-1} \tag{4.17}$$

Perfect disturbance rejection:

$$\dot{u}_{max} \geq \max_{\omega \leq \omega_d} \left|\omega \left(G(j\omega) G_d(j\omega)^{-1} - 1\right)^{-1}\right| \tag{4.18}$$

Again, the required input rates for command tracking can be found for by substituting R for G_d.

Example 4.3 *For the unstable process in example 4.1 and 4.2, equation (4.17) gives the new bound* $\dot{u}_{max} \geq 0.4$ *for stabilization. For performance, (4.18) gives new bounds for perfect disturbance rejection,* $\dot{u}_{max} \geq 0.61$*, and for perfect command tracking,* $\dot{u}_{max} \geq 0.0069$*. The bounds using the exact input limitation in (4.3) are 0.22, 0.45 and 0.0072, respectively. The bound for stabilization is thus significantly increased when the approximate bound is introduced.*

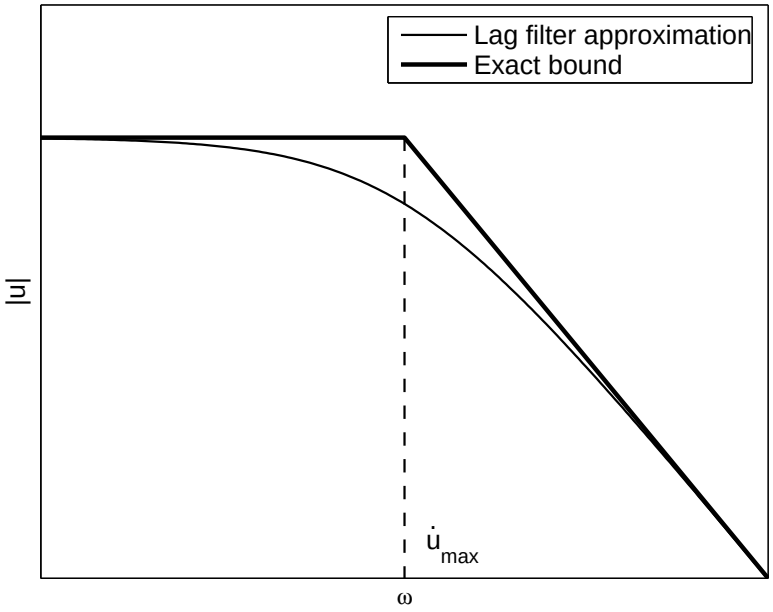

Figure 4.3: Exact bound and lag filter approximation

4.6.2 $\mathcal{H}_\infty$ controller design

To illustrate the controller design procedure, we design a $\mathcal{H}_\infty$ controller that minimizes $\|W_u KSG_d\|_\infty$ for the unstable process from example 4.1. The input rate limitation is set to the minimum value computed from (4.17) ($\dot{u}_{max} = 0.4$). The corresponding input weight is $W_u = 2.5s + 1$.

The $\mathcal{H}_\infty$ controller design was performed using the *hinfsyn* command in Matlab, yielding the controller:

$$K(s) = \frac{-0.01(10s+1)(s+1)(0.00025s+1)}{(1.5s+1)((0.003s)^2 + 0.0043s + 1)(0.0285s+1)} \tag{4.19}$$

Since the minimum input rate is used, the resulting frequency response for $|W_u KSG_d(j\omega)|$ is "flat" with $\|W_u KSG_d\|_\infty = 1$. This is not surprising since $\mathcal{H}_\infty$ controller design usually results in flat responses if possible and the peak value of one is given by (4.6) and (4.17) with equality. This implies that the controller in (4.19) just manages to keep the input away from saturation for sinusoidal disturbances of magnitude 1 if the input limitations are described by W_u^{-1}. However, there is some conservatism introduced for frequencies around $\dot{u}_{max}$ through the use of the lag filter W_u from (4.16) instead of the exact bound in (4.3). The transfer function KSG_d is plotted together with the input weight W_u^{-1} in figure 4.5.

Figure 4.6 shows a simulation where the process in figure 4.4 is stabilized by the controller in (4.19). A sinusoidal disturbance with magnitude 1 and frequency $p = 0.5$ is imposed on the process. The upper plot shows the process output (y), the middle one shows the

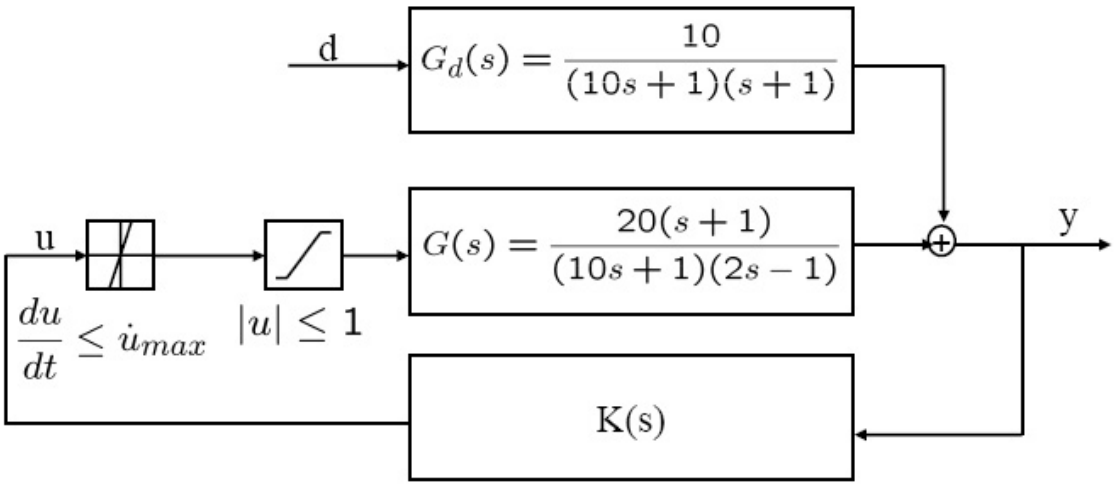

Figure 4.4: Unstable process from example 4.1

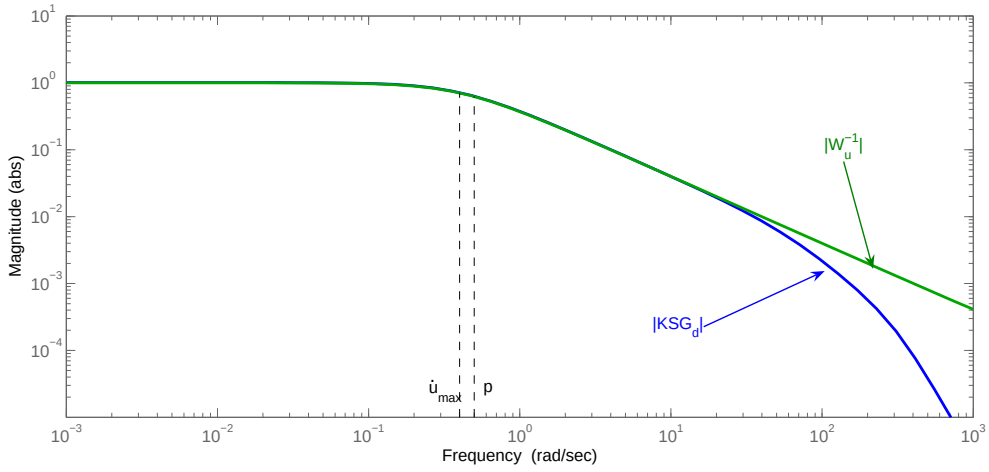

Figure 4.5: Transfer function KSG_d from disturbance d to plant input u together with input weight W_u^{-1}

controller output (u) and the lower plot shows the difference, due to the rate and magnitude limitations, between the output from the controller and the input to the plant. For the simulation on the left hand side, the input limitation is set to $du/dt \leq \dot{u}_{max} = 0.4$. The system is stable, and the rate and magnitude limitations do not affect the system at all. If the maximum input rate is reduced by 30% to 0.28, as in the simulations on the right hand side in figure 4.6, the rate limitations results in saturation, and the system goes unstable.

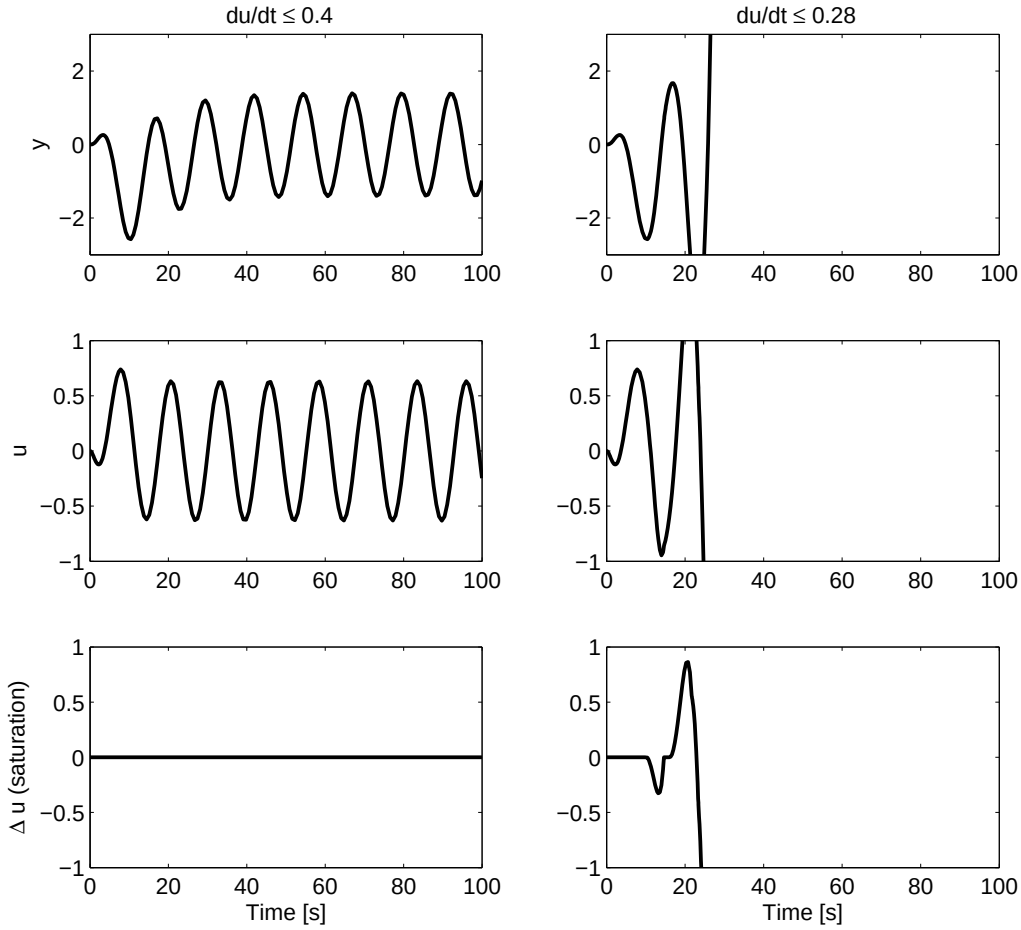

Figure 4.6: Effect of input limitation on $\mathcal{H}_\infty$ stabilizing controller for example 4.1

This design has stabilization as its sole target. There are no performance or robustness targets, and, as can be observed from the simulation in figure 4.6, the resulting controller can not keep the output y within its desired range of $|y| \leq 1$. Also, the design has other weaknesses. For instance, the weighted closed-loop transfer function from measurement noise n to plant input u, $W_u KSN$, where $N = 0.1$ is the noise model, has a peak value of $\|W_u KSN\|_\infty = 922$, indicating that the plant input would be very sensitive to measurement noise. If the controller design targets is extended to also minimize $\|W_u KSN\|_\infty$ by solving

the problem $\min_K \left\| \begin{array}{cc} W_u KSG_d & W_u KSN \end{array} \right\|_\infty$, then $\|W_u KSG_d\|_\infty$ and $\|W_u KSN\|_\infty$ both exceed unity ($\|W_u KSG_d\|_\infty = 1.2$ and $\|W_u KSN\|_\infty = 1.26$). To avoid input saturation due to both disturbances d and noise n, the allowed input rate has to be increased by about 60% to $du/dt \leq 1.6 \cdot \dot{u}_{max} = 0.64$ yielding $\|W_u KSG_d\|_\infty = 0.99$ and $\|W_u KSN\|_\infty = 0.99$.

If performance targets in terms of S are added to the design objective, the input rate has to be further increased. The input rate requirement for perfect disturbance rejection for this plant is $\dot{u}_{max} = 0.61$ (example 4.3), and the combined effect of stabilization and performance requirements in addition to the effect of measurement noise will, as we will see in the next section, require a input rate that is higher than the individual bounds.

4.7 Input rate limitations for stabilization of slug flow

Stabilizing control of multiphase flow in pipeline-riser systems at riser slugging conditions provides a good and relevant example for illustrating the importance of input rate limitations. The actuator in these systems is the valve opening of a large choke valve located on the top of the riser. For safety reasons, the choke valves should be slow-acting. The reason for the safety restriction on the valve rate is that if the valve were to open quickly at a time when the pressure drop over the valve is high, flow in to the inlet separator would increase dramatically. This could result in overfilling or over-pressurizing of the separator. Thus, we would like to design a choke valve that is just fast enough for achieving the control targets, and being able to quantify the required input rate may be a critical factor in the design of stabilizing controllers.

The pipeline-riser system studied in chapters 2 and 3 provides a simple, yet representative example of a case where riser slugging can be removed using stabilizing feedback control. We will use the model derived in chapter 3 to calculate the required input rate for stabilizing control of the pipeline-riser system.

The process is linearized around the operating point corresponding to a choke valve opening of 30%, giving the (unscaled) process model from the valve opening $u = Z$ to the inlet pressure measurement $y = P_I$

$$\hat{G}(s) = \frac{-4.87(260.8s + 1)}{(0.218s + 1)(6808s^2 - 51.75s + 1)} e^{-10s} \tag{4.20}$$

The hat (ˆ) is used to indicate that the model has not been scaled. Note that a 10 second delay is included the model. This is done based on the analysis in chapter 3, were it was concluded that, because of the neglected pipeline dynamics, a delay of about 10 seconds was missing in the simplified model.

The disturbance models from gas feed flow W_G, liquid feed flow W_L and downstream (separator) pressure P_O are

$$\hat{G}_d(s) = \begin{bmatrix} \frac{31.56(20.3s-1)(0.23s+1)}{(0.218s+1)(6808s^2-51.75s+1)} \\ \\ \frac{0.82(30s+1)}{(0.218s+1)(6808s^2-51.75s+1)} \\ \\ \frac{1.07(260.8s+1)}{(0.218s+1)(6808s^2-51.75s+1)} \end{bmatrix} \tag{4.21}$$

Table 4.1: Minimum input rate for stabilization of the pipeline-riser system. The disturbance model augmented to include measurement noise ($G_{d,aug} = [G_d\ N]$)

Bound	Eq. #	$\dot{u}_{max}$	Opening Time [min]
$\|pG_s(p)^{-1}G_{d,aug,ms}(p)\|_2$	(4.9)	0.0074	4.5
$1/\underline{\sigma}_H\left(\mathcal{U}\left(G_{d,aug,ms}^{-1}Gs^{-1}\right)\right)$	(4.11)	0.0052	6.6

The plant input is scaled with the maximum positive input deviation ($70\% \Rightarrow D_u = 0.7$), the output is scaled with the maximum allowed deviation ($\Delta P_I = 1\ bar\ \Rightarrow D_y = 1$) and the disturbances are scaled by the following scaling matrix

$$D_d = \begin{bmatrix} \frac{0.072\left(\frac{2\pi}{180}s+1\right)\left(\frac{2\pi}{160}s+1\right)}{\left(\frac{2\pi}{90}s+1\right)\left(\frac{2\pi}{30}s+1\right)^2} & 0 & 0 \\ 0 & \frac{1.728\left(\frac{2\pi}{180}s+1\right)\left(\frac{2\pi}{160}s+1\right)}{\left(\frac{2\pi}{90}s+1\right)\left(\frac{2\pi}{30}s+1\right)^2} & 0 \\ 0 & 0 & \frac{1}{(10s+1)} \end{bmatrix}$$

The basis for the disturbance scaling is given in section 2.6.3. The resulting scaled models are found as $G = D_y^{-1}\hat{G}D_u,\ G_d = D_y^{-1}\hat{G}_d D_d$.

The plant has a complex pair of unstable poles, $p_i = 0.0038 \pm 0.0115i$ and three disturbances. To include the effect of measurement noise, the disturbance model is augmented with the disturbance model $N = 0.1$. Table 4.1 shows the minimum input rates for stabilization using the bounds in (4.11) and (4.9). The bound in (4.11), which applies for plants with multiple unstable poles, is difficult to evaluate for non-square disturbance models and is thus evaluated one disturbance at a time. The value 0.0052 for the worst disturbance is shown. On the other hand, the bound 0.0074 in (4.9) applies to multiple disturbances ($\|d\|_2 \leq 1$), but is not tight for multiple unstable poles. The actual value for $\dot{u}_{max}$ will therefore exceed 0.0074.

4.7.1 Design 1 - Stabilization with input limitation

For controller design, we use the approximate input limitation description W_u in (4.16) and the rate limitation $\dot{u}_{max} = 0.0103$, which is obtained from (4.17). This resulting input weight is $W_u = 97s + 1$. The stabilizing controller is then found by solving the control problem

$$\min_K \left\| \begin{array}{cc} W_u KSG_d & W_u KSN \end{array} \right\|_\infty \tag{4.22}$$

The frequency response for the resulting controller is shown in the top plot in figure 4.7. The input usage for the different disturbances are shown in the middle plot together with the input weight W_u^{-1}. The middle plot shows that neither the disturbances d nor the measurement noise n can individually drive the input into saturation. This is confirmed by the closed-loop norms $\|W_u KSG_d\| = 0.96$ and $\|W_u KSN\| = 0.96$. The lower plot in figure 4.7 shows the sensitivity function S and the complementary sensitivity function T. The sensitivity function S is high at all frequencies, which implies that there is no reference

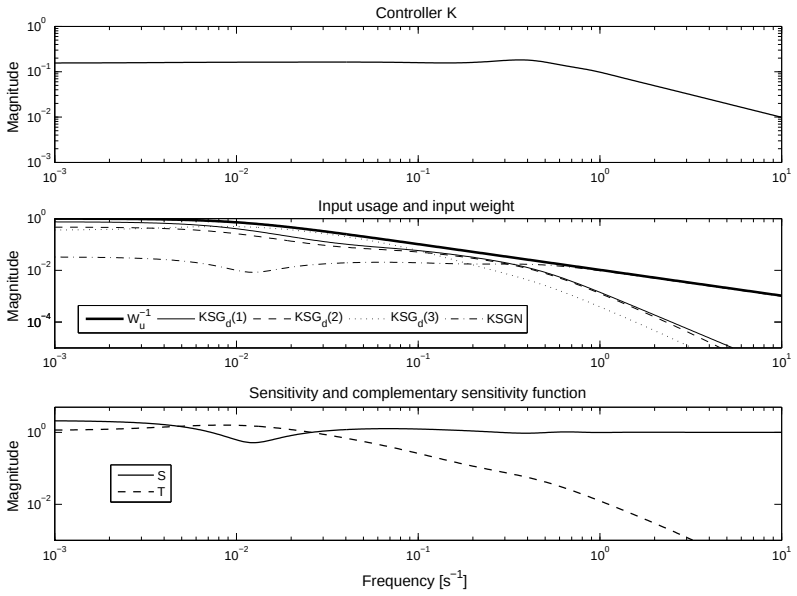

Figure 4.7: Controller, input usage and performance for riser slugging case, design 1.

tracking properties in the design. This is not surprising, since there are no low-frequency performance requirements in the design.

Low-frequency performance is not strictly needed for stabilizing control, but without it, the process might drift away from its operating point even for small disturbances. This is indeed what happens with design 1, as shown in figure 4.8, where, as a result of a 5 % reduction in the feed at t=1 h, the process drifts off and the input saturates. Thus, to stabilize the pipeline-riser system in practice, a low-frequency performance condition has to be added to the design.

4.7.2 Design 2 - Stabilization with input limitation and low-frequency performance

To avoid the process drifting off from its operating point, a performance weight is added to design problem. The weight

$$W_p = \frac{s/M + \omega_B^*}{s + \omega_B^* A} \tag{4.23}$$

on the control error $e = r - y$ will demand the sensitivity function S to be less than A at low frequencies. At high frequencies, S is required to be less than M. ω_B^* constitutes the approximate bandwidth requirement for the closed loop process. The control problem with input and performance requirements is

$$\min_K \left\| \begin{array}{ccc} W_u K S G_d & W_u K S N & W_u K S R \\ W_p S G_d & W_p S N & W_p S R \end{array} \right\|_\infty \tag{4.24}$$

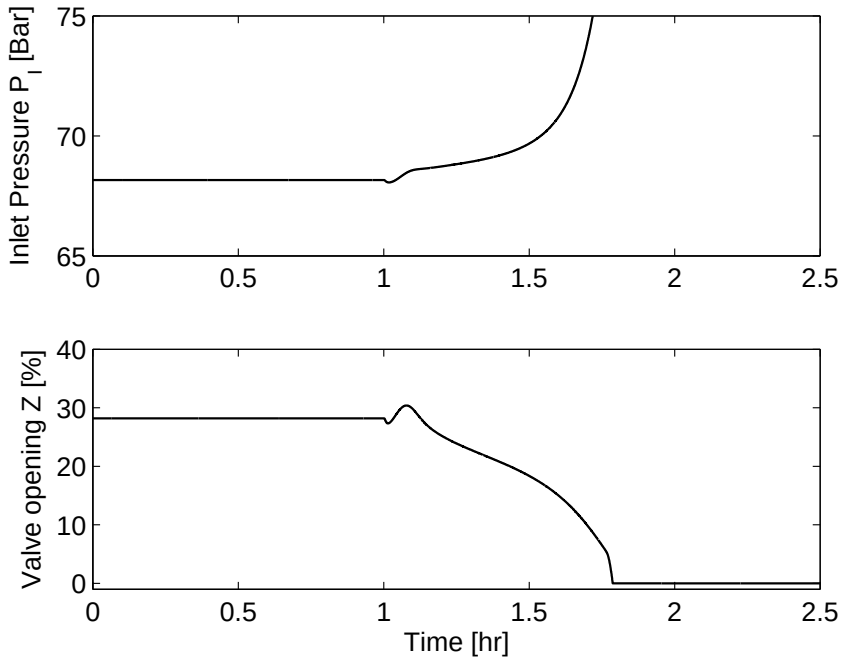

Figure 4.8: Simulation of riser slugging case with controller design 1 showing that the operating point drifts off and the input saturates when the feed flow is slightly reduced.

where R is the weight for setpoint tracking.

With the extended control problem defined by (4.24), a higher input rate is required to fulfill the design objectives. With $M = 5$, $\omega_B^* = 0.01$, $A = 0.1$ and $R = 1/(100s + 1)^2$, the obtained peak values for the weighted closed loop transfer functions for setpoint tracking (W_pSR), disturbance suppression (W_pSG_d), input usage due to noise (W_uKSN) and input usage due to disturbances (W_uKSG_d) for different input rates are given in table 4.2. Table 4.2 shows that the required valve rate for achieving the performance target whilst avoiding input saturation is $\dot{u}_{max} = 0.021$, a value 2 times higher than the one computed from (4.6.1).

From (4.15), the required input rate for perfect control of the pipeline-riser system, is $\dot{u}_{max} = 0.014$. Thus, as expected, the combined effect of stabilization and disturbance rejection requires a higher input rate than the individual requirements for stabilization and

Table 4.2: Input usage and performance for increasing valve rates

$\dot{u}_{max}$	$\|W_pSR\|_\infty$	$\|W_pSG_d\|_\infty$	$\|W_uKSG_d\|_\infty$	$\|W_uKSN\|_\infty$
0.012	0.34	1.29	1.40	1.38
0.015	0.27	1.11	1.22	1.19
0.018	0.22	0.99	1.09	1.06
0.021	0.19	0.89	1.00	0.97

disturbance rejection.

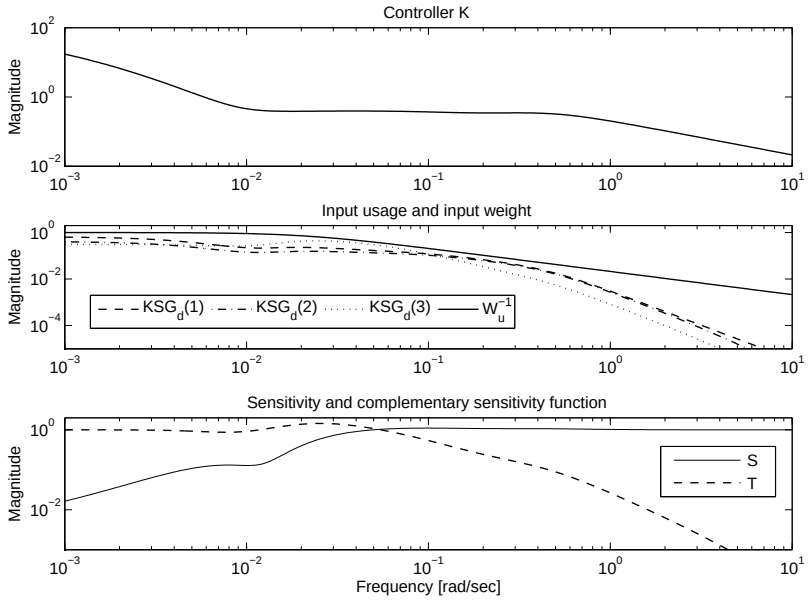

Figure 4.9: Controller, input usage and performance for riser slugging case, 2nd design

Figure 4.9 shows the controller, the input usage and the sensitivity functions for the controller designed based on the input rate $\dot{u}_{max} = 0.021$. This control system should be able to stabilize the system under the influence of all the disturbances considered in the design. An interesting observation is that the structure of the resulting $\mathcal{H}_\infty$ optimal controller is very similar to a PI controller with gain around 0.3 bar^{-1}, integral time of about 200 seconds and a lag filter on the measurement with a filter constant of about 1.5 seconds.

This example has shown that a theoretical lower bound on the required input movement rate can be computed for a "real" system. It has also shown that, as more design objectives are added, a faster and faster input is needed. We will not pursue the controller design for the riser slugging case further in this chapter, as this is left for a more thorough treatment in the next two chapters.

4.8 Conclusion

Simple equations for computing the minimum input rate required for control of both stable and unstable systems have been derived. For stabilizing control of an unstable plant, the minimum input rate $\dot{u}_{max}$ is bounded by

$$\left| pG_s(p)^{-1} G_{d,ms}(p) \right| \leq \dot{u}_{max}$$

Correspondingly, the minimum input rate for perfect disturbance rejection is bounded by

$$\max_{\omega \leq \omega_d} \left| \omega G\left(j\omega\right)^{-1} G_d\left(j\omega\right) \right| \leq \dot{u}_{max}$$

For an unstable plant, the requirements for perfect control will be stricter than the requirements for stabilization for process where disturbance rejection is needed at frequencies around the instability, that is, when $|G_{d,ms}(p)| > 1$, approximately. For processes where the disturbance gain is low at frequencies around the instability (i.e. $|G_{d,ms}(p)| < 1$), the requirements for stabilization will usually be stricter.

The input rates can be included in a frequency-dependent weight $W_u(s)$, which can be used in controllability analysis and controller design.

Two examples have been provided that illustrate the importance of the input rate. The examples have also shown that if both input limitations and performance requirements are included in the controller design objective for an unstable plant, the input rate must be higher than the theoretical minimum for both stabilization and performance.

For the simulated OLGA cases with riser slugging, which is used as the main case study in this thesis, a minimum input rate is $\dot{u}_{max} = 0.0074s^{-1}$ for stabilization and $\dot{u}_{max} = 0.014s^{-1}$ for perfect disturbance rejection. The $\mathcal{H}_\infty$ controller designed in this chapter, with both input limitations and performance requirements, required a valve rate of $\dot{u}_{max} = 0.021s^{-1}$.

Chapter 5

Stabilization of multiphase flow in pipelines with single-loop and cascade controllers

Espen Storkaas and Sigurd Skogestad

Manuscript in preparation

Abstract

Stabilizing PID anti-slug controllers are designed for the OLGA pipeline-riser system case studied in chapters 2 and 3. The controller parameters are optimized based on the simplified, three-state model developed in chapter 3, and the choice of measurements are based on the controllability findings from chapters 2 and 3. The controllers are tested with simulations on both the simplified three-state model, the two-fluid model from chapter 2 and the OLGA model.

Control is based on manipulating the valve position ($u = Z$). Single-loop (SISO) PID controllers based on an upstream pressure measurement ($y =$ inlet pressure P_I or $y =$ riser base pressure P_{Rb}) perform well if tuned to minimize $\|S\|_\infty$ (the peak of the sensitivity function S). Minimizing $\|T\|_\infty$ results in too aggressive controllers. A flow controller (with $y = Q$) can also stabilize the process, but the low-frequency performance is, as expected, poor.

The stabilizing flow controller is, however, well suited as an inner loop in a cascade controller ($y_2 = Q$). If the inlet pressure ($y_1 = P_I$) is used as the primary measurement in the cascade controller, the performance is slightly improved over the SISO pressure controller. A cascade controller can also stabilize the process with only topside (downstream) measurement by using the pressure drop over the choke valve DP or the valve position Z as a primary control variable (y_1). These controllers are, however, slower due to the inherent controllability limitations in the process.

5.1 Introduction

Chapters 2 and 3 dealt with modeling of and controllability analysis for multiphase flow in pipeline-riser systems at riser slugging conditions. Two different models were described, a conventional two-fluid model and novel simplified dynamic model with only 3 dynamic states. For both these models, controllability analysis show that it should be possible to avoid riser slugging in the system by stabilizing an unstable operating point that exists at the same boundary conditions that uncontrolled would yield riser slugging. It has also been shown that the choice of control variable is crucial. We now consider the design of controllers based on the controllability findings from these two chapters.

The focus of this chapter will be on PID controllers, either as single-loop or cascade controllers. These controllers are by far the most common in practice, and can be easily implemented in most control systems. The controller parameters are optimized based on the simplified model introduced in chapter 3, but the resulting controllers are tested on both the simplified model, the two-fluid model used in chapter 2 as well as on the OLGA model that provides the reference data for the model tuning. The use of three different models to test the controllers provides some insight into the robustness properties of the controllers. Testing the controllers designed based on the simplified model on other models also gives further information regarding the quality of the simplified model.

We will first, in section 5.2, discuss the requirements for a stabilizing control of a pipeline-riser system. These requirements are based the set of properties that the resulting closed-loop system should have in order to guarantee stable operation. Section 5.3 deals with single-loop (SISO) stabilizing PID controllers for three different measurements alternatives, namely inlet pressure (P_I), riser base pressure (P_{Rb}) and volumetric flow out of the riser (Q). We will design PID controller with these measurements that meet the control requirements and evaluate their performance. Section 5.4 deals with cascade controllers where the volumetric flow Q is used as a secondary measurement in an inner loop. The main goal of this section is to design controllers based on only topside measurements, and evaluate the performance of these controllers compared to the controllers based on upstream measurements. This chapter will thus give good insight into the achievable performance with PID anti-slug controllers for a wide range of control structures.

5.2 Control objectives

The main control objective for any stabilizing controller is obviously to keep the process stable. This implies that the (nominal) closed loop system needs to have all its poles in the left half plane (nominal stability, NS). Keeping the process stable will also impose requirements on the input usage, on low-frequency performance (at least for nonlinear systems) and on the robustness of the system. These requirements will in this section be formalized to form a set of control objectives for the controller design process.

5.2.1 Input usage

All real processes have hard constraints on the inputs determined by the equipment used to manipulate the process. A valve, which is the most common manipulated input in the process industry, cannot be more than fully open or fully closed and there is a limit to how fast it can be opened. When the process input is at one of its constraints (that is, it is saturated) it is impossible to implement the action demanded by the control system.

To ensure that the process input u stays away from saturation, we will require that neither the disturbances d nor the measurement noise n bring the input into saturation. The closed-loop transfers functions from disturbances and measurement noise to process input are KSG_d and KSN, respectively. Assuming that the inputs are bounded by an input weight $W_u(s)$ such that $|u(j\omega)| \leq |W_u(j\omega)^{-1}|$, and the models G_d and N contain scaling such that the disturbance and noise signals are less than one in magnitude ($|d|, |n| \leq 1$), input saturation will be avoided if

$$|W_u KSG_d| \leq 1 \, \forall \, \omega \quad \Leftrightarrow \quad \|W_u KSG_d\|_\infty \leq 1 \tag{5.1}$$

$$|W_u KSN| \leq 1 \, \forall \, \omega \quad \Leftrightarrow \quad \|W_u KSN\|_\infty \leq 1 \tag{5.2}$$

These two requirements will hence form a part of the design objective for the controller design.

5.2.2 Low-frequency performance

Low-frequency performance is not really a requirement for stabilizing control, at least not for linear systems. However, real systems are nonlinear and the lack of low-frequency performance might cause the process to drift into an operating region where the linear model is not valid and the controller no longer manages to keep the process stable. Thus, in practice we need low-frequency performance to ensure stability.

A low value for the closed-loop transfer function S at low frequencies will ensure that disturbances have little steady-state effect on the process. We will require

$$|S(0)| \leq 0.1 \tag{5.3}$$

corresponding to less than 10% offset for a reference change. This is consistent with the performance bounds that will be used in the next chapter. Note, however, that we for most of the PID-controllers used in this chapter include integral action, which yields $S(0) = 0$.

5.2.3 Robust stability

Robust stability implies that the control system is able to maintain closed-loop stability even though the plant on which it is implemented differs from the one its design was based on. Differences between the mathematical model of the plant and the actual plant are always present, and it is important for the control system to be insensitive to these differences. For the riser slugging case, one indication of robust stability would be that a controller that

stabilizes the simplified 3-state model would also stabilize the two-fluid model from chapter 2 and the more detailed OLGA model that provided the reference data.

In chapter 3, we compared the properties of the simplified 3-state and the two-fluid model. The comparison showed that there were some differences in the pole and zero locations. There were also some differences in the process gain, particularly at frequencies around the instability. This indicates that there are some errors in the model which we may represent as uncertainty.

Uncertainty can be represented in different ways (Skogestad and Postlethwaite, 1996), depending on the source of the uncertainty. Once the uncertainty is described, the block diagram with uncertainty Δ may be rearranged into the $M\Delta$-structure depicted in figure 5.1 to test for robust stability. Minimizing $\|M\|_\infty$ will maximize the robust stability, or more precisely, maximize the allowed magnitude of the uncertainty such that the system remains stable.

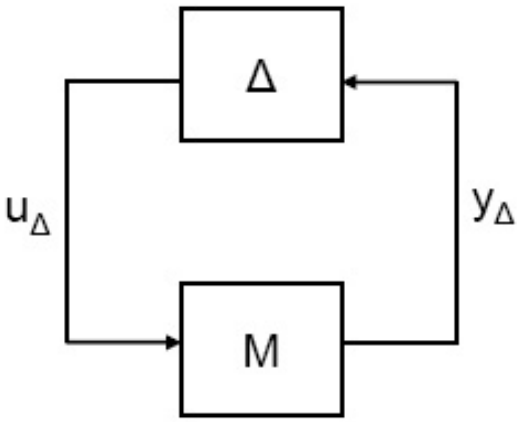

Figure 5.1: M Δ structure for robust stability analysis

Table 5.1: Uncertainty sources, mathematical description, and transfer function to be minimized.

Source	Type	Set of plants	M
Relative gain and zeros	Multiplicative input	$G_p = G(I + \omega_I \Delta_I)$	T
Relative pole location	Inverse multiplicative input	$G_p = G(I + \omega_{iI} \Delta_{iI})^{-1}$	S
Absolute gain and zeros	Additive	$G_p = G + \omega_A \Delta_A$	KS

Table 5.1 shows some sources of (assumed) model uncertainty, the corresponding uncertainty type, mathematical representation of the set of possible plants, and the expression for M. The resulting M for the three uncertainty sources are $S,\ T$ and KS, respectively. It is, however, difficult to determine *a priori* which of the uncertainties that are most limiting

in practice. One simple approach is to design controllers for all three (S, T and KS) and evaluate the result by simulating on the three nonlinear process models (3-state, two-fluid, OLGA).

5.2.4 Startup of anti-slug controllers

In most cases, the anti-slug controller can be started up by first bringing the process into the stable region by manually reducing the choke valve (see for example figure 2.5 on page 15) and then turning on the controller to move the process to the desired operating point inside the unstable region. However, this will result in an increased pipeline pressure, which in some cases may be a problem, and the controller may have to be able to bring the system directly from riser slugging to the desired operating point. To deal with this problem, Havre and Dalsmo (2002) introduced a startup condition in the presented control system to ensure that the controller was turned at a suitable place in the slug cycle. In this work we test the controllers ability to bring the process from riser slugging to the desired operating point, but we will not include any start-up design criteria in the control objectives.

5.3 Single-loop stabilizing control of pipeline-riser systems

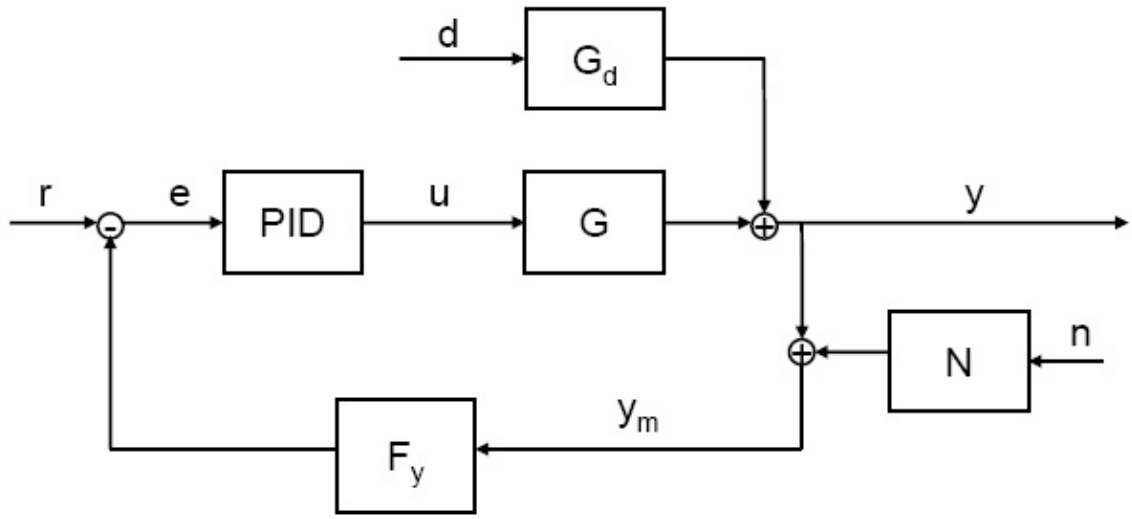

Figure 5.2: Block diagram for feedback control using a PID controller and a measurement filter F_y

In this section we design stabilizing PID controllers using the setup in figure 5.2. The transfer functions G and G_d for the inputs u and the disturbances d are obtained from lineariz-

ing the simplified 3-state model described is chapter 3. A measurement filter F_y is included in the feedback loop to filter out some of the measurement noise. The PID controller and the measurement filter are

$$PID = K_c \left(\frac{\tau_I s + 1}{\tau_I s} \right) \left(\frac{\tau_D s + 1}{\alpha \tau_D + 1} \right), \quad F_y = \frac{1}{\tau_F s + 1} \tag{5.4}$$

where $\alpha = 0.1$ is used to limit the derivative action to one decade.

The controllability analysis performed in chapter 2 and confirmed in chapter 3 concluded that an upstream pressure measurement, either located at the pipeline inlet ($y = P_I$) or at the riser base ($y = P_{Rb}$), would be a good control variable for stabilizing control. The analysis also showed that it should be possible to stabilize the process using a flow measurement located at the pipeline outlet (either volumetric flow $y = Q$ or mass flow $y = W$), but that there might be problems with low-frequency performance and disturbance rejection. The analysis showed that a pressure measurement at the top of the riser (e.g. pressure drop over the valve DP) could *not* be used for stabilizing control because of RHP-zeros located close to the RHP -poles. In this section we design SISO (single-input single-output) PID controllers and check the results from the controllability analysis.

5.3.1 Control of inlet pressure P_I

Linear model and process scaling

We use the simple three-state model developed in chapter 3. The unscaled process model from valve opening $u = Z$ to inlet pressure measurement $y = P_I$, linearized around the operating point corresponding to a choke valve opening of 30%, is

$$\hat{G}(s) = \frac{-4.87(260.8s + 1)}{(0.218s + 1)(6808s^2 - 51.75s + 1)} e^{-10s} \tag{5.5}$$

The hat (ˆ) is used to indicate that the model has not been scaled.

Note that a 10 second delay is included in the model. This is done based on the analysis in chapter 3, were it was concluded that, because of the neglected pipeline dynamics, a delay of about 10 seconds was missing in the simplified three-state model.

The disturbance models from gas feed flow W_G, liquid feed flow W_L and downstream (separator) pressure P_O are

$$\hat{G}_d(s) = \begin{bmatrix} \frac{31.56(20.3s-1)(0.23s+1)}{(0.218s+1)(6808s^2-51.75s+1)} \\ \\ \frac{0.82(30s+1)}{(0.218s+1)(6808s^2-51.75s+1)} \\ \\ \frac{1.07(260.8s+1)}{(0.218s+1)(6808s^2-51.75s+1)} \end{bmatrix} \tag{5.6}$$

The plant input is scaled with the maximum positive input deviation ($70\% \Rightarrow D_u = 0.7$), the output is scaled with the maximum allowed deviation ($\Delta P_I = 1\ bar \ \Rightarrow D_y = 1$) and

the disturbances are scaled by the following scaling matrix

$$D_d = \begin{bmatrix} \frac{0.072\left(\frac{2\pi}{180}s+1\right)\left(\frac{2\pi}{160}s+1\right)}{\left(\frac{2\pi}{90}s+1\right)\left(\frac{2\pi}{30}s+1\right)^2} & 0 & 0 \\ 0 & \frac{1.728\left(\frac{2\pi}{180}s+1\right)\left(\frac{2\pi}{160}s+1\right)}{\left(\frac{2\pi}{90}s+1\right)\left(\frac{2\pi}{30}s+1\right)^2} & 0 \\ 0 & 0 & \frac{1}{(10s+1)} \end{bmatrix} \tag{5.7}$$

This scaling, which was introduced in chapter 2.6.3, allows for feed variations and variations in the separator pressure. The resulting scaled models are $G = D_y^{-1}\hat{G}D_u$ and $G_d = D_y^{-1}\hat{G}_d D_d$.

Input weight

In section 4.7, the minimum required valve rate for this control problem was found to be $\dot{u}_{max} \geq 0.0074s^{-1}$, corresponding to an opening time for the valve of 4.5 minutes. This bound is based only on stabilization and does not include performance requirements. Avoiding saturation with this valve rate would also require an optimal controller with respect to input usage. Thus, when using a simple PID controller and imposing low-frequency performance demands, the input needs to be faster than the minimum value computed in section 4.7. Therefore, in the simulations and in designing the controllers, a opening time for the valve of 1 min is used, corresponding to a valve rate of $\dot{u}_{max} = 1/(D_u \cdot 60s) = 0.024s^{-1}$. The corresponding input weight is then:

$$W_u(s) = \dot{u}_{max}^{-1}s + 1 = 40s + 1 \tag{5.8}$$

PID controller design

To achieve the design objectives described in section 5.2, the controller parameters K_c, τ_I, τ_D and τ_F must be found. To both simplify the design and assure reasonable setpoint tracking properties, the integral time is fixed at $\tau_I = 600s$. This is slower than the bandwidth of the system, and should therefore not interfere with the stabilization. The remaining controller parameters are found by solving the following optimization problem:

$$\min_{K_c,\tau_D,\tau_F} \left(\|M\|_\infty\right) \tag{5.9}$$

$$s.t. \quad \begin{matrix} \|W_u KSG_d\|_\infty \leq 1 \\ \|W_u KSN\|_\infty \leq 1 \end{matrix} \tag{5.10}$$

where M is the closed-loop transfer function to be minimized ($M = S, T$ or KS).

Table 5.2 shows the results from the optimization problem defined by (5.9) and (5.10). In the last row, we give the lowest achievable norms with PID control, obtained by minimizing $\|S\|_\infty$, $\|T\|_\infty$ and $\|KS\|_\infty$, respectively, without the constraints in (5.10). Table 5.2 reveals that the cost of the input limitations (5.10) in terms of robustness is not very high, as the differences between the achieved norms and lowest achievable are fairly small.

Table 5.2: Controller tunings for PID control with $y = P_I$

Minimized (M)	$K_c[bar^{-1}]$	$\tau_I[s]$	$\tau_D[s]$	$\tau_F[s]$	$\|S\|_\infty$	$\|T\|_\infty$	$\|KS\|_\infty$
$\|S\|_\infty$, $\|KS\|_\infty$[a]	-0.098	600	14.2	6.9	**1.26**	1.91	**0.29**
$\|T\|_\infty$	-0.20	600	14.3	12.3	1.60	**1.44**	0.50
Lowest achievable with PID controller					1.18	1.18	0.29

[a]The controller that minimizes $\|KS\|_\infty$ is not unique; these parameters minimize $\|S\|_\infty$ and achieves $\min_K(\|KS\|_\infty)$

Integral action in the controller ensures $T(0) = 1$. This imposes a lower bound on KS, $\|KS\|_\infty = \|G^{-1}T\|_\infty \geq |G^{-1}(0)| = 0.29$, and since in our case the required input usage is highest at low frequencies, it implies that the controller that minimizes $\|KS\|_\infty$ is not unique. The controller that minimizes $\|S\|_\infty$ in table 5.2 achieves the lower bound on $\|KS\|_\infty$ and should be robust toward uncertainty in relative pole location as well as absolute gain and zero location. Note that the same controller parameters are found by minimizing $[S \quad KS]^T_\infty$. The controller that minimizes T is more aggressive with higher controller gain.

Simulation results

To test the controllers, the following scenario is simulated: The process is started up in open-loop with a valve opening of $Z = 30\%$. This valve opening brings the process well within the riser slugging region, and riser slugging develops for all three models. The controller is turned on after 30 minutes with a setpoint for P_I corresponding to a valve opening of $Z = 17.5\%$. After 90 minutes, the setpoint is reset to the lower pressure corresponding to a valve opening of $Z = 30\%$. The gradual lowering of the setpoint is done both to test the working range of the controller and to make the transition from riser slugging to stabilized flow easier. White measurement noise $|n|$ of magnitude about 0.1 is added to the measurement.

In figure 5.3, the controller that minimizes S and KS ($K_c = -0.1bar^{-1}$, $\tau_I = 600s$, $\tau_D = 14.2s$, $\tau_F = 6.9s$) is tested on the simplified model, the two-fluid model, and the OLGA model. The controller stabilizes the process with all three models, and the responses are in fact remarkably similar. The only slight difference is in the transition from riser slugging to the first operating point, where the input usage is different. This is because the controller is turned on at different phases of the slug cycle for the different models. Noise suppression, input usage and setpoint tracking is very good for all three models. Based on the simulations in figure 5.2 and the data in table 5.2, we conclude that the controller that minimizes $\|S\|_\infty$ (and also $(\|KS\|_\infty)$) achieves robust stability.

The controller that minimizes $\|T\|_\infty$ ($K_c = -0.2bar^{-1}$, $\tau_I = 600s$, $\tau_D = 14.3s$, $\tau_F = 12.3s$) produces similar responses as those in figures 5.3(a) and 5.3(b) with the simplified and the two-fluid model. However, the controller is more aggressive ($\|KSG_d\|_\infty = 0.50$) with higher loop gain, and thus closer to instability. The problems are even more profound with the OLGA model, as shown in figure 5.4, where the controller barely manages to stabilize the process. Thus, we conclude that with inlet pressure measurement, minimizing $\|S\|_\infty$ results in more robust controllers than minimizing $\|T\|_\infty$.

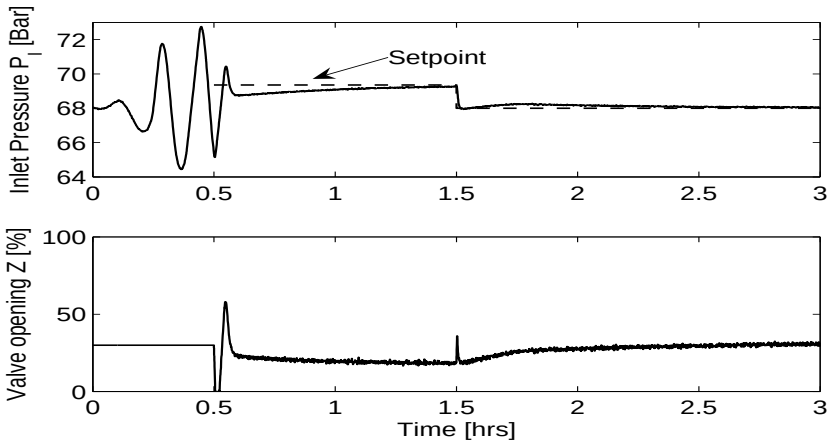

(a) Simplified 3-state model

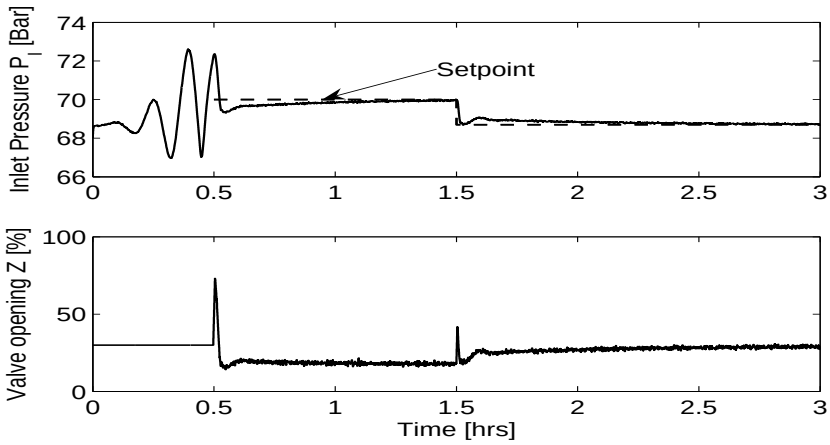

(b) Two-fluid model

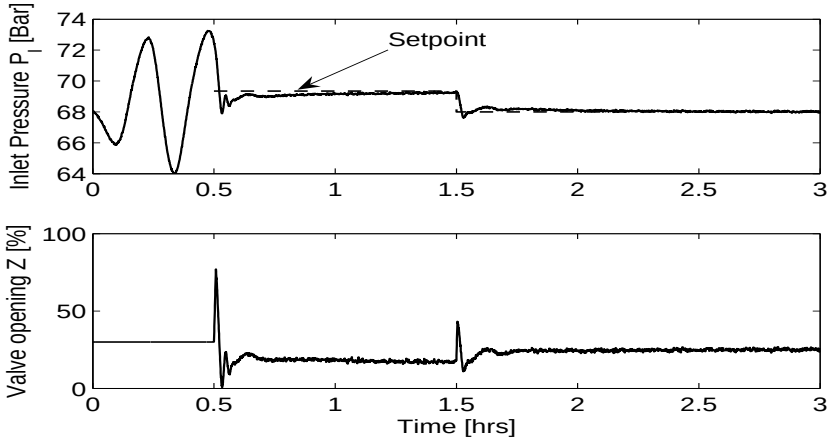

(c) OLGA model

Figure 5.3: Anti-slug control ($y = P_I$) with three different nonlinear process models. PID tuning: $\|S\|_\infty$ minimized.

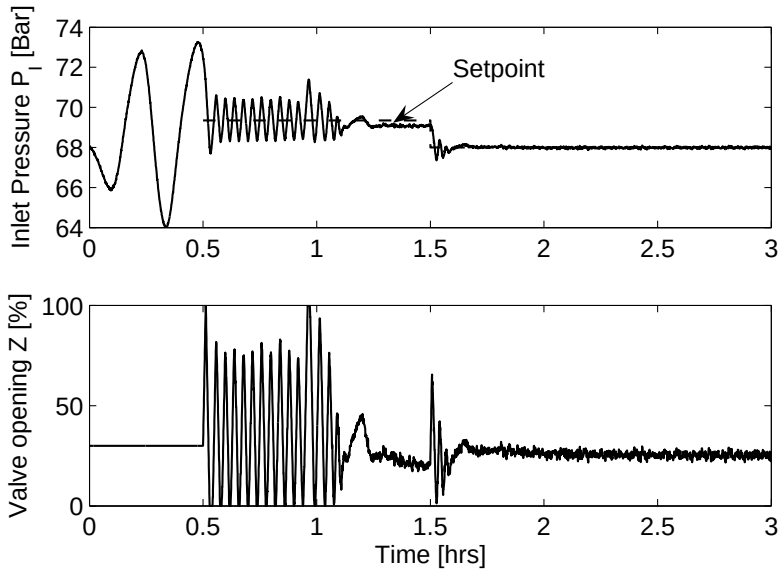

Figure 5.4: Anti-slug control ($y = P_I$) with OLGA model. PID tuning: $\|T\|_\infty$ minimized

In the following we will only show simulations with the OLGA model which generally is the most difficult to control. Simulations with all three models are found in appendix C.

5.3.2 Control of riser base pressure P_{Rb}

Linear model and process scaling

The unscaled process model from valve opening $u = Z$ to riser base pressure measurement $y = P_{Rb}$, linearized around the operating point corresponding to a choke valve opening of 30%, is

$$\hat{G}(s) = \frac{-4.73(242.6s + 1)}{(0.437s + 1)(6431s^2 - 53.34s + 1)} \tag{5.11}$$

The disturbance models from gas feed flow W_G, liquid feed flow W_L and downstream (separator) pressure P_0 are

$$\hat{G}_d(s) = \begin{bmatrix} \frac{27.8(20.58s-1)(0.46s+1)}{(0.437s+1)(6431s^2-53.34s+1)} \\ \\ \frac{0.75(30.8s+1)}{(0.437s+1)(6431s^2-53.34s+1)} \\ \\ \frac{1.07(242.6s+1)}{(0.437s+1)(6431s^2-53.34s+1)} \end{bmatrix} \tag{5.12}$$

Note that the model parameters in the simple 3-state model have been slightly changed to represent the riser base pressure instead of the inlet pressure. This is the reason for the slightly different pole locations. However, the process and disturbance model are almost identical to the models with $y = P_I$, except for the lacking time delay. The process is scaled

in the same manner as with $y = P_I$; that is, with the tuning matrices described in the first section of chapter 5.3.1. The missing time delay does not significantly affect the required input rate, so we use the same input weight (5.8) as before.

PID controller design

Table 5.3: Controller tuning for PID control with $y = P_{Rb}$

Minimized (M)	$K_c[bar^{-1}]$	$\tau_I[s]$	$\tau_D[s]$	$\tau_F[s]$	$\|S\|_\infty$	$\|T\|_\infty$	$\|KS\|_\infty$
$\|S\|_\infty$, $\|KS\|_\infty$[a]	-0.16	600	0	0.9	**1.03**	1.52	**0.30**
$\|T\|_\infty$	-0.30	600	0	2.0	1.11	**1.25**	0.45
Lowest achievable with PID controller					1.00	1.00	0.30

[a]The controller that minimizes $\|KS\|_\infty$ is not unique; these parameters minimize $\|S\|_\infty$ and achieves $\min_K(\|KS\|_\infty)$

Table 5.3 shows the optimized controller parameters for the design problem defined by (5.9) and (5.10). Compared to the controller design in section 5.3.1, the $\mathcal{H}_\infty$ norms for the closed-loop transfer functions S and T are lower, whereas the norm for KS is almost the same. This is expected, since there is no time delay in this case.

Simulation results

The controllers that minimizes $\|S\|_\infty$ and $\|T\|_\infty$ perform well for all three models, and the responses are very similar to the those in the previous section. Figure 5.5 shows the OLGA simulation with $\|S\|_\infty$ minimized ($K_c = -0.16bar^{-1},\ \tau_I = 600s,\ \tau_D = 0s,\ \tau_F = 0.9s$). The remaining simulations are given in appendix C.

5.3.3 Control of volumetric flow Q

We have already stated, based on the controllability analysis, that the volumetric flow Q should not be used alone in a single-loop control scheme. This conclusion was further strengthened by the simulations example in chapter 2.7.2, where a step in the liquid feed flow resulted in instability for a pipeline-riser system stabilized by a $\mathcal{H}_\infty$ flow controller. To confirm this conclusion, we now design PID controllers using (5.9) and (5.10).

Linear model and process scaling

The unscaled process model from valve opening $u = Z$ to topside volumetric flow rate $y = Q$, linearized around the operating point corresponding to a choke valve opening of 30%, is

$$\hat{G}(s) = \frac{8.1 \cdot 10^{-4}(1301s+1)(292.7s+1)(0.3184s+1)}{(0.218s+1)(6808s^2 - 51.75s + 1)} \tag{5.13}$$

We note the very low steady-state gain of 0.0008.

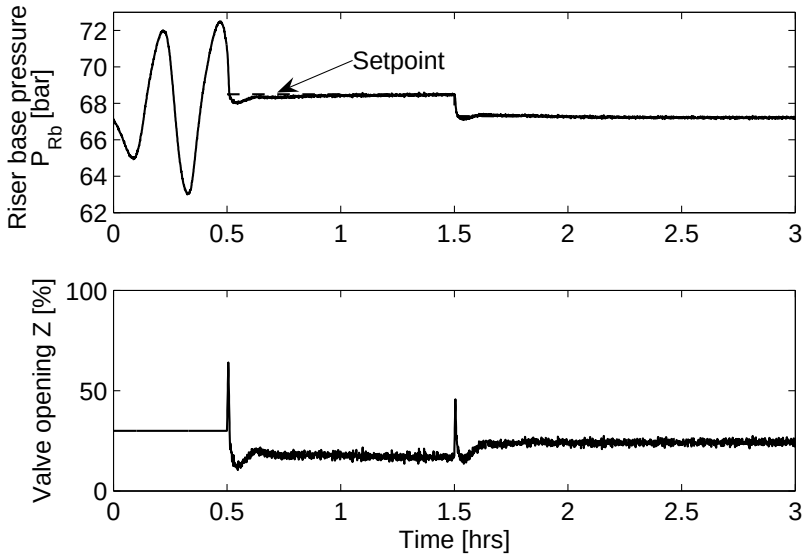

Figure 5.5: Anti-slug control ($y = P_{Rb}$) with OLGA model. PID tuning: $\|S\|_\infty$ minimized

The disturbance models from gas feed flow W_G, liquid feed flow W_L and receiving (separator) pressure P_O are

$$\hat{G}_d(s) = \begin{bmatrix} \frac{-0.025(259s+1)(0.56s-1)}{(0.22s+1)(6808s^2-51.75s+1)} \\ \frac{0.0012(212.7s-1)(10.57s-1)}{(0.22s+1)(6808s^2-51.75s+1)} \\ \frac{-1.8\cdot 10^{-4}(1301s+1)(292.7s+1)(0.32s+1)}{(0.22s+1)(6808s^2-51.75s+1)} \end{bmatrix} \tag{5.14}$$

The process is scaled as described in the first section of chapter 5.3.1. The same scaling matrices is also used, except for the process output y, where $D_y = 0.002$ is used. We use the same input weight (5.8) as before.

PID controller design

To achieve the low-frequency performance criteria $S(0) \leq 0.1$, the stationary gain in the controller must satisfy $|1 + G(0)K(0)| \geq 0.1^{-1}$ which gives $|K(0)| \geq 9/|G(0)| = 11100\ s/m^3$. For the scaled model this gives $\|W_u KSG_d\|_\infty \geq \|W_u KSG_d(0)\|_2 = 4.36$. This is larger than 1 and means that low-frequency performance cannot be achieved because of input saturation. This is consistent with the controllability findings in chapters 2 and 3. Avoiding input saturation is more important than low-frequency performance, so the low-frequency performance requirement will be dropped as a control objective. This implies that integral action is removed from the controller, resulting in a PD-controller plus a measurement filter.

Table 5.4 shows the resulting controller tunings. We note that derivative action is not used such that we in effect have proportional control. None of this controllers will be effective

Table 5.4: Controller tuning for PD control with $y = Q$

Minimized (M)	$K_c[s/m^3]$	$\tau_D[s]$	$\tau_F[s]$	$\|S\|_\infty$	$\|T\|_\infty$	$\|KS\|_\infty$
$\|S\|_\infty$[a]	120	0	145	**1.00**	1.34	0.31
$\|T\|_\infty$	270	0	135	1.00	**1.16**	0.63
$\|KS\|_\infty$	55	0	135	1.35	2.02	**0.15**

[a]Design not unique, these parameters achieves $\|S\|_\infty = 1$ with minimal input usage

for setpoint tracking, and should not be considered for stabilizing control without an outer loop (cascade) that keep the process at its desires operating point. Again, the controller that minimizes $\|T\|_\infty$ is the most aggressive with $\|KS\|_\infty = 0.63$ for the nominal model, and since the process gain with this measurement increases strongly as the valve opening is reduced (based on the data for the stationary gain data in tables 3.4 and 3.5 on page 54), this controller will not robustly stabilize the process due to saturation.

Simulation results

The responses with the controller that minimizes $\|S\|_\infty$ ($K_c = 120s/m^3$, $\tau_F = 145s$) is shown in figure 5.6. We observe that the controller stabilizes the process quite effectively, but, as expected, the setpoint tracking is poor. The controller that minimizes $\|KS\|_\infty$ gives similar responses whereas designs based on minimizing $\|T\|_\infty$ performs poorly. Simulations where $\|KS\|_\infty$ and $\|T\|_\infty$ are minimized are given in appendix C.

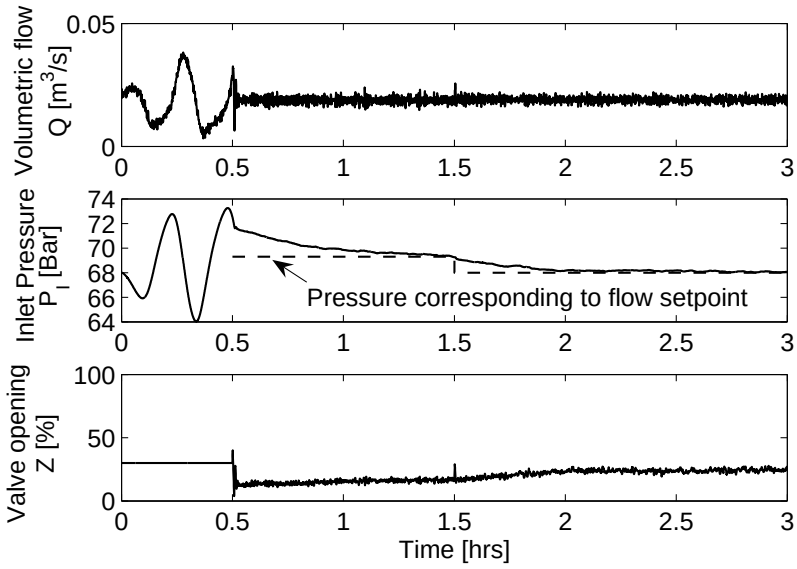

Figure 5.6: Anti-slug flow control ($y = Q$) with OLGA model. PID tuning: $\|S\|_\infty$ minimized

5.3.4 Summary of SISO anti-slug PID control

The design of single-loop PID controllers has shown that minimizing either $\|S\|_\infty$ or $\|KS\|_\infty$ results in robustly stable controllers. This is consistent with the normal practice for tuning stabilizing controllers, where one usually seeks to minimize input usage. Minimizing $\|T\|_\infty$ results in controllers that are too aggressive to robustly stabilize the pipeline-riser system.

5.4 Cascade control of pipeline riser systems

Section 5.3 showed that a flow measurement should not be used in a single-loop stabilizing control scheme for the pipeline-riser system. The flowrate can, however, be used as a secondary measurement in a cascade controller ($y_2 = Q$), since the primary (outer) loop in a cascade would take care of the low-frequency performance in the system, and the flow measurement could be used only for stabilization.

An additional argument for cascade control of the pipeline-riser system, see chapter 2, is that an upstream pressure measurement is not well suited for suppressing mid-to-high frequency disturbances ($\omega > 0.1$). Finally, there are cases with no upstream pressure measurement available. In this section we therefore investigate cascade controllers with the secondary measurement $y_2 = Q$.

5.4.1 Cascade control: Theory

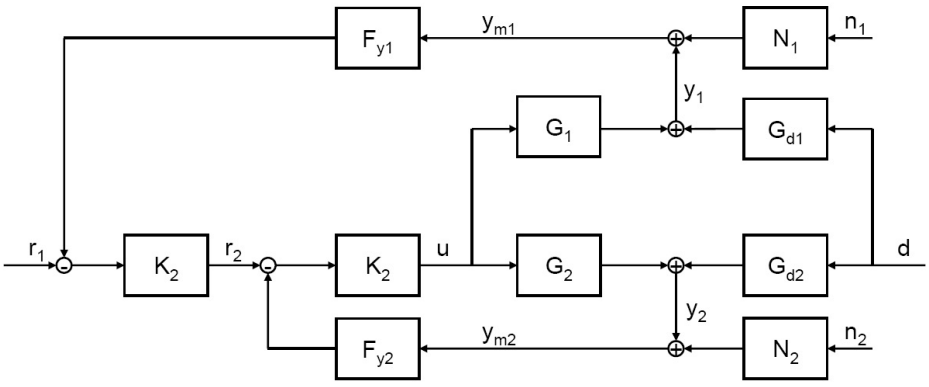

Figure 5.7: Block diagram for cascade control system, 1 - primary (outer) loop, 2 - secondary (inner) loop

We first derive some transfer functions in order to better understand the stability and performance properties of the cascaded system in figure 5.7. The secondary controller K_2 controls the process G_2 from the input u to the secondary measurement y_2. The setpoint r_2 to the inner loop is the output from the primary controller K_1, which is controlling the primary

measurement y_1. The disturbances d affects the outputs y_1 and y_2 through the disturbances models G_{d1} and G_{d1}, respectively. The measurement filters F_{y1} and F_{y2} are included to reduce the sensitivity to measurement noise.

Transfer functions

To find controller parameters for the outer loop based on the same approach as we have used earlier in this chapter, we need the transfer functions for the closed-loop system. With both loops closed the response is

$$\begin{bmatrix} y_1 \\ y_2 \end{bmatrix} = \begin{bmatrix} G_1 \\ G_2 \end{bmatrix} \cdot K_1 K_2 S \cdot r_1 + \begin{bmatrix} (1 + G_2 K_2 F_{y2}) G_{d1} - G_1 K_2 F_{y2} G_{d2} \\ -K_1 F_{y1} K_2 G_2 G_{d1} + (1 + K_1 F_{y1} K_2 G_1) G_{d2} \end{bmatrix} \cdot S \cdot d - \begin{bmatrix} G_1 K_1 F_{y1} & G_1 F_{y2} \\ G_2 K_1 F_{y1} & G_2 F_{y2} \end{bmatrix} K_2 S \begin{bmatrix} N_1 n_1 \\ N_2 n_2 \end{bmatrix} \quad (5.15)$$

The corresponding plant input signal is

$$u = K_2 K_1 S \cdot r_1 - (K_1 F_{y1} G_{d1} + F_{y2} G_{d2}) K_2 S \cdot d - K_2 \begin{bmatrix} K_1 F_{y1} & F_{y2} \end{bmatrix} S \begin{bmatrix} N_1 n_1 \\ N_2 n_2 \end{bmatrix} \quad (5.16)$$

and the control error is

$$\begin{aligned} e_1 = y_1 - r_1 &= (G_1(1 - F_{y1}) K_1 K_2 - G_2 K_2 F_{y2} - 1) S \cdot r_1 + \\ &((1 + G_2 K_2 F_{y2}) G_{d1} - G_1 K_2 F_{y2} G_{d2}) S \cdot d - \begin{bmatrix} G_1 K_1 F_{y1} & G_1 F_{y2} \end{bmatrix} K_2 S \begin{bmatrix} N_1 n_1 \\ N_2 n_2 \end{bmatrix} \end{aligned} \quad (5.17)$$

with the sensitivity function S for the system given by:

$$S = (1 + G_2 K_2 F_{y2} + K_2 K_1 G_1 F_{y1})^{-1} = (1 + \tilde{G}_1 K_1 F_{y1})^{-1} \quad (5.18)$$

$$\tilde{G}_1 = G_1 S_2 K_2 = G_1 (1 + G_2 K_2 F_{y2})^{-1} K_2 \quad (5.19)$$

These closed-loop responses for cascade control yields the following equivalents for the usual SISO closed-loop transfer functions:

$$T = 1 - S \quad (5.20)$$

$$KS = K_2 \cdot \begin{bmatrix} K_1 F_1 & F_2 \end{bmatrix} S \quad (5.21)$$

$$KSG_d = KS \cdot \begin{bmatrix} G_{d1} \\ G_{d2} \end{bmatrix} \quad (5.22)$$

$$KSN = KS \cdot \begin{bmatrix} N_1 & 0 \\ 0 & N_2 \end{bmatrix} \quad (5.23)$$

where the sensitivity function S is given by (5.18).

Effect of stabilized RHP-poles on outer loop

In this work, the task for the inner loop is to stabilize the process and the task for the outer loop is to provide low-frequency performance. Thus, the process as seen from the outer loop ($\tilde{G}$) is stable, but the original instability will in some cases still affect this outer control loop.

With the inner loop closed, the transfer function $\tilde{G}$ for the remaining control problem is given by (5.19), and includes the sensitivity function for the inner loop, $S_2 = (1 + G_2K_2F_{y2})^{-1}$. Since the requirement for internal stability prohibits the unstable poles in G_2 from being canceled by K_2, S_2 must have RHP-zeros in the same location as the RHP-poles of G_2. Depending on the primary process G_1, the stabilized RHP-poles will have one of the following effects on the primary loop:

- If the unstable modes in G_2 are observable in y_1 (G_1 contains the same unstable poles as G_2), the RHP-zeros in S_2 will be canceled out by the RHP-poles in G_1 and the stabilized modes will not affect the primary loop. Thus, any bandwidth limitation due to RHP-zeros in the primary loop must come from G_1 itself.

- If the unstable modes in G_2 are not present in G_1, the RHP-zeros in S_2 will not be canceled. Thus, $\tilde{G}$ will have RHP-zeros at the same location as the RHP-poles in G_2, and these RHP-zeros will limit the bandwidth in the primary loop. For example, this will be the case if we choose the input as primary output ($y_1 = u,\ G_1 = 1$)

The latter of these two cases has an interesting implication; The slower the instabilities in G_2 (easy stabilization), the slower the inverse response through $\tilde{G}$ and the lower the allowed bandwidth in the primary loop (slower control). In other words, the harder job the secondary controller has, the better control can be achieved in the primary loop.

5.4.2 Cascade control with P_I in outer loop

It is not necessary to use a cascade controller if an upstream pressure measurement is available, but, as discussed in chapter 2, an inner flow control loop might help with disturbance rejection. Furthermore, the cascade controller with inlet pressure as a primary control variable ($y_1 = P_I$) and volumetric flow through the choke valve as a secondary variable ($y_2 = Q$) will serve as performance reference for the other cascade systems that will be developed in this section. Because the system can be stabilized using the primary control variable alone, the inner loop does not necessarily have to stabilize the process. An alternative to use a stabilizing inner loop could be to use an inner loop that provides local disturbance rejection and "linearizes" the actuator. However, to unify the treatment of the cascade controllers, we will in this work use a stabilizing inner loop.

Secondary (inner) loop

When tuning a cascade controller, the inner loop is usually tuned first, with little regard for the outer loop. This implies that we should be able to use the flow control parameters derived in section 5.3.3 for the inner loop, and should thus be able to rely on a robustly stable inner

loop. Note that the $\mathcal{H}_\infty$ sensitivity norms in table 5.4 are the norms for the stabilizing loop, so for the purposes of cascade control, we should replace S, T and KS in section 5.3.3 by S_2, T_2 and K_2S_2, respectively.

In section 5.3.3 we found that minimizing $\|S_2\|_\infty$ or $\|K_2S_2\|_\infty$ yield flow controllers suitable for stabilizing the process. This implies that the gain in the inner loop should be in the range $55s/m^3 \leq K_{c2} \leq 120s/m^3$. It turns out, from simulations, that when combining the inner flow loop with $y_1 = P_I$ in the outer loop, minimizing input usage ($\|K_2S_2\|_\infty$) in the inner loop results in the best controller. Thus, we use $K_{c2} = 55s/m^3$ and $\tau_{F2} = 135s$ in the inner flow control loop.

Primary (outer) loop

Integral action in the primary loop provides the desired low-frequency performance. Minimizing the peak value for the overall sensitivity function S with the inner loop parameters constant gives the controller parameters $K_{c1} = -0.001m^3/(bar \cdot s)$, $\tau_{I1} = 600s$ and $\tau_{F1} = 135s$. These controller parameters achieves for the total control system $\|S\|_\infty = 1$, $\|T\|_\infty = 1.9$, $\|KS\|_\infty = 0.29$, $\|W_uKSG_d\|_\infty = 0.93$ and $\|W_uKSN\|_\infty = 0.17$ based on the expressions for the closed-loop transfer functions on page 87. Compared with the SISO PID controller from section 5.3.1, $\|S\|_\infty$ is reduced from 1.25 to 1 and the noise sensitivity $\|W_uKSN\|_\infty$ is reduced from about 0.8 to 0.17. The other transfer function peaks are unchanged by the inner flow loop. The bandwidth for the system (the frequency where S first crosses $1/\sqrt{2}$ from below) is $\omega_B \approx 0.001s^{-1}$.

Simulation results

The simulation with the OLGA model is shown in figure 5.8. The performance is similar to the single-loop PID controller in section 5.3.1, but with slightly less input usage (Z) due to better noise suppression. Simulations with the 3-state model and the two-fluid model are shown in appendix C.

5.4.3 Cascade control with DP in outer loop

Without upstream pressure measurements such as P_I or P_{Rb} available, a topside measurement has to be used in the outer loop. In real systems, the topside density ρ_T is usually too noisy to be used directly for control, so we will only consider the pressure drop over the valve DP. The controller parameters for the inner loop ($y_2 = Q$) are, as in the previous section, $K_{c2} = 55s/m^3$ and $\tau_{F2} = 135s$.

With the inner loop closed, the scaled model for the process as seen from the outer loop is

$$\tilde{G}_1 = G_1S_2K_2 = \frac{-0.95(135s+1)(63s-1)(0.7s-1)}{(82s+1)(0.22s+1)(10692s^2+64s+1)}$$

Thus, the process is stabilized, but there are two unstable (RHP) zeros in the model $\tilde{G}_1$, stemming from the original unstable zeros in the response from z to DP (G_1). These unstable zeros are also the reason for not using DP for stabilizing control. When using DP in the

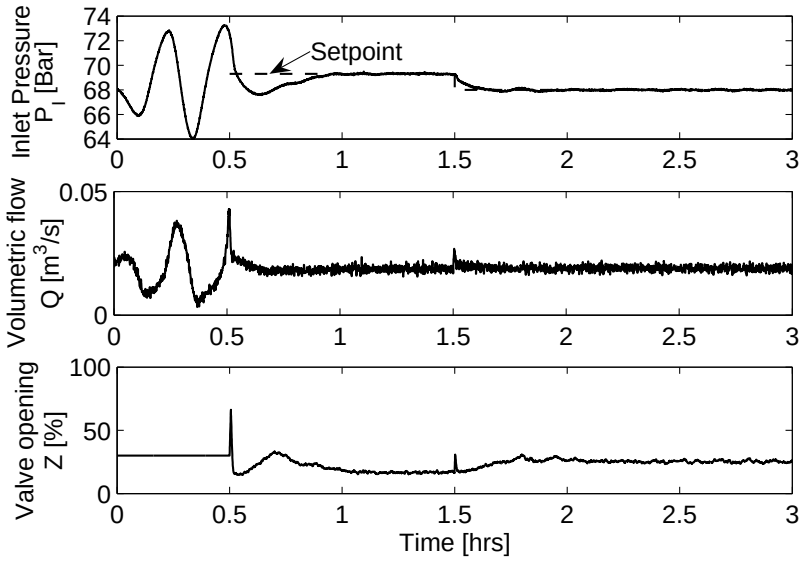

Figure 5.8: Cascade control ($y_1 = P_I$, $y_2 = Q$) with OLGA model.

outer loop, these unstable zeros will limit the bandwidth of the system, and the controller based on only topside measurements are therefore slower than control systems based on upstream pressure measurements.

The controller parameters $K_{c1} = -0.00015m^3/(bar \cdot s)$, $\tau_{I1} = 600s$, $\tau_{F1} = 135$ for the outer loop constitutes a compromise between lowering the peaks for the closed-loop transfer functions and achieving a reasonable bandwidth for the system. With these tuning parameters, $\|S\|_\infty = 1.42$, $\|T\|_\infty = 2.1$, $\|KS\|_\infty = 0.16$, $\|W_u KSG_d\|_\infty = 0.98$, $\|W_u KSN\|_\infty = 0.16$. The closed-loop bandwidth is $\omega_B \approx 0.0001$, which is ten times slower than with the controller with inlet pressure as a primary measurement.

The OLGA simulation is shown in figure 5.9. Note that since the setpoint response is considerably slower with this controller, the simulation time is extended compared to the previous simulations in this chapter. Apart from the slower response, the controller performs very well.

5.4.4 Cascade control with valve position Z in outer loop

An alternative is to use the valve opening Z in the outer loop ($y_1 = Z$). This may seem a bit strange since Z is also the input ($u = Z$), but note that the objective of the outer loop is to avoid steady-state drift and this may be achieved by slowly "resetting" Z to its desired value.

Secondary (inner) loop

With $y_1 = Z$, the disturbances does not affect the primary measurement directly ($G_{d1} = 0$). The primary measurement is however affected by disturbances through the inner loop, as can be seen from (5.15). Because of this interaction, we need tighter control in the inner loop to

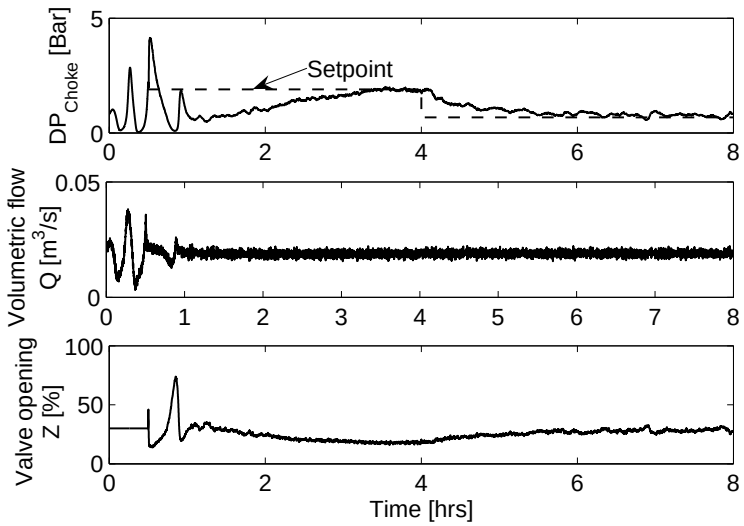

Figure 5.9: Cascade control ($y_1 = DP$, $y_2 = Q$) with OLGA model. Note the extended simulation time.

reject disturbances, and the controller gain K_{c2} in the inner loop is increased compared to the previous cascade controllers. The controller parameters $K_{c2} = 90s/m^3$, $\tau_{D2} = 0$ and $\tau_{F2} = 135$ for the inner loop will stabilize the process and at the same time enables us to design an outer loop that can provide low-frequency performance.

Primary (outer) loop

With $y_1 = Z$, the process model for the outer loop is $G_1 = 1$ (figure 5.7). With the inner loop closed, the transfer function as seen from the outer loop is

$$\tilde{G}_1 = G_1 S_2 K_2 = \frac{0.17(135s+1)(6808s^2 - 52s + 1)}{(44s+1)(19457s^2 + 142s + 1)}$$

Again, we note that the transfer function $\tilde{G}_1$, with the inner loop closed, contains unstable (RHP) zeros that will limit performance. The RHP-zeros are located at the same location as the original unstable (RHP) poles. As noted earlier, this is a fundamental limitation when we select $y_1 = u$. Thus, whereas with $y_1 = DP$, the RHP-zeros originate from the RHP-zeros of the measurement, with $y_1 = Z$ they originate from the RHP-poles of the process.

With the controller parameters $K_{c1} = 0.002$, $\tau_{I1} = 600$, $\tau_{F1} = 135$ for the primary controller, the process is stabilized with a reasonable bandwidth of $\omega_B = 0.0004$. With this controller, the peak values for the closed-loop transfer functions are $\|S\|_\infty = 1.14$, $\|T\|_\infty = 1.54$, $\|KS\|_\infty = 1.42$, $\|W_u KSG_d\|_\infty = 0.88$ and $\|W_u KSN\|_\infty = 0.1$.

Simulation results

The OLGA simulation is shown in figure 5.10. The setpoint tracking is slow but otherwise, the controller performs well.

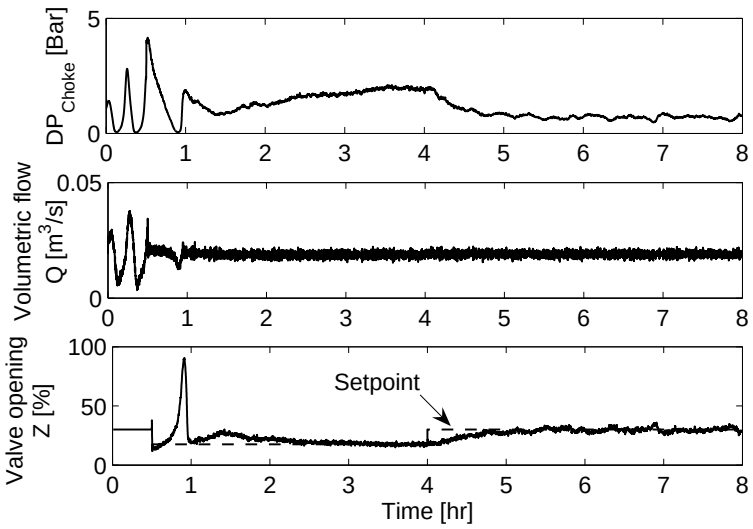

Figure 5.10: Cascade control ($y_1 = Z$, $y_2 = Q$) with OLGA model. Note the extended simulation time.

5.5 Conclusions

This chapter has confirmed, mainly through simulations, the conclusions from the controllability analysis performed in chapters 2 and 3. When the valve position is used as a manipulated input ($u = Z$):

- Upstream pressure measurements (inlet pressure P_I or riser base pressure P_{Rb}) are well suited for stabilizing control of pipeline-riser systems
- Volumetric flow through the choke valve (Q) can be used to stabilize the process, but the low-frequency performance is poor
- The flow measurement is well suited for an inner loop in a cascade controller, $y_2 = Q$.
- With $y_2 = Q$, the valve position may be used in the outer loop, but performance is limited by unstable zeros caused by the original unstable poles.
- Alternatively, the pressure drop over the valve $y_1 = DP$ may be used in the outer loop, but in this case performance is limited by unstable zeros in the measurement.

The controller design has shown that minimizing the input usage (that is, minimizing $\|KS\|_\infty$) or the sensitivity peak $\|S\|_\infty$ (alternatively $[S \quad KS]^T_\infty$) results in robust stability. This has been proved by testing the controllers on the simplified model developed in chapter 3, the two-fluid model used in chapter 2 and the OLGA model that provided the reference data.

Chapter 6

Model-based anti-slug controllers

Espen Storkaas and Sigurd Skogestad

Manuscript in preparation

Abstract

A SISO $\mathcal{H}_\infty$ controller based on the inlet pressure P_I is found to be almost identical to the PID controller designed earlier in this thesis. This indicates that, as long as an upstream pressure measurement (e.g. inlet pressure P_I or riser base pressure P_{Rb}) is available, a PID controller is well suited for stabilizing control of the pipeline-riser system.

Cascade controllers based on topside measurements are fundamentally limited by RHP-zeros and have poor setpoint tracking properties. A MISO $\mathcal{H}_\infty$ controller based on the same measurements is not limited by RHP-zeros, and show significantly faster setpoint responses. Attempts were also made to design an LQG controller with an extended (non-linear) Kalman filter based on these measurements. It also stabilizes the process, but the achieved performance is significantly worse than with the $\mathcal{H}_\infty$ controllers.

The success of designing controllers based on the simplified 3-state model introduced in chapter 3 provides additional confirmation of the applicability of the model.

6.1 Introduction

Chapter 5 demonstrated that PID controllers, either as single-loop or cascade controllers, can stabilize the flow in pipeline-riser systems. The PID controllers based on upstream pressure measurements provided excellent performance, both in terms of disturbance rejection, noise suppression and setpoint tracking. The cascade controllers based on only topside pressure measurements are also good for disturbance rejection and noise suppression, but the setpoint tracking is slow. The slow setpoint tracking is illustrated in figure 6.1, where we compare the responses with stabilizing SISO control (y = riser base pressure P_{Rb}, solid lines) and cascade control with topside measurement s (y_1 = pressure drop over topside valve DP and y_2 = flow out of riser Q, dashed line).

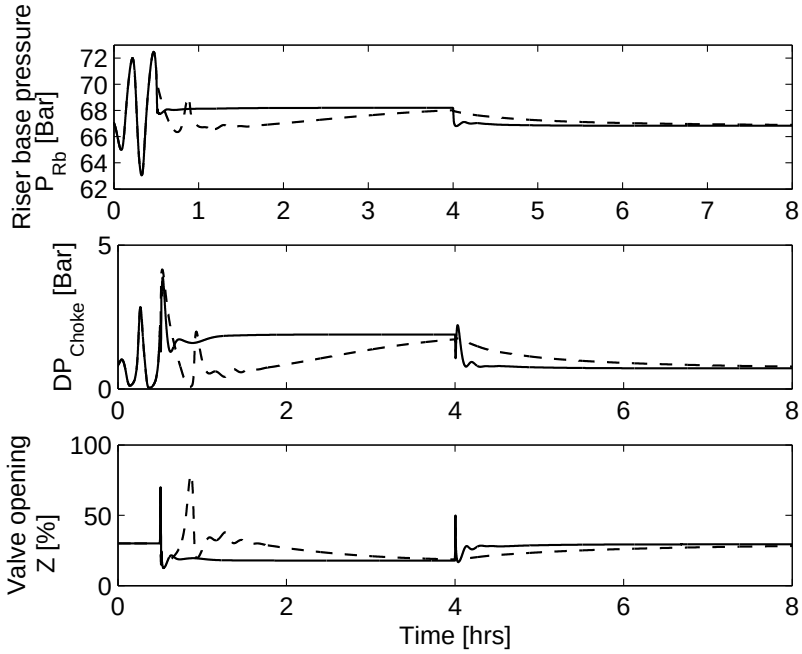

Figure 6.1: Comparison of SISO controller based on riser base measurement ($y = P_{Rb}$, solid line) and cascade controller with topside measurement s ($y_1 = DP$ and $y_2 = Q$, dashed line).

The slow setpoint tracking for the cascade controller based on topside measurements is caused by unstable (RHP) zeros for the measurement $y_1 = DP$. The other topside measurement ($y_2 = Q$) does not contain these RHP-zeros, so we may expect that a controller that utilize the two measurements simultaneously (MISO, Multiple Input - Single Output) does not suffer from these performance limitations. However, MISO controllers are more difficult to design and tune than PID controllers, and direct model-based controller design is usually needed.

There are also several other reasons for investigating model-based controllers and the added performance they might provide:

- The model-based controllers are optimal (based on some optimality criteria) and will hence serve as a benchmark that allows us to better assess the quality of the PID controllers.
- The improved performance and robustness provided by model-based controllers might be necessary for more complex cases for which PID controllers may no longer be sufficient.
- The controllers will be based directly on the simplified 3-state model from chapter 3. Testing the controllers on the two-fluid model from chapter 2 and the OLGA model will give additional verification of the simplified model

Section 6.2 discusses $\mathcal{H}_\infty$ controllers, both based on an upstream pressure measurement as a benchmark for the PID controllers and on topside measurements to achieve good low frequency performance. Section 6.3 deals with LQG controllers with an extended Kalman filter based on the 3-state simplified model.

6.2 $\mathcal{H}_\infty$ controller design for stabilizing control of pipeline riser systems

$\mathcal{H}_\infty$optimization was introduced as method to design robust controllers by Zames (1981). In short, the method involves finding the controller K that minimizes the maximum singular value ($\mathcal{H}_\infty$ norm) of one or more (weighted) closed loop transfer functions and thereby maximizing robustness and, through the weights, shaping the closed loop response.

6.2.1 General control problem formulation

For the general control configuration depicted in figure 6.2, the $\mathcal{H}_\infty$ optimization can be interpreted as minimizing the worst-case "error" signal z for all exogenous signals w. The exogenous signals w can include disturbances d, commands r and measurement noise n. The process in figure 6.2 is described by

$$\begin{bmatrix} z \\ v \end{bmatrix} = P(s) \begin{bmatrix} w \\ u \end{bmatrix} = \begin{bmatrix} P_{11} & P_{12} \\ P_{21} & P_{12} \end{bmatrix} \begin{bmatrix} w \\ u \end{bmatrix} \tag{6.1}$$

$$u = K(s)v \tag{6.2}$$

where u is the control variables and v is the measured variables. The control problem is to find the controller(s) K that minimizes

$$\|F_l(P,K)\|_\infty \triangleq \max_\omega \bar{\sigma}(F_l(P,K)(j\omega)) \tag{6.3}$$

where

$$F_l(P,K) = P_{11} + P_{12}K(I - P_{22}K)^{-1}P_{21} \tag{6.4}$$

is the linear fractional transformation for the system in figure 6.2.

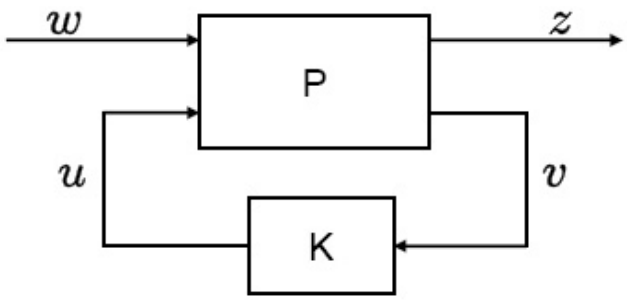

Figure 6.2: General control configuration

6.2.2 Mixed sensitivity $\mathcal{H}_\infty$ control: performance requirements and input limitations

Problem formulation

For the pipeline riser system, chapter 4.7 showed that it was important to include performance requirements in the design objectives. It has also been stressed in this thesis that avoiding input limitations is essential for stabilizing controllers. Thus, the signals that we want to minimize are the error signal $e = y - r$ and the control signal u. Weighing these signals with the weights W_P and W_u respectively aims to achieve $|u(\omega)| \leq |W_u(j\omega)^{-1}|$ and $|e(\omega)| \leq |W_P(j\omega)^{-1}|$. The exogenous signals that affect the process are disturbances d, measurement noise n and commands r. With these exogenous signals, the generalized plant P is given in figure 6.3.

The expression for the generalized plant P can easily be derived from figure 6.3:

$$P_{11} = \begin{bmatrix} W_pR & -W_pN & -W_pG_d \\ 0 & 0 & 0 \end{bmatrix} \quad P_{12} = \begin{bmatrix} -W_pG \\ W_u \end{bmatrix}$$
$$P_{21} = \begin{bmatrix} R & -N & -G_d \end{bmatrix} \qquad P_{22} = -G \tag{6.5}$$

This yields for the linear fractional transformation (6.4)

$$F_l(P,K) = \begin{bmatrix} W_pSR & -W_pSN & -W_pSG_d \\ W_uKSR & -W_uKSN & -W_uKSG_d \end{bmatrix} \tag{6.6}$$

Note that minimizing $\|F_l(P,K)\|_\infty$ in (6.6) is different from the PID parameter optimization in chapter 5. This is both because we in this chapter minimize weighted transfer functions (e.g. W_pSG_d) and because we minimize the maximum singular value of the matrix in (6.6) rather than the individual transfer functions. This may result in higher $\mathcal{H}_\infty$-norms for individual transfer function (e.g. S), but it should, provided that sensible weights are chosen, result in better overall robustness and performance.

Thus, using $\mathcal{H}_\infty$ controller design to minimize $\|F_l(P,K)\|_\infty$ is a systematic way to avoid input saturation and achieve the performance targets for the riser slugging case.

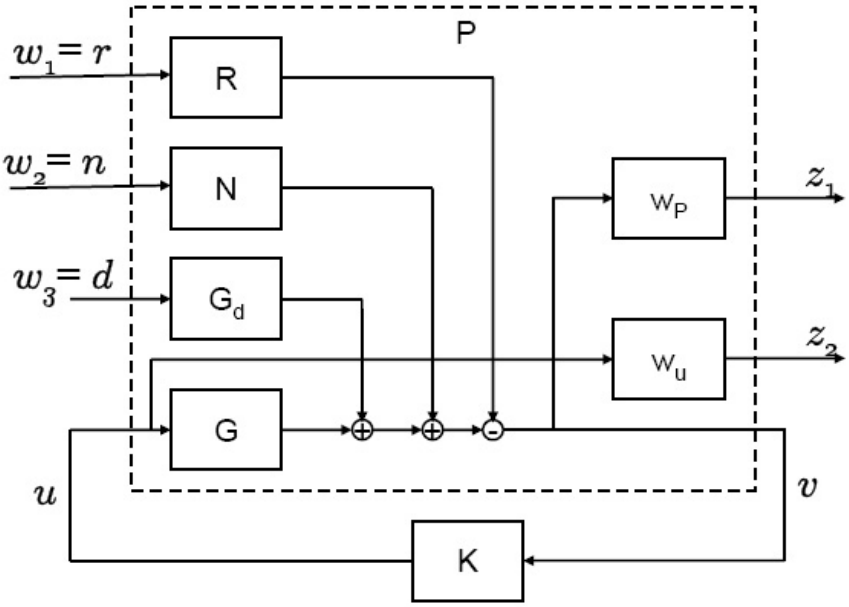

Figure 6.3: Mixed sensitivity minimization for the pipeline riser case

Input and performance weight

To enable direct comparison with the PID controllers from chapter 5 we use the same input weight (derived in chapter 4) and the same valve rate ($\dot{u}_{max} = 1/(D_u \cdot 60s) = 0.024s^{-1}$, corresponding to an opening time of 1 minute). However, to be able to balance the input limitation with the performance requirement, the input weight is multiplied by a constant k:

$$W_u(s) = k(\dot{u}_{max}^{-1}s + 1) = k(40s + 1) \tag{6.7}$$

The performance weight w_P is given by

$$W_P(s) = \frac{s/M + \omega_B^*}{s + \omega_B^* A} \tag{6.8}$$

where $|S(0)| \leq A$ is the requirement for low-frequency performance, ω_B^* is the bandwidth requirement and $|S| \leq M$ is the requirement for higher frequencies above the bandwidth.

6.2.3 $\mathcal{H}_\infty$ control of inlet pressure P_I

The PID-controller in section 5.3.1, which was based on inlet pressure as measurement ($y = P_I$), performed well with all the three models on which it was tested. As a benchmark for the PID controller, we design and test a $\mathcal{H}_\infty$ controller using the same measurement.

The PID-controller is used as a starting point for the $\mathcal{H}_\infty$ controller design. Fitting the performance weight W_P to the sensitivity function for the PID-controller results in $A = 0.1$ (allowing for 10% steady state error), $M = 1.26$ (maximum peak) and $\omega_B^* = 0.001$ (desired

bandwidth). To guarantee that the input does not saturate, we use $k = 2$ in the input weight (6.7).

With these weights, the resulting controller K is shown together with the PID controller in figure 6.4. The two controllers are remarkably similar, which indicates that the PID controller is close to optimal for this control problem. This is confirmed by simulations with all the three models used in this thesis. The OLGA simulation is shown in figure 6.5, and is almost identical to the response with the PID controller (figure 5.3(c), page 81). Simulations with the other two models (3-state, two-fluid) are given in appendix C.

Comparing the closed-loop norms, we find that $\|S\|_\infty$ and $\|KS\|_\infty$ are higher for the $\mathcal{H}_\infty$ controller than for the PID controller (1.48 vs. 1.26 and 0.43 vs. 0.29, respectively). However, the norm for $\|T\|_\infty$ is lower for the $\mathcal{H}_\infty$ controller (1.35 vs. 1.91). The higher norms are, as previously mentioned, caused by the problem formulation for the $\mathcal{H}_\infty$ optimization, where *weighted* closed loop transfer functions are minimized. The weighted transfer functions in (6.6) are generally lower for the $\mathcal{H}_\infty$ controller than for the PID controller.

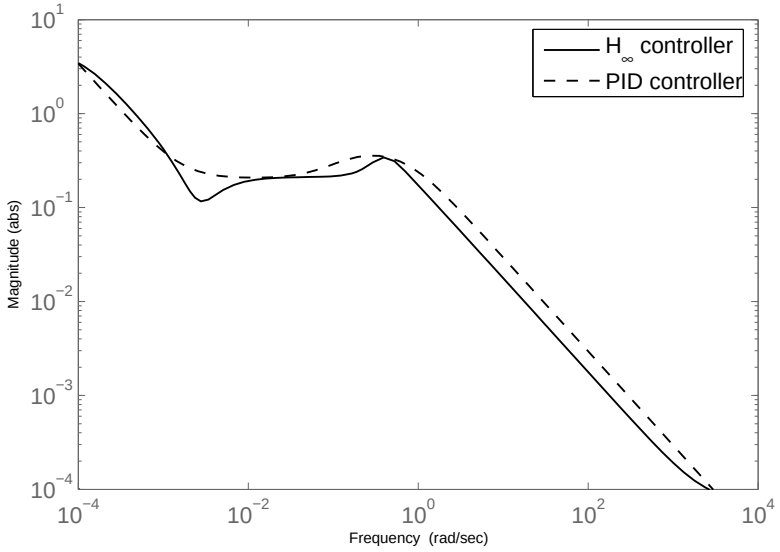

Figure 6.4: Comparison of $\mathcal{H}_\infty$and PID controller for the case with $y = P_I$

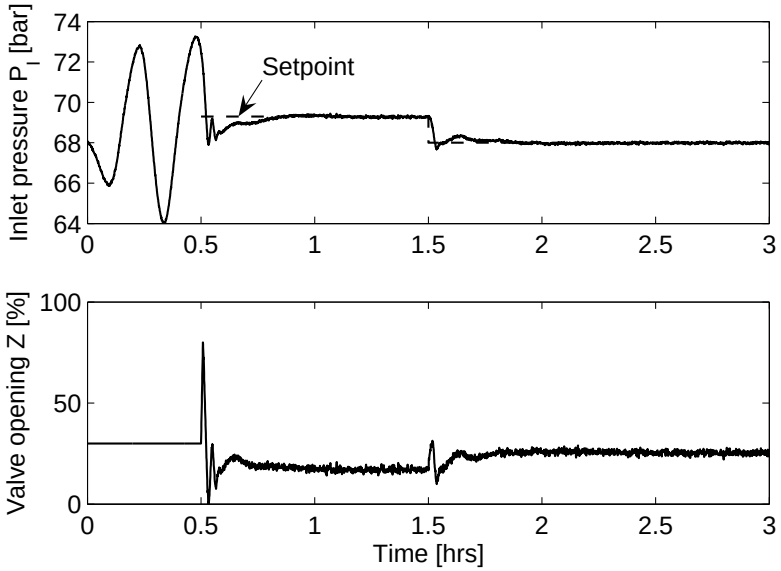

Figure 6.5: $\mathcal{H}_\infty$stabilizing control with $y = P_I$, OLGA model.

6.2.4 $\mathcal{H}_\infty$ control using only topside measurements

Stabilizing control of pipeline riser systems based on upstream pressure measurements performs well, and is, with good reason, the preferred practice on real pipelines. There may, however, be systems that need stabilizing control where an upstream pressure measurement is not available. Skofteland and Godhavn (2003) as well as section 5.4 showed that a cascade controller based on a secondary flow measurement and a primary topside pressure measurement could stabilize the system without relying on an upstream measurement.

As mentioned in the introduction to this chapter, the cascade controllers based on topside measurements are slow due to (SISO) bandwidth limitations caused by RHP-zeros. These occur both with valve opening $y_1 = Z$ as well as with pressure drop over the topside valve $y_1 = DP$ in the outer loop. Note that processes with more outputs (y) than inputs (u) rarely have RHP-zeros, except when the RHP-zero is pinned to one of the outputs. In our case there are no pinned RHP-zeros, and to see if performance can be improved, we will in this section design $\mathcal{H}_\infty$ MISO controllers for the same two topside measurement combinations used in chapter 5: 1) $y = [DP \;\; Q]^T$, with pressure drop over valve DP as primary control variable (meaning that we want low-frequency performance for this measurement) and 2) $y = [Z \;\; Q]^T$, with valve opening Z as a primary control variable. Neither of these controllers will be limited by RHP-zeros, and we expect significantly improved low-frequency performance compared with the corresponding cascade controllers. As noted in section 5.4.4, it may seem strange to use the valve opening Z as both controller input and output, but the purpose of this is to provide low-frequency performance, and we shall see that using this "measurement" yields a good controller.

The design objective for the $\mathcal{H}_\infty$-optimization will be the same as in the previous section: minimize the worst-case effect of disturbances d, measurement noise n and commands r on

the weighted process input u and the control error $e = r - y_1$. . To avoid input saturation, we must put more emphasis on the input usage by setting $k = 3$ in (6.7), but other than that, the input weight and the performance weight is the same.

Table 6.1 shows closed-loop norms and bandwidth for the resulting MISO controllers compared to the cascade controller in section 5.4. The major improvement provided by the MISO controllers is the bandwidth, which is increased by a factor of 25 for $y = [DP \;\; Q]^T$ and a factor of 2.5 for $y = [DP \;\; Q]^T$. $\|T\|_\infty$ is also significantly reduced, whereas there are only small differences for other closed-loop norms.

Table 6.1: Closed-loop norms and bandwidth for MISO $\mathcal{H}_\infty$ controllers compared to corresponding cascade controllers.

	$y = [DP \;\; Q]^T$		$y = [Z \;\; Q]^T$	
	$\mathcal{H}_\infty$	Cascade	$\mathcal{H}_\infty$	Cascade
$\|S\|_\infty$	1.27	1.42	1.16	1.14
$\|T\|_\infty$	0.94	2.10	0.91	1.54
$\|KS\|_\infty$	0.37	0.16	0.91	1.42
$\|W_u KSG_d\|_\infty$	0.61	0.98	0.61	0.88
$\|W_u KSN\|_\infty$	0.33	0.16	0.61	0.10
ω_B	0.0025	0.0001	0.0010	0.0004

Figure 6.6 shows OLGA simulations with the $\mathcal{H}_\infty$ controllers. The setpoint tracking is significantly faster than with the cascade controllers (figure 5.9, page 91 and figure 5.10, page 92), but still a bit slower than with controllers based on upstream pressure measurements. Simulations with the other two models, given in appendix C, shows equally good performance.

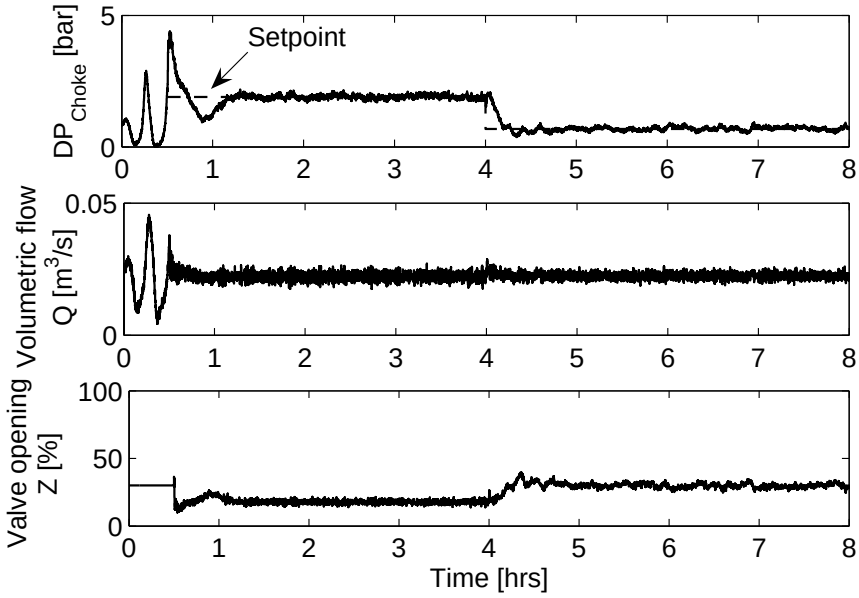

(a) Measurements $y = [DP \quad Q]^T$

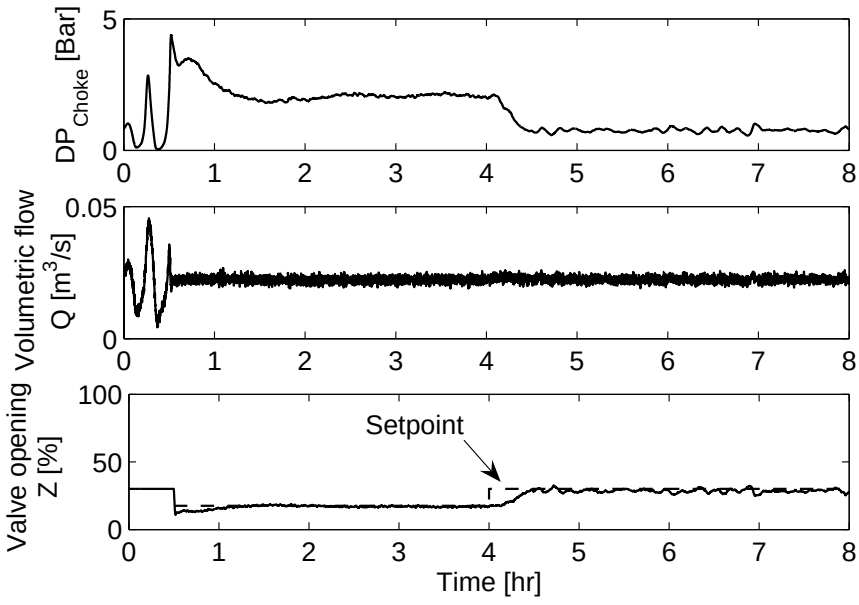

(b) Measurements $y = [Z \quad Q]^T$

Figure 6.6: MISO $\mathcal{H}_\infty$ anti-slug control with OLGA model.

6.3 LQG control

LQG control, which reached maturity in the 1960's, has been successfully applied to many control problems, especially for mechanical systems, which are characterized by accurate mathematical models and well defined optimization problems. For other control problems, where the models are less accurate and the assumption of white noise disturbance is not always well founded, LQG control has not been as successful, particularly because of robustness issues (Skogestad and Postlethwaite, 1996). We will in this section design LQG controllers for the pipeline-riser system.

In his diploma thesis, Trudvang (2003) designed LQG controllers based on the simplified three-state model from chapter 3 for a case that was similar to the simulated OLGA case used as the main case study in this thesis. He found that linear Kalman filters should not be used to estimate the states for the pipeline-riser system since the linear model, on which the Kalman filter is based, are valid for a too limited region of the state space. On the other hand, an extended (non-linear) Kalman filter, with the non-linear 3-state model used in the filter instead of the linearized model, was found to estimate the states quite effectively, and was thus well suited for stabilizing control.

Section 6.2 proved that PID controller were close to optimal if upstream pressure measurement, either at the pipeline inlet ($y = P_I$) or at the riser base ($y = P_{Rb}$), were used as a primary control variable. Because it is unlikely that a LQG controller will improve performance when these measurements are available, we will only consider LQG control based on the topside measurements $y_1 = DP$ (pressure drop over valve) and $y_2 = Q$ (volumetric flow out of riser).

6.3.1 Theory

Traditional LQG control is based on a (known) linear process model with stochastic measurement noise w_n and disturbance signals w_d (process noise) of known variance:

$$\dot{x} = Ax + Bu + w_d \tag{6.9}$$

$$y = Cx + w_n \tag{6.10}$$

If the states x are known, the optimal solution to the LQR control problem

$$J_r = \int_0^\infty \left(x(t)^T Q x(t) + u(t)^T R u(t) \right) dt \tag{6.11}$$

were Q and R are weighting matrices (design parameters), is a constant state feedback

$$u(t) = -K_r x(t) \tag{6.12}$$

The controller gain K_r is found by solving an algebraic Ricatti equation.

If the states x cannot be measured, an estimate $\hat{x}$ is obtained from a Kalman filter. The filter gain K_f can be found from an algebraic Ricatti equation, and depend on the statistical properties of the noise signals. The combination of a Kalman filter and optimal state feedback is called a LQG controller. We will in this work us an extended (nonlinear) Kalman

filter. For this filter, the filter gain K_f normally depends on the state estimate $\hat{x}$, but we will, for simplicity, use a constant filter gain, computed from the linear model. The same approach was used in Trudvang (2003) with good results.

The LQG controller have only proportional action, and to avoid steady-state deviations and safeguard against input saturation, we modify the LQG controller to include an integrating loop acting on a subset y_I of the measurements, as shown in figure 6.7. To compute the controller gain K_r for this controller, the state space matrices are augmented to include the measurement model for the measurements with integral action ($y_I = C_I x + D_I u$) (Skogestad and Postlethwaite, 2005):

$$A^* = \begin{bmatrix} A & 0 \\ -C_I & 0 \end{bmatrix}, \; B^* = \begin{bmatrix} B \\ -D_I \end{bmatrix} \tag{6.13}$$

With integral action, only the measurements are weighted in Q (eq. (6.11)). Thus, Q and R are given by

$$Q = \begin{bmatrix} 0 & 0 \\ 0 & I \end{bmatrix}, \; R = k \cdot I \tag{6.14}$$

where k is used to adjust input usage vs. output performance.

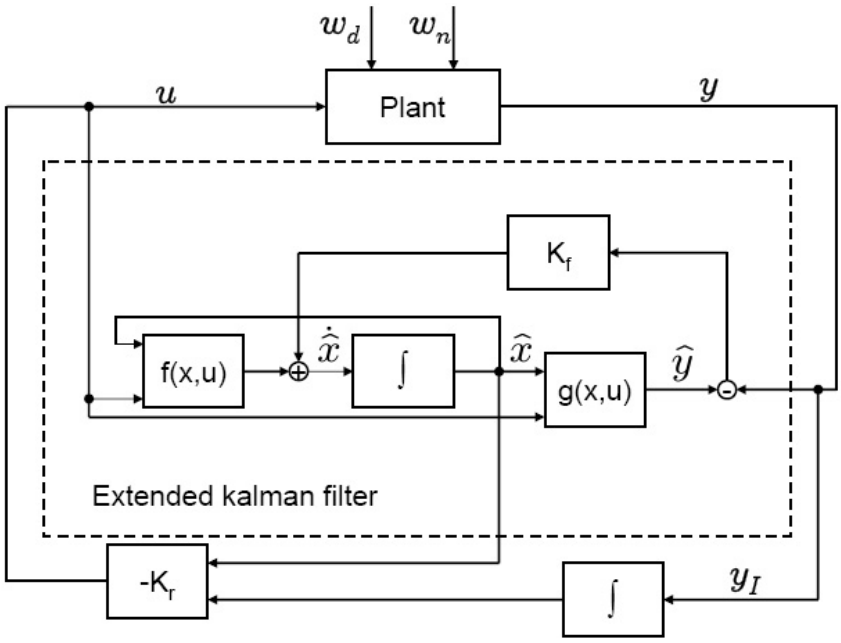

Figure 6.7: LQG controller with extended (nonlinear) Kalman filter, and integral action

6.3.2 LQG controller for the pipeline-riser system

The controller tuning is based on the linear model obtained from linearizing the simplified three-state model around the operating point for a valve opening of 30%. The filter gain K_f

is computed using the matlab routine *kalman.m* based on 2% variance for the process noise (disturbances) and 2% variance for the measurement noise. As mentioned above, we will use a constant filter gain even though we are using a nonlinear Kalman filter. The controller gain K_r is computed using the matlab rutine *lqr.m* with $k = 80e6$ in the weighting matrices in (6.14). The high value for k is is used because the states x are not scaled and have a significantly higher numerical value than the input u.

The resulting LQG controller performs well for the simplified three-state model and, with the same simulated scenario as earlier in this thesis, stabilizes the operating points corresponding to both a valve opening of 17.5% and 30%. If model error is introduced by testing the LQG controller on the two-fluid and OLGA model, the controller manages to stabilize the first operating point (Z=17.5%), but after the setpoint change, the systems starts to oscillate. This indicates that the LQG controller is not robust enough towards the errors in the simplified three-state models. Also, since the controller manages to stabilize an operating points with slower instabilities than the one it is designed for ($Z = 17.5\%$), but not the operating point it was designed for ($Z = 30\%$), the failure of the extended LQG controller can indicate that the simplified model predicts too slow instabilities for high valve openings.

By design the controller for a higher valve opening than the desired operation point we can get around the robustness problems. It turns out that it is sufficient to design the state feedback gain K_r for a more aggressive operating point, and designing K_r from the model linearized around $Z = 40\%$ and retaining the extended Kalman filter designed at $Z = 30\%$, the LQG controller is able to stabilize all three models used in this thesis. However, the close loop sensitivity peaks are very high for the resulting design ($\|S\|_\infty$ and $\|T\|_\infty$ both exceed 10), and the bandwidth is low ($\omega_B = 0.0004$, which equals the bandwidth for the corresponding cascade controller). Even though the input usage is low, with $\|KS\|_\infty = 0.43$, we would not recommend using this controller in practice, especially since the $\mathcal{H}_\infty$ controllers designed in the previous section provides much better performance and are easier to design.

The OLGA simulation with the LQG controller, shown in figure 6.8, confirms the slow setpoint tracking.

6.4 Conclusions

The $\mathcal{H}_\infty$ controllers designed in this chapter stabilize the flow in the pipeline-riser system with little input usage and quick and accurate setpoint tracking, and must, both based on closed loop norms and simulations, be said to be close to optimal. The $\mathcal{H}_\infty$ controller based the inlet pressure ($y = P_I$) is very similar to the PID controller designed in chapter 5.3.1, indicating that using a PID controller based on an upstream pressure measurement is a very good control strategy.

The $\mathcal{H}_\infty$ controllers based on topside measurements ($y = [DP \;\; Q]^T$) and ($y = [Z \;\; Q]^T$) show that good performance with fast setpoint tracking can be achieved even without relying on an upstream pressure measurement. The setpoint response with these MISO $\mathcal{H}_\infty$controllers are significantly faster than with the cascade controllers designed in section 5.4.3. The rea-

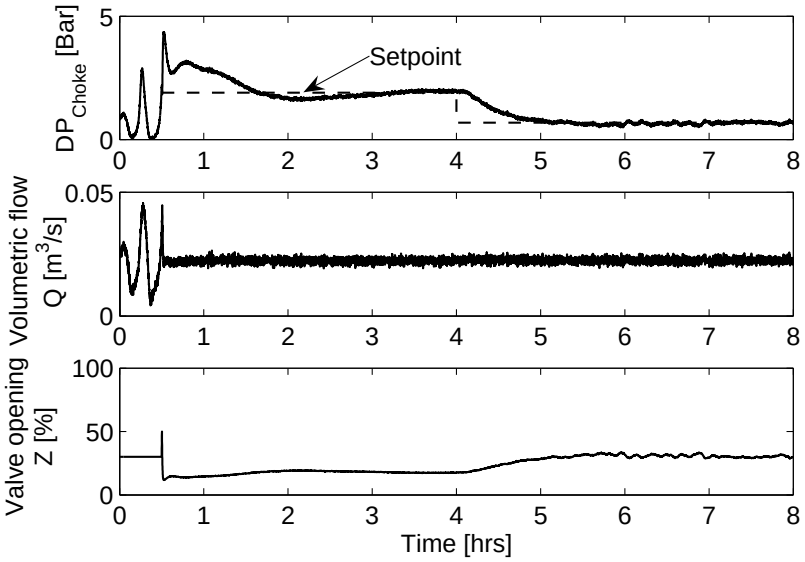

Figure 6.8: LQG control with extended Kalman filter, $y_1 = DP$ and $y_2 = Q$, OLGA model,

son for the faster setpoint response with the $\mathcal{H}_\infty$ controllers is that their bandwidth is not limited by RHP-zeros.

An LQG controller with an extended Kalman filter based on the simplified 3-state model can also be used for stabilizing control of the pipeline riser system, even if only topside measurements are available. However, due to model errors in the simplified 3-state model, the achieved performance is poor. The LQG controller had to be designed for a more aggressive operating point than it is intended to be used at to achieve robust stability.

The success of the $\mathcal{H}_\infty$ controllers design from the simplified 3-state model introduced in chapter 3 provides the final confirmation of the applicability of the model. However, the problems with designing the LQG controller may imply that 3-state model predicts too slow instabilities at higher valve openings.

Chapter 7

Extended Slug Control - An industrial application

Espen Storkaas, John-Morten Godhavn and Sigurd Skogestad

Based on a paper accepted for publication at Multiphase ’05

Abstract

Control systems that prevent the development of riser slugging in pipeline-riser systems have in recent years been introduced on several offshore processing facilities. These anti-slug control systems are based on active use of the topside choke valve to control a pressure measured somewhere upstream of the riser. Anti-slug control systems have been a great success, and are emerging as the standard method to avoid riser slugging in multiphase production pipelines.

There are several other multiphase phenomena occurring in pipeline-riser systems that can cause operational problems for the downstream production facilities. Among these are 1) Surge waves, which are large liquid waves that can occur when the production rate in a gas-condensate pipeline is increased and 2) Start-up slugs, which can occur when the pipeline is started up from shut-in conditions. The start-up slugs are similar to surge waves but can be even more serious as they potentially can initiate riser slugs and thereby cause even larger peaks in the liquid production.

In this chapter we introduce a novel control structure that extends the scope of pipeline control by including suppression of surge waves and start-up slugs. The control system combines a stabilizing anti-slug controller with individual flow controllers for each phase seamlessly through a minimum select function. The flow controllers use the pipeline as a buffer volume to smear out the flow variations that can not be handled by the separator. The performance of the control system is illustrated with simulations of an industrial case study.

7.1 Introduction

Many remaining offshore oil and gas reserves in the North Sea are in small fields. Subsea installations and long multiphase tie-in lines to existing infrastructure are emerging as the preferred solutions for extracting the reserves in these smaller fields. This development is made possible by technological advances in the last twenty years. In this chapter we address some of the challenges associated with multiphase transport of hydrocarbons in these tie-in lines and introduce a control system to meet these challenges.

This thesis has so far focused on avoiding riser slugging in pipeline-riser systems with stabilizing anti-slug controllers. Riser slugging has been one of the main operational concerns with these systems, and, over the last few years, several such anti-slug control systems that stabilize the flow at operating conditions that uncontrolled would yield riser slugging have been implemented (Courbot, 1996; Havre et al., 2000; Havre and Dalsmo, 2002; Skofteland and Godhavn, 2003; Kovalev et al., 2003). A typical control structure for an anti-slug controller is shown in figure 7.1. The anti-slug controller has removed a major obstacle for multiphase transport of hydrocarbons, and has also introduced the use of the topside choke valve for control purposes.

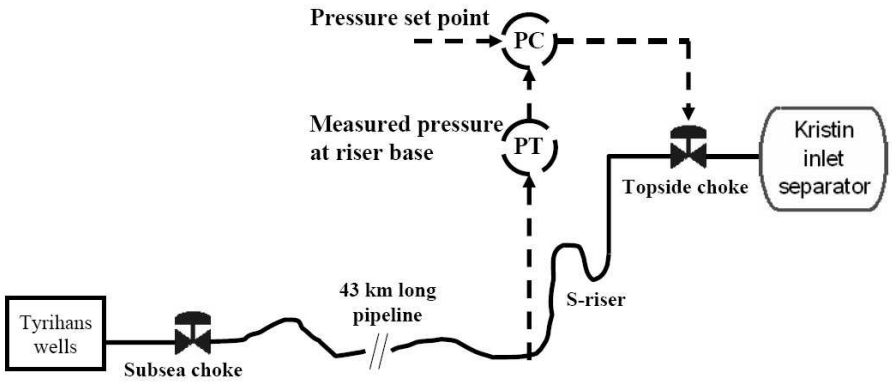

Figure 7.1: Control structure for a conventional slug control system

Due to the success of the control systems for avoiding riser slugging, the focus for pipeline control has recently broadened to include other troublesome multiphase flow phenomena as targets for an extended slug controller. The goal of such a controller would be to handle most, if not all, of the operational challenges caused by transient multiphase flow phenomena, thus minimizing the need for operator intervention and at the same time optimizing production.

Other types of slug flow, such as hydrodynamic and terrain induced slugging, have been considered in this thesis as disturbances affecting the anti-slug control system. The small hydrodynamic and terrain induced slugs are usually not a big operational problem for the receiving facilities, and, although some emphasis has been put on reducing the effect of these smaller slugs (i.e. smoothing them out), the motivation for the disturbance rejection has been aiding the anti-slug controller (avoid input saturation) rather than suppressing the

disturbances.

The last of the four types of slug flow defined in the chapter 1 is transient slugging, where slugs or large waves are caused by changes in operating conditions. These transient slugs can be very large and cause significant problems for the receiving facilities. We will in this chapter introduce controllers that suppress these transient slugs by manipulating the valve opening of the topside choke valve ($u = Z$). These controllers are combined with the anti-slug controller to form an extended slug controller.

In section 7.2, we describe the physical phenomena that are causing the control challenges and in section 7.3, we introduce the Extended Slug Controller. The case study in section 7.4 is based on the development of the Tyrihans field in the North Sea, and illustrates the actions and benefits of the proposed control structure.

7.2 Challenges for an extended slug controller

7.2.1 Surge waves

The liquid holdup in a pipeline is a function of the fluid velocities, and therefore a function of the production rate for the pipeline. Low production implies high liquid holdup and vice versa, as illustrated in figure 7.2. This means that during a rate change from low to high production, the excess volume of liquid relative to the new stationary liquid holdup will have to be transported out of the pipeline during the transition period. As a consequence, the peak liquid production will exceed the new stationary liquid production, and possibly also the liquid processing capacity of the receiving facility. The peak rate will depend on the ramp-up time from low to high production, and a possible strategy for avoiding capacity problems is to slowly ramp up the production during rate transitions.

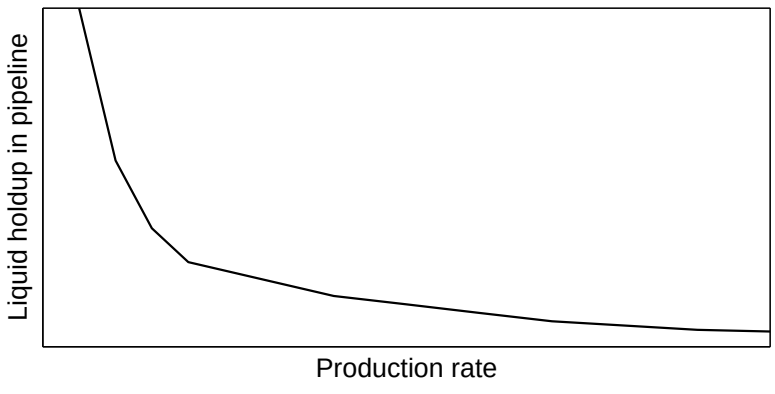

Figure 7.2: Typical relationship between liquid holdup and production rate

A slow ramp-up will lead to loss of production in the transition period, and the goal for an extended slug controller would be to facilitate faster rate transitions whilst keeping the feed to the processing facility within its operating range.

7.2.2 Start-up slugs

Startup of pipelines from shut-in condition is a phenomenon closely related to rate increases resulting in surge waves. The major difference is that the flow variations resulting from an (fast) startup usually are more severe, as the waves in the pipeline can initiate riser slugs. The flow variations at the outlet have characteristics as a combination of surge waves and riser slugs, and must be handled either by a slow start-up procedure or by an automatic control system. Again, the goal of such a control system would be to minimize the time it takes to start up the production in a safe manner.

7.2.3 Other possible tasks

Surge waves and start-up slugs are mainly challenging the processing capacity (in terms of maximum throughput) of the receiving process, including the separators, the water treatment facilities and compressor trains. Other types of equipments could potentially also impose restriction on the allowed rate out of the pipeline. For example, a condensate heater has only a limited amount of heating medium available, and if too much cold condensate enters the process, the temperature controller for the condensate heater would saturate. In this situation, it would be wise to limit the production of cold condensate, but these types of restrictions are outside the scope of this work. However, the extended slug controller could easily be extended to include these types of limitations.

Also, we assume fixed, time-invariant limitations on the fluid processing capacity. As there are usually more than one pipeline producing to a common separator and compressor train, the limitations for one pipeline will depend on the production rate from other sources. A natural extension to the control system would be to connect the available capacity in the processing facility to the extended slug controller to optimize the production. To limit the scope and complexity of the work herein, this is assumed to be done manually by an operator.

7.3 Extended Slug controller

The goal of the extended slug controller developed here is, in addition to prevent riser slugging from developing, to keep the flow of all three phases (gas, oil and water) within the capacity limitations imposed by the receiving facility. To achieve this, the controller utilizes an upstream pressure measurement and flow rate measurements for each phase as illustrated in figure 7.3. The flow rate measurements can either be obtained from a multiphase meter located close to the control valve or estimated from separator measurements.

The controller itself is shown in figure 7.4. It consists of a regular anti-slug controller (in this case controlling the riser base pressure) and flow controllers for each phase. The minimum select functionality ensures that only the controller that demands the lowest valve opening is active. This ensures a consistent system and, when properly tuned, prioritizes between the different tasks according to its importance.

Note, however, that the anti-slug controller can only stabilize the flow in the system when the flow controllers are inactive, as stabilization is based on continuously manipulating the input $u = Z$. If one of the flow controllers ”take over” while the anti-slug controller is

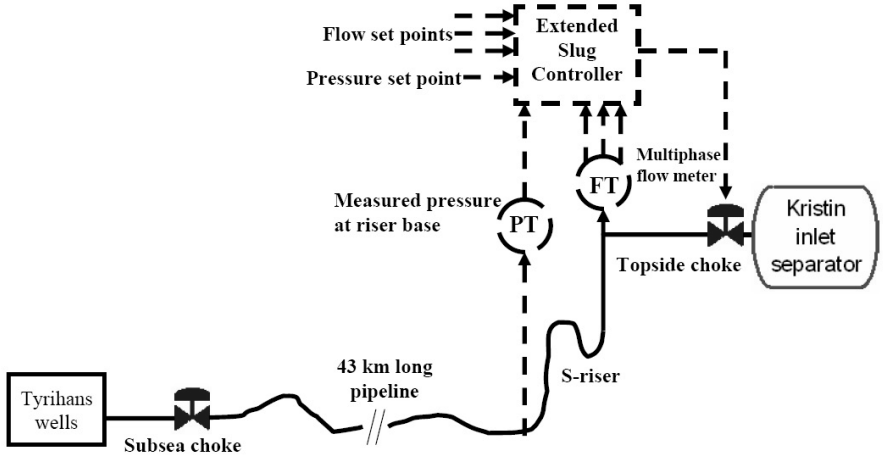

Figure 7.3: Control structure for an extended slug control system

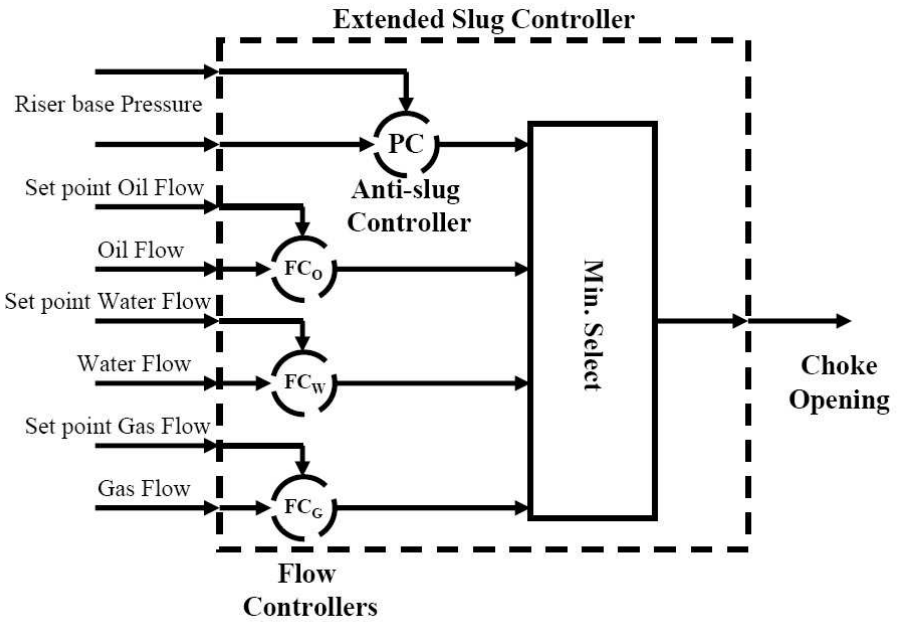

Figure 7.4: Extended slug controller

stabilizing the process, the feedback loop for the stabilizing anti-slug controller is broken and the controller can no longer keep the process stable. Thus, the extended slug controller can only handle the situation where riser slugging occurs at reduced flow rates. This is not as limiting as it may seem since surge waves and startup slugs are mainly a problem in pipelines where the GOR (Gas-to-Oil Ratio) is above a certain value, and at these GOR values, riser slugging only occurs at low flow rates.

The flow controllers are selected to be simple P-controllers (proportional action only), possibly with gain scheduling to reduce the controller gain if the pressure drop over the control valve, and by that also the process gain, gets significantly higher than its nominal value. Integral action is not included in the controllers because 1) the steady-state gain is low and 2) we are only interested in the dynamical behavior anyway.

If the flow rate for a given phase exceeds the setpoint for that phase, the flow controller will close the choke valve and retain more fluid in the pipeline. Thus, the effect of the flow controllers is to use of the pipeline volume as a buffer. It makes perfect sense to do this, as the pipeline volume far exceeds the available volume in the inlet separator. Therefore, the main philosophy behind the extended slug controller is, in addition to stabilizing any (desired) unstable flow regimes, to use the choke and the pipeline volume to average out the flow variations that can not be handled by the separator. This is similar to ”averaging level control”.

The flow controllers should be tuned with equal gain relative to the maximum allowed deviation for the given phase. This implies that the flow controllers whose nominal rates are close to their maximal rates (as imposed by the downstream processing capacity) should have higher gains than the flow controllers for the phases where there are more leeway in terms of production rates. If these tuning principles are used, the extended slug controller would always limit the production based on the most ”critical” phase. The setpoint for the flow controllers should be at or slightly above the nominal values to give the controllers a certain working range for the flows.

The pressure- and flow controllers will usually be active in different phases of the production, except possibly when dealing with start-up slugs. The switch between the pressure and flow modes of the controller is done seamlessly by the minimum select functionality.

Example 7.1 *To illustrate the tuning of the flow controllers, consider the following simple example: We want to control a pipeline with nominal flow rates and processing capacity as given in table 7.1. As stated above, the gain relative to the maximum allowed deviation should be constant, which means that for each phase i, the controller gain should be $K_i = K/\Delta W_i$. Setting K = 100 yields the controller gains for the flow controllers given in table 7.1.*

Table 7.1: Data for example 7.1

	Oil	*Water*	*Gas*
Nominal rate / Setpoint r_i [kg/s]	*10*	*5*	*20*
Processing capacity [kg/s]	*13*	*10*	*30*
Max deviation ΔW_i[kg/s]	*3*	*5*	*10*
Controller gain [s/kg]	*33*	*20*	*10*

Now assume that, at some point during the operation, the flow rates are measured to be 12 kg/s oil, 7 kg/s water and 15 kg/s gas. A P-controller has the simple algorithm $u = u_0 + K \cdot (r - y)$. Here, u is the controller output, u_0 is the bias (set to u_0 = 100%, corresponding to a fully open valve in this example), K is the controller gain, r is the reference (setpoint) and y is the measurement. For this example, this yields a valve opening of u = 34% from the oil flow controller ($u = u_0 + K \cdot (r - y) = 100 + 33 \cdot (10 - 12) = 34\%$), u = 60% for the water flow controller and u =150% for the gas flow controller. Because of the minimum select functionality, only the smallest one of these will be used, and the controller will set the valve opening to u = 34%. Thus, the oil flow controller limits the production as the oil flow rate is closest to maximum value (66% of its allowed deviation).

7.4 Case Study - Tyrihans

The simulation example for this work is based on models for the Tyrihans field, owned by Statoil, ExxonMobil, Norsk Hydro, Total and Eni, and currently under development by Statoil. The Tyrihans field consists of the reservoirs Tyrihans Nord and Tyrihans Sør, and is located in the Halten area about 35 km southeast of the Åsgard field and about 35 km east of the Kristin field. The fields were discovered in 1983 (Sør) and 1984 (Nord) and the sea depth is about 290 meters. The production from Tyrihans will be tied in to the Kristin production platform with a scheduled production startup in July 2009.

The Tyrihans pipeline will be about 43 km long, with a 16” pipeline (0.4 m inner diameter) along the seabed. The characteristics of the pipeline geometry is a slight downward inclination and a hill close to the riser. The riser is a 14” S-riser (0.36 m inner diameter). The receiving pressure at Kristin will be about 88 bar, and typical pressures in the pipeline are as shown later in figures 7.7 and 7.11. Exact values for flow rates, GOR and water cut cannot be revealed, but the values are fairly typical for such a pipeline.

The flow in the Tyrihans pipeline will initially be oil-dominated, but the GOR will increase as the field matures, resulting in gas-dominated flow in the pipeline for the later production years. Riser slugging can be a problem when the flow is oil dominated, especially when the production is reduced. Surge waves will primarily be an issue when the flow is gas dominated. Start-up slugs need to be handled for all operating conditions.

To test the extended slug controller’s ability to handle the flow related challenges described in section 7.2, a scenario including start-up slugs, maximum production, reduced production with riser slugging and surge waves are investigated. Figure 7.5 shows the inflow profile for the simulated production scenario. The production (feed rate) is ramped up from 0 to 100% during the first 4 hours and kept at maximum production for 8 hours. Problems with start-up slugs are expected in this phase (A). Then the production in ramped down to 33% over the next 4 hours and kept at reduced production for 8 hours. For oil-dominated flow, we expect riser slugging in this phase (B). Finally, the production is ramped back up to maximum production over 2 hours and kept there for the last 10 hours of the simulation. The last phase (C) of the simulation will produce surge waves that may cause problems.

In the simulations, the initial condition is a shut-in, cold, low pressure pipeline resulting from a controlled shutdown. The feed into the pipeline is assumed to be independent of the pipeline pressure. We have also assumed constant inlet separator pressure.

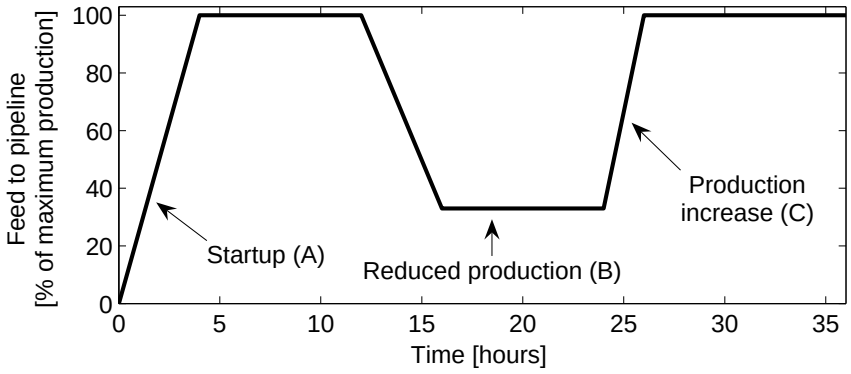

Figure 7.5: Illustration of simulation scenario represented by inflow to the pipeline

Below we present simulation results for both the oil-dominated (low GOR) and the gas-dominated (high GOR) production phase. For oil dominated production we will focus on suppressing start-up slugs and avoiding riser slugging at reduced rates, whereas for gas dominated flow we will focus on surge waves.

The simulations were preformed with OLGA2000 v.4.10.1, a commercial multiphase flow simulator. The controllers were implemented in Matlab and the link between the two programs was done with the OLGA-Matlab toolbox available in the OLGA distribution.

7.4.1 Oil-Dominated Case

The oil-dominated case will occur during the first years of production from Tyrihans. In figure 7.6 we show the simulated flows of the individual phases into the separator and the choke valve opening for the production profile in figure 7.5. The dashed line is without control and the solid line is with the Extended Slug Controller. The pressure profile in the pipeline for the same simulations is shown in figure 7.7, where the subscripts I, MP and RB denotes Inlet, Middle of the Pipe and Riser Base, respectively.

At first glance, we observe that the peak flow rates for the start-up slugs are reduced significantly and that the riser slugging occurring at reduced production is removed by the extended slug controller. We will now focus on the different phases of the production scenario to explain and discuss the actions of the controller.

Startup slug suppression for oil dominated flow

Figure 7.8 shows the start-up slugging part of the simulation in figures 7.6 and 7.7. With control, the peak in the oil production is reduced from about 100% to about 50% above the nominal rate and the water peak is reduced from 140% to 70% above its nominal rate. The gas flow is less affected, the peak is slightly reduced, but the gas phase still needs control due to the otherwise deteriorating effect the control of the other phases would have on the gas production.

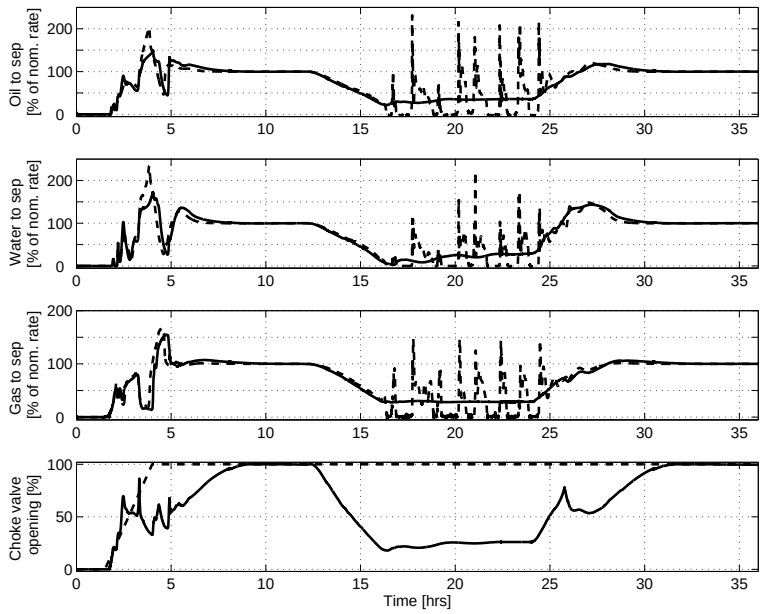

Figure 7.6: Simulated flows for oil-dominated case. Solid lines for controlled case, dashed lines for uncontrolled.

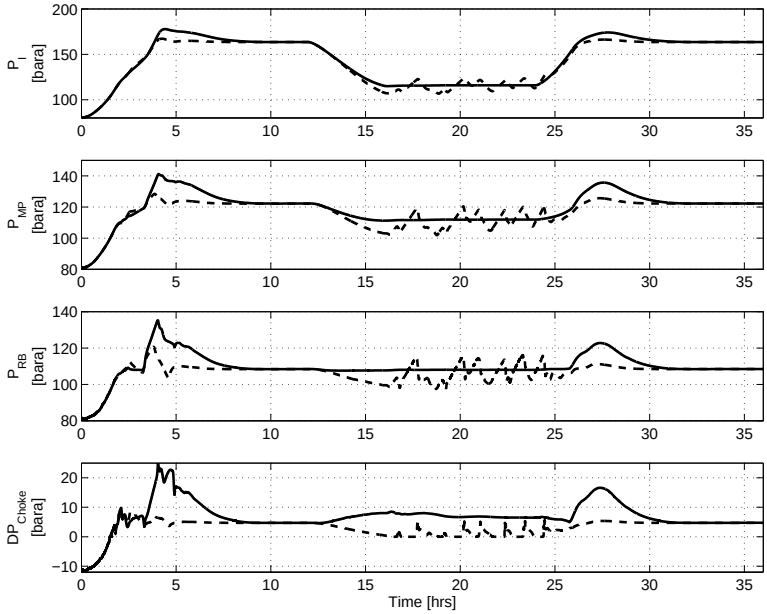

Figure 7.7: Simulated pressures for oil-dominated case. Solid lines for controlled case, dashed lines for uncontrolled.

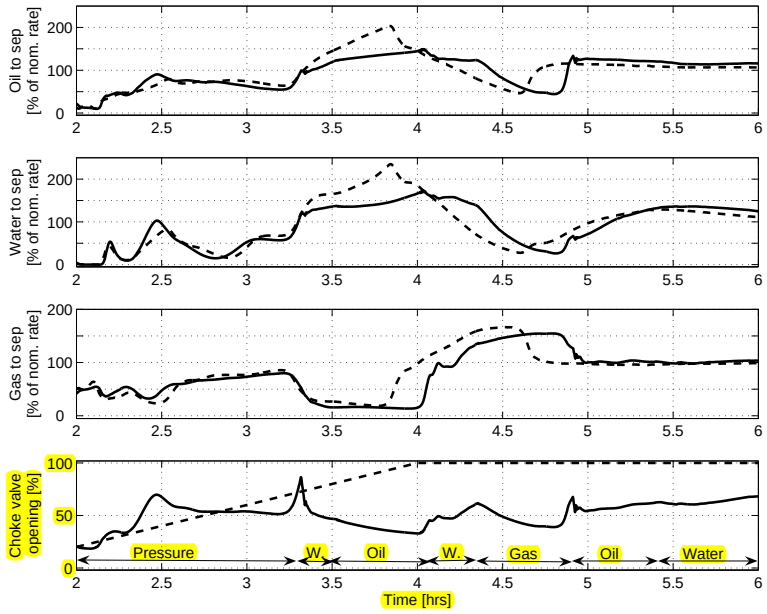

Figure 7.8: Startup-phase (A) for the oil-dominated case. Solid lines for controlled case, dashed lines for uncontrolled.

In the lower plot in figure 7.8, the choke valve action is given together with a indication of the active controller mode selected by the min. select in figure 7.4. We see that the pressure controller takes care of the ramp-up phase. When start-up slugs starts to appear around t = 3.3 hours, the flow controllers take over. The major peak in liquid production between 3.3 and 4.3 hours consists of both water and oil and the controller switches between these two modes to limit the flow of the most critical phase. Also the gas flow controller is active in order to reduce the peak in gas production that follows the liquid peak. As the start-up slugs dies out, the extended slug controller will slowly and gently open the choke valve as the production rates approach their nominal values.

One concern with using the choke to smooth out the flow during start-up is that the pressure in the pipeline could increase to the extent that it would severely affect the production. It can be observed from figure 7.7 that the pipeline inlet pressure (P_I) is only slightly increased by the choking, and the total production would not be significantly affected by this (transient) pressure increase. This argument is further strengthened by remembering that the alternative to the control is a slower start-up. The reduction in production volume due to increased pressure in the pipeline for the controlled case will probably be significantly lower than the reduction in production during a slow start-up. This could, however, not be tested in this work since we have assumed that the inflow is independent on the pipeline pressure.

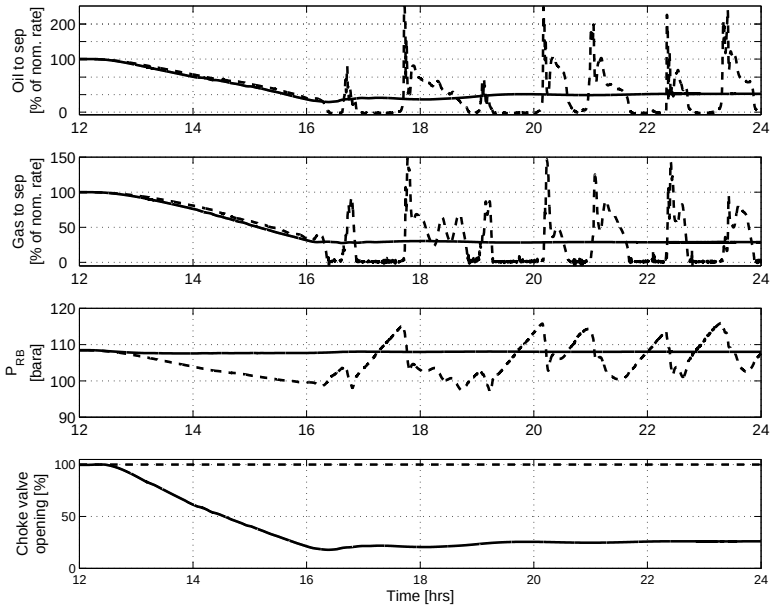

Figure 7.9: Reduced production phase (B) for oil-dominated case.

Stabilization of riser slugging

Figures 7.6 and 7.7 show that there will be riser slugging in the system at reduced production for the uncontrolled case. The rates will be well below the setpoints for the flow controller when the production is reduced, so the flow controllers are inactive. This means that the extended slug controller will work as a regular anti-slug controller during this phase. Figure 7.9 shows the details of the transition to slug flow for the uncontrolled case (dashed line) and the stabilized operating point for the controlled case (solid line).

The control system stabilizes the flow in the pipeline and keeps the riser base pressure P_{Rb} at its setpoint. The setpoint is chosen to achieve a suitable pressure drop (around 2 bars) over the choke valve to ensure enough process gain for the stabilizing controller to be effective. Note that feedback control is essential for keeping the flow stable, as a constant valve opening of 30% (which is the same as average valve opening implemented by the control system) would result in riser slugging.

7.4.2 Gas-Dominated Case

We now repeat the simulations for the gas-dominated case, which will occur as the Tyrihans field matures. From the simulations in figures 7.10 and 7.11, we see, as expected, that riser slugging at reduced rates no longer occurs. The startup slugs have a similar effect as in the oil-dominated flow section, but the surge waves arising during the production increase have a more serious effect in this case.

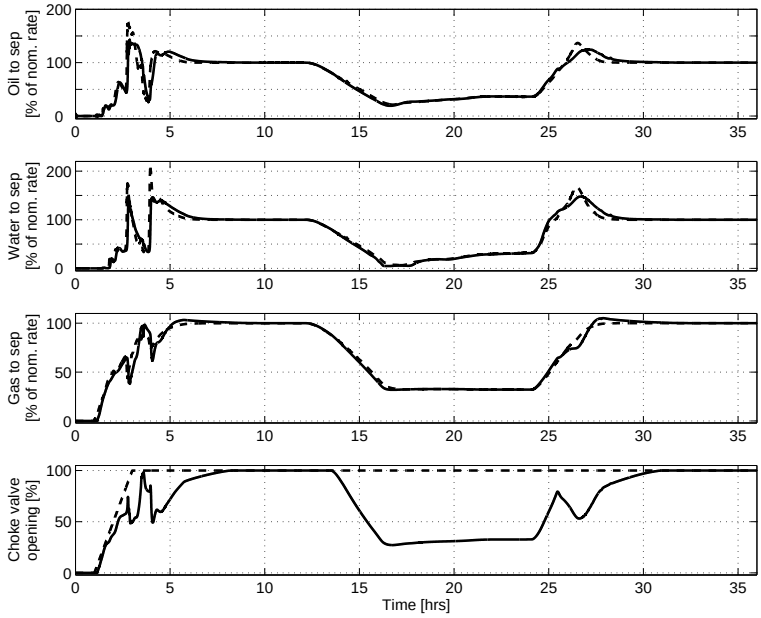

Figure 7.10: Simulated flows for the gas-dominated case. Solid lines for controlled case, dashed lines for uncontrolled.

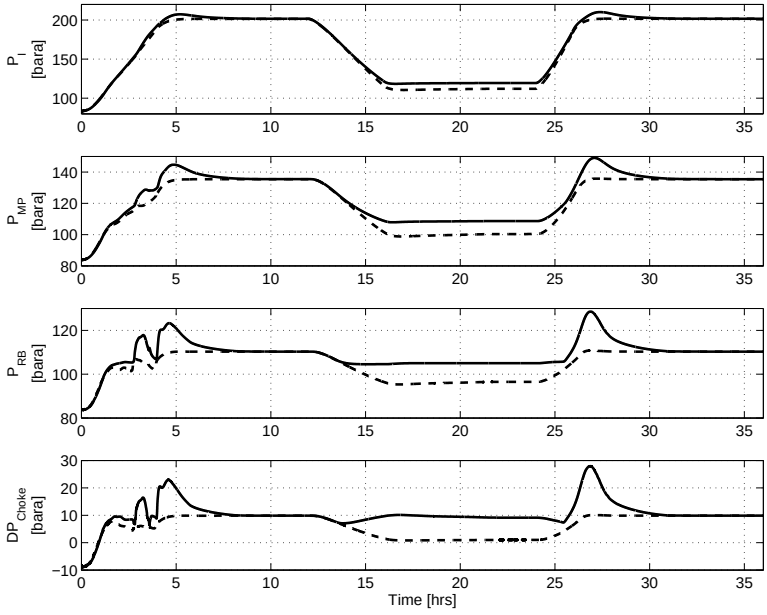

Figure 7.11: Simulated pressures for the gas-dominated case.

Surge wave suppression

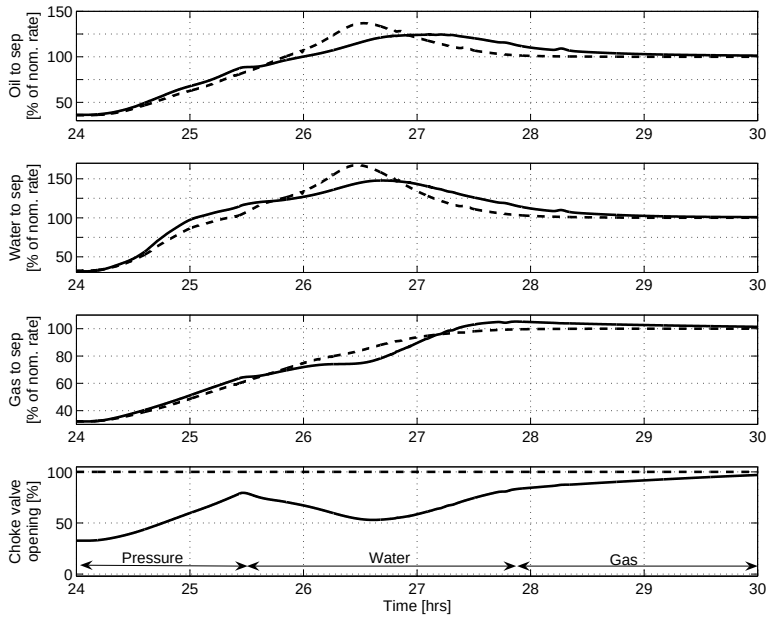

Figure 7.12: Simulated flows for production increase phase (C) for the gas-dominated case.

The suppression of surge waves, shown in more detail in figure 7.12, is very similar to the suppression of start-up slugs described in section 7.4.1. The ramp-up from reduced flow is handled by the pressure controller and when the wave arises the flow controllers take over and limit the flow. For this case, the water is regarded by the controller (through the tuning parameters) as the most critical phase. Again the pipeline volume is used as a buffer to smear out the wave(s). After the majority of the liquid wave has passed through the choke valve, the gas flow controller takes over to avoid a burst of (compressed) gas following the liquid surge wave.

Figure 7.11 shows that the inlet pressure P_I is only marginally affected by the choking to suppress the surge waves. Thus, the total production volume during the rate transition would not be significantly affected (see also discussion in section 7.4.1).

7.5 Conclusions

The extended slug controller introduced in this paper is designed to avoid riser slugging and suppress both start-up slugs and surge waves. Riser slugging is avoided by a anti-slug controller that stabilize the flow based on measuring the riser base pressure. Start-up slugs and surge waves are averaged out with individual proportional action flow controllers for each phase. The flow controllers reduce the choke valve opening if the flow for the given

phase exceeds its setpoint and will hence use the pipeline as a buffer volume, rather than letting the waves enter the inlet separator, which has a significantly lower volume than the pipeline.

The flow and pressure controller that constitute the extended slug controller are combined through a minimum select functionality. This ensures, through the tuning principles introduced in this paper, that the controller effectively limits the flow based on the most critical phase (relative to its maximum allowed production as defined by the downstream production capacity). The minimum select functionality also ensures a bumpless switch between the pressure and flow modes of the controller.

The actions and benefits of the proposed extended slug controller are illustrated by simulations from an industrial case study. The case study clearly shows that the controller effectively eliminates riser slugging, and that the peak rates of the start-up slugs and surge waves are significantly reduced by smearing out the waves.

Chapter 8

Conclusions and further work

8.1 Conclusions

Chapter 2

A controllability analysis based on a simplified two-fluid model finds that an upstream pressure measurement, located either at the pipeline inlet or at the riser base, is well suited for stabilizing control. A topside pressure measurement cannot be used for stabilizing control due to unstable zeros dynamics. A flow measurement can be used for stabilizing control, but due to low steady-state gain, it should only be used in an inner loop in a cascade controller or in combination with another measurement in a MISO (multiple-input single-output) controller. The chapter also concludes that a simpler model of the system could be used for control purposes.

Chapter 3

A simplified, nonlinear model with only 3 dynamic states for a pipeline-riser system is introduced. The model fitted it to both experimental data and data from a simulated OLGA test case with good results. The model is further verified by a controllability analysis that shows the same results as for the two-fluid model used in chapter 2. The model is easy to fit to experimental data, and is well suited for controllability analysis and controller design.

Chapter 4

Simple equations are derived for computing the minimum input rate required for both stable and unstable systems. The input rate limitation is combined with the input magnitude limitation to form a frequency dependent bound on the input that can be used in controllability analysis and controller design. The applicability of the bounds are demonstrated on a simple example and on the simulated OLGA case, where input rate limitations can be a limiting factor for stabilizing control.

Chapter 5

A anti-slug PID controller based on an upstream pressure measurement (located either at the pipeline inlet or at the riser base) is shown to provide good performance, and can possibly also be extended with an inner flow loop to further improved the disturbance rejection. A cascade controller based on only topside measurements (flow control in inner loop, pressure drop over valve or valve position as measurement in outer loop) can also be used to stabilize the process, but the setpoint tracking is slow due to unstable zeros dynamics in the outer loop.

Chapter 6

A SISO $\mathcal{H}_\infty$ controller based on an upstream pressure measurement is almost identical to a PID controller, which confirms that a PID controller is a good choice when this measurement is used for stabilizing control. MISO $\mathcal{H}_\infty$ controllers based on only topside measurements show significantly improved low-frequency performance compared to the cascade controllers in chapter 5. We were not able to design an LQG controller based on topside measurements that could provide the same performance as the corresponding $\mathcal{H}_\infty$ controller.

Chapter 7

An extended slug controller based on an anti-slug controller combined with individual flow controllers for each phase is shown to be effective for both avoiding riser slugging and suppressing transient slugs (i.e. surge waves and startup slugs). The suppression of the transient slugs are based on using the pipeline as a buffer volume to average out the flows, rather that the (significantly smaller) inlet separator.

8.2 Directions for future work

Model extensions

The simplified model developed in chapter 3 are based on a simple pipeline-riser system with a regular L-shaped riser. Another limitation is the assumption of constant liquid holdup in the pipeline leading into the riser, which prevents that both frequency and amplitude of the oscillations can be fitted simultaneously. The following extensions of the simplified 3-state model should thus be investigated

- Other pipeline and riser configurations, including S-shaped risers
- Varying liquid holdup in the pipeline
- Extension to three-phase (inclusion of water)
- Gas lift entering at the riser base

The last point would also mean that the a common model for both casing-heading instabilities in gas-lifted systems (Jansen et al., 1999; Eikrem et al., 2004) and riser slugging should be developed. A model that combines both these phenomena would also be useful to study the stabilizing effect that gas lift has on pipeline-riser systems.

New measurements or combination of measurements for anti-slug controllers

When only topside measurements are available, fundamental limitations in the process (e.g. unstable zero dynamics, low steady state gain) prevents us from using SISO (single-input single-output) anti-slug controllers. There may exist other physical measurements, or alternatively combinations of existing measurements, that are not limited by these fundamental limitations. For example, the model for the flow out of the riser does not contain any unstable zeros, whereas the model for both the topside pressure and density both contain unstable zeros. However, flow measurement is often obtained from a density and a pressure measurement by using a valve equation (Skofteland and Godhavn, 2003). This shows that (nonlinear) combinations of measurements have different properties than the original measurements and that it may be possible to find topside measurements or combinations of measurements that can be used for SISO stabilizing control.

Bibliography

Baker, D. (1954), 'Simultanous flow of oil and gas', *Oil and Gas J.* **53**, 183–195.

Barnea, D. (1987), 'A unified model for predicting flow pattern transitions for the whole range of pipe inclinations', *Int. J. Multiphase Flow* **13**, 1–12.

Bendiksen, K., Malnes, D. and Nydal, O. (1985), 'On the modeling of slug flow', *Chemical Engineering Science* **40**, 59–75.

Bewley, T. (2000), 'Flow control: new challenges for a new renaissance', *Progress in Aerospace Sciences* **37**, 21–58.

Buller, A., Fuchs, P. and Klemp, S. (2002), 'Flow assurance', Statoil's Research & Technology Memoir No. 1, Available on request from authors.

Chen, J. (2000), 'Logarithmic integrals, interpolation bounds and performance limitations in MIMO feedback systems', *IEEE Transactions on Automatic Control* **AC-45**(6), 1098–1115.

Courbot, A. (1996), 'Prevention of severe slugging in the Dunbar 16" multiphase pipeline', Offshore Technology Conference, May 6-9, Houston, Texas.

Eikrem, G., Imsland, L. and Foss, B. (2004), Stabilization of gas lifted wells based on state estimation, *in* 'Proc. of 7th international symposium on advanced control of chemical processes, Hong Kong, 11-14 Jan. 2004'.

Fard, M., Godhavn, J.-M. and Sagatun, S. (2003), 'Modeling and slug control within OLGA', Submitted to SPE Journal.

Glover, K. (1986), 'Robust stabilization of linear multivariable systems: relations to approximation', *Int. J. Control* **43**(3), 741–766.

Godhavn, J.-M., Mehrdad, P. F. and Fuchs, P. (2005), 'New slug control strategies, tuning rules and experimental results', *Journal of Process Control* (15), 547–577.

Godhavn, J.-M., Strand, S. and Skofteland, G. (2005), 'Increased oil production by advanced control of receiving facilities', IFAC world congress, Prague, Czech Republic.

Havre, K. and Dalsmo, M. (2002), 'Active feedback control as a solution to severe slugging', SPE *Production and Facilities* pp. 138–148. SPE 79252.

Havre, K. and Skogestad, S. (1997), Limitations imposed by rhp zeros/poles in multivariable systems, *in* 'Proc. European Control Conference, Brussels'. number Tu-A H1.

Havre, K. and Skogestad, S. (2001), 'Achievable performance of multivariable systems with unstable zeros and poles', *International Journal of Control* **48**, 1131–1139.

Havre, K. and Skogestad, S. (2003), 'Selection of variables for stabilizing control using pole vectors', *IEEE Trans. Autom. Control* **74**(8), 1393–1398.

Havre, K., Stornes, K. and Stray, H. (2000), 'Taming slug flow in pipelines', *ABB review* **4**, 55–63.

Hedne, P. and Linga, H. (1990), 'Suppression of terrain slugging with automatic and manual riser choking', *Advances in Gas-Liquid Flows* pp. 453–469.

Henriot, V., Courbot, A., Heintze, E. and Moyeux, L. (1999), 'Simulation of process to control severe slugging: Application to the Dunbar pipeline', SPE Annual Conference and Exhibition in Houston,Texas. SPE 56461.

Hollenberg, J., de Wolf, S. and Meiring, W. (1995), 'A method to supress severe slugging in flow line riser systems', Proc. 7th Int. Conf. on Multiphase Technology Conference.

Jansen, B., Dalsmo, M., Nøkkelberg, L., Havre, K., Kristiansen, V. and Lemetayer, P. (1999), 'Automatic control of unstable gas lifted wells', paper SPE 56832 presented at the 1999 SPE Annual Technical Conference and Exhibition, Houston, Texas, Oct. 3-6, 1999.

Kovalev, K., Cruickshank, A. and Purvis, J. (2003), 'The slug suppression system in operation', Offshore Europe 2003, Aberdeen, UK. SPE 84947.

Mandhane, J., Gregory, G. and Aziz, K. (1974), 'A flow pattern map for gas-liquid flow in horizontal pipes', *Int. J. Multiphase Flow* **1**, 537–553.

Patankar, S. (1980), *Numerical Heat Transfer and Fluid Flow*, Series in Computational Methods in Mechanics and Thermal Sciences, Hemisphere Publishing Company.

Sachdeva, R., Schmidt, Z., Brill, J. and Blais, R. (1986), 'Two phase flow through chokes'. SPE 15657.

Sarica, C. and Tengesdal, J. (2000), 'A new teqnique to eliminating severe slugging in pipeline/riser systems', SPE Annual Technical Conference and Exibition, Dallas, Texas. SPE 63185.

Schmidt, Z., Brill, J. and Beggs, H. (1979*a*), 'Choking can eliminate severe slugging', *Oil and Gas Journal* pp. 230–238.

Schmidt, Z., Brill, J. and Beggs, H. (1979*b*), 'Experimental study of severe slugging in a two-phase pipeline-riser system'. SPE 8306.

Sivertsen, H. and Skogestad, S. (2005), 'Anti-slug control experiments on a small scale two-phase loop', Escape'15, Barcelona, Spain, 29 May - 1 June 2005.

Skofteland, G. and Godhavn, J.-M. (2003), Suppression of slugs in multiphase flow lines by active use of topside choke - field experience and experimental results, *in* 'Proc. of MultiPhase '03, San Remo, Italy, 11-13 June 2003'.

Skogestad, S. and Postlethwaite, I. (1996), *Multivariable feedback control*, John Wiley & sons.

Skogestad, S. and Postlethwaite, I. (2005), *Multivariable feedback control, 2. ed.*, John Wiley & sons.

Storkaas, E. (2003), Matlab source code. *www.chembio.ntnu.no/users/skoge/software/index2.html

Taitel, Y. (1986), 'Stability of severe slugging', *Int. J. Multiphase Flow* **12**(2), 203–217.

Taitel, Y. and Barnea, D. (1990), 'Two phase slug flow', *Advances in Heat Transfer* **20**, 71–103.

Taitel, Y., Barnea, D. and Dukler, A. (1980), 'Modeling flow pattern transitions for staedy upward gas-liquid flow in vertical tubes', *AIChE J.* **26**, 345–354.

Taitel, Y. and Dukler, A. (1976), 'A model for predicting flow regime transitions in horizontal and near horizontal gas-liquid flow', *AIChE J.* **22**, 47–55.

Thompson, J. and Stewart, H. (1986), *Nonlinear dynamics and chaos*, John Wiley & sons.

Trudvang, C. (2003), 'Modellbasert stabiliserende regulering av gravitasjonsindusert slugging i pipeline-riser systemer', Diploma Thesis, NTNU (in norwegian).

Weisman, J., Duncan, D., Gibson, J. and Crawford, T. (1979), 'Effect of fluid properties and pipe diameter on two-phase flow patterns in horizontal lines', *Int. J. Multiphase Flow* **5**, 437–460.

Zames, G. (1981), 'Feedback and optimal sensitivity; model reference transformations, multiplicative seminorms, and approximate inverse', *IEEE Transactions on Automatic Control* **AC-26**, 301–320.

Zuber, N. and Findlay, J. (1965), 'Average volumetric concentration in two-phase flow systems', *Journal of Heat Transfer* **87**, 453–468.

Appendix A

Two-fluid model for a pipeline-riser systems

A.1 Modeling details

The PDE-based two-fluid model consist of mass balances (eq. A.1 and A.2) and momentum balances (eq. A.3 and A.4) for the liquid and gas phase. The balance equations combined with the summation equation for the phase fraction (eq. A.5) will give the four states $\alpha_L\rho_L$, $\alpha_G\rho_G$, $\alpha_L\rho_L u_L$ and $\alpha_G\rho_G u_G$.

$$\frac{\partial}{\partial t}\left(\alpha_L\rho_L\right) + \frac{1}{A}\frac{\partial}{\partial x}\left(\alpha_L\rho_L u_L A\right) = 0 \tag{A.1}$$

$$\frac{\partial}{\partial t}\left(\alpha_G\rho_G\right) + \frac{1}{A}\frac{\partial}{\partial x}\left(\alpha_G\rho_G u_G A\right) = 0 \tag{A.2}$$

$$\frac{\partial}{\partial t}\left(\alpha_L\rho_L u_L\right) + \frac{1}{A}\frac{\partial}{\partial x}\left(\alpha_L\rho_L u_L^2 A\right) = -\alpha_L\frac{\partial P}{\partial x} + \alpha_L\rho_L g_x - \frac{S_{Lw}}{A}\tau_{Lw} + \frac{S_i}{A}\tau_i \tag{A.3}$$

$$\frac{\partial}{\partial t}\left(\alpha_G\rho_G u_G\right) + \frac{1}{A}\frac{\partial}{\partial x}\left(\alpha_G\rho_G u_G^2 A\right) = -\alpha_G\frac{\partial P}{\partial x} + \alpha_G\rho_G g_x - \frac{S_{Gw}}{A}\tau_{Gw} - \frac{S_i}{A}\tau_i \tag{A.4}$$

$$\alpha_L + \alpha_G = 1 \tag{A.5}$$

The following assumptions form the basis for the model:

- One-dimensional flow
- Constant liquid density ρ_L
- Constant pressure over a pipe cross-section, implying equal pressure in both phases
- No mass transfer between the phases
- No liquid droplet field in the gas
- Isothermal conditions

Table A.1: Notation used for the two-fluid model

Symbol	Description	Unit
α_k	Volume fraction	
ρ_k	Density	kg/m^3
x	Axial distance	m
u_k	Local phase velocity	m/s
A	Pipe cross-section	m^2
g_x	Gravity vector in pipe direction	m/s^2
S_{kw}	Wetted perim., phase k and wall	m
S_i	Wetted interphase perim.	m
τ_{kw}	Wall friction	Nm^2
τ_i	Inter-phase friction	Nm^2
ϵ	Wall roughness	m
D_{hk}	Hydraulic diameter for phase k	m
Re_k	Reynolds number	-
Db	Bubble diameter	m

- Ideal gas equation of state corrected with a compressibility factor.

The notation used for phases k = L and G are given in table A.1

Since we assume constant liquid density ρ_L, we can extract phase fractions α_k, gas density ρ_L and phase velocities u_k directly from the states. To solve the balance equations, we need to relate the shear stresses against the wall τ_{kw}, the inter-phase shear stress τ_i, the friction factors f_w and f_i and the wetted perimeters S_i and S_{kw} to the state information. The algebraic relations used for friction correlations are:

$$\tau_{kw} = f_w \rho_k \frac{u_k^2}{2} \tag{A.6}$$

$$\tau_i = f_i \rho_g \frac{(u_G - u_L)^2}{2} \tag{A.7}$$

$$f_w = \max\left(\frac{64}{Re_k}, 0.005\left(1 + \left(\frac{2 * 10^4 \epsilon}{D_{hk}} + \frac{10^6}{Re_k}\right)^{1/3}\right)\right) \tag{A.8}$$

$$f_i = 0.02\frac{1 + 75\alpha_L}{4} \tag{A.9}$$

The wetted perimeters are implicit in phase fraction, and are approximated by polynomials:

$$S_i(\text{stratified}) = \left(\alpha_{\text{L}}^2 - \alpha_{\text{L}}\right)(-4\text{D}) \tag{A.10}$$

$$S_i(\text{annular}) = \pi \text{D}\sqrt{\alpha_{\text{G}}} \tag{A.11}$$

$$S_i(\text{bubble}) = \frac{\pi \alpha_{\text{G}} \text{D}^2}{\text{Db}} \tag{A.12}$$

$$S_{kw} = \pi \alpha_k D \tag{A.13}$$

A.1.1 Discretization of the PDEs

In order to solve the system of PDEs, we discretize in space and solve the resulting set of Ordinary Differential Equations (ODEs). A staggered grid approach is used, where the momentum equations is solved on a grid that are displaced by half a cell relative to the grid used for the mass conservation equation. This is required for numeric stability of the solution with standard ODE solvers (in this work we use the built-in MatLab solver ODE23tb). We used 13 grid points for the mass conservations equations and 12 grid points the momentum equations, resulting in a set of 50 ODEs. The grids points were unequally distributed, with highest density of grid points around the bottom of riser. The spatial derivatives are computed using a backward difference scheme (Patankar, 1980). Since the direction of the flow can change in this system, care has to be taken when allocating data to the ODEs. For forward flow, the data for the spatial derivatives is collected upstream the control volume, when the flow reverses, the data is collected downstream.

A.1.2 Dealing with different flow regimes

Multiphase flow may change between different flow regimes. Flow regime maps, showing the stability region of the various flow patterns as function of liquid and gas velocity, have been developed based on experimental data. Baker (1954) was one of the first to investigate the stability of the different flow regimes, the resulting map for horizontal flow of oil and gas is shown in figure A.1.

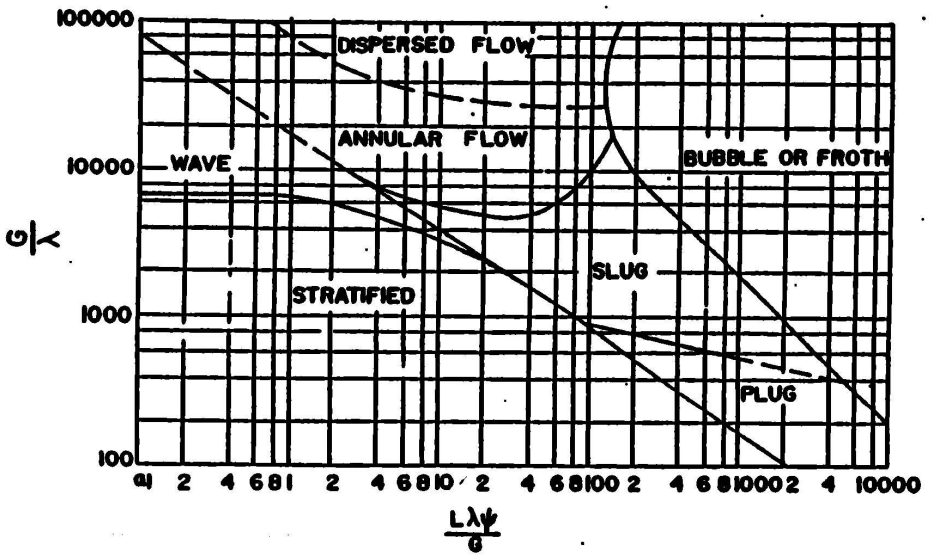

Figure A.1: Flow regime map for horizontal flow of oil and gas

The parameters used on the axis in figure A.1 are

$$\gamma = \left[\left(\frac{\rho_G}{0.075}\right)\left(\frac{\rho_L}{62.3}\right)\right]^{0.5}, \psi = \frac{73}{\sigma}\left[\mu_L\left(\frac{62.3}{\rho_L}\right)^2\right]^{1/3} \tag{A.14}$$

More recent work can be found in Schmidt et al. (1979*b*). Friction, phase distribution and other system properties which depends on flow regimes are computed either by algebraic correlations or interpolated from experimental data based on the predicted flow regime. Commercial multiphase flow simulators use flow regime maps and the experimental data behind these maps to determine the flow regime and the suitable correlations for the problem at hand. However, the flow regime maps are, as already mentioned, based on *open loop* experimental data. In this work, where we are concerned with operation in open-loop unstable operating points, the maps do not apply. Because of this, we do not use flow regime dependent correlations (except for the possibility for annular and bubbly flow in the riser, where we only consider this change to be a function of phase fraction)

Appendix B

Simplified model for a pipeline-riser systems

This appendix contains the set of equations that constitutes the simplified model of a pipeline-riser system at riser slugging conditions that was developed in chapter 3. The model is implemented in Matlab and the model files are available at the web (Storkaas, 2003)

B.1 Model Assumpions

A1 The liquid dynamics in the feed pipeline are neglected by assuming constant liquid velocity.

A2 Constant gas volume V_{G1} in the feed pipeline. This follows from assumption A1 if we also neglect the liquid volume variations due to variations in the liquid level h_1 at the low-point.

A3 Only one dynamical state for liquid holdup (the control volume V_L with holdup m_L includes both the riser and the part of the feed pipeline from the low-point to the level h_1)

A4 Two dynamical states for gas holdup ,m_{G1} and m_{G2}, occupying the volumes V_{G1} and V_{G2}, respectively. The gas volumes are separated by the low point, and connected through a pressure-flow relationship.

A5 Ideal gas behavior

A6 Stationary pressure balance over the riser (between pressures P_1 and P_2)

A7 Simplified valve equation for gas and liquid leaving the system at the top of the riser

A8 Constant temperature

B.2 Model Equations

Conservation equations

$$\frac{d}{dt}m_L = w_{L,in} - w_{L,out} \tag{B.1}$$

$$\frac{d}{dt}m_{G1} = w_{G,in} - w_{G1} \tag{B.2}$$

$$\frac{d}{dt}m_{G2} = w_{G1} - w_{G,out} \tag{B.3}$$

Calculation of state-dependent internal variables

$$P_1 = \frac{m_{G1}RT}{V_{G1}M_G} \tag{B.4}$$

$$\rho_{G1} = \frac{m_{G1}}{V_{G1}} \tag{B.5}$$

$$V_L = \frac{m_L}{\rho_L} \tag{B.6}$$

$$h_1 A_1 + V_{LR} = V_L \tag{B.7}$$

$$V_T = A_2\left(H_2 + L_3\right) \tag{B.8}$$

$$V_{G2} = V_T - V_{LR} \tag{B.9}$$

$$\rho_{G2} = \frac{m_{G2}}{V_{G2}} \tag{B.10}$$

$$\alpha_L = \frac{V_{LR}}{V_T} \tag{B.11}$$

$$P_2 = \frac{m_{G2}RT}{V_{G2}M_G} \tag{B.12}$$

$$\bar{\rho} = \frac{m_{G2} + V_{LR}\rho_L}{V_T} \tag{B.13}$$

$$\bar{\rho}g\left(H2 + H3\right) - \rho_L g h_1 = P_1 - P_2 \tag{B.14}$$

$$\alpha_{LT} = \left(V_{LR} > H_2A_2\right)\alpha^*_{LT} + \frac{w^n}{1+w^n}\left(\alpha_L - \left(V_{LR} > H_2A_2\right)\alpha^*_{LT}\right) \tag{B.15}$$

$$\alpha^*_{LT} = \frac{V_{LR} - A_2H_2}{A_2L_3} \tag{B.16}$$

$$w = \frac{K_3\rho_{G1}v^2_{G1}}{\rho_L - \rho_{G1}} \tag{B.17}$$

$$\rho_T = \alpha_{LT}\rho_L + \left(1-\alpha_{LT}\right)\rho_{G2} \tag{B.18}$$

$$\alpha^m_L = \frac{\alpha_{LT}\rho_L}{\alpha_{LT}\rho_L + \left(1-\alpha_{LT}\right)\rho_{G2}} \tag{B.19}$$

Flow equations

$$v_{G1} = (h_1 < H_1)\, K_2 \frac{H_1 - h_1}{H_1} \sqrt{\frac{P_1 - P_2 - \rho_L g \alpha_L H_2}{\rho_{G1}}} \tag{B.20}$$

$$w_{G1} = v_{G1} \rho_{G1} \hat{A} \tag{B.21}$$

$$m_{mix,out} = K_1 z \sqrt{\rho_T \left(P_2 - P_0\right)} \tag{B.22}$$

$$w_{G,out} = \left(1 - \alpha_L^m\right) m_{mix,out} \tag{B.23}$$

$$w_{L,out} = \alpha_L^m m_{mix,out} \tag{B.24}$$

Geometric equations

$$H_1 = \frac{2r}{cos\left(\theta\right)}$$

$$A_1 = \frac{A_2}{sin\left(\theta\right)}$$

$$\phi = \left(\pi - acos\left(1 - \frac{(H1 - h1)\, cos\left(\theta\right)}{r}\right)\right)$$

$$\hat{A} = r^2 \left(\pi - \phi - cos\left(\pi - \phi\right) sin\left(\pi - \phi\right)\right) \tag{B.25}$$

B.3 Notation

Symbol	Description	Unit	Remarks
m_{Gi}	Mass of gas in volume i	Kg	State variable
m_L	Mass of liquid	Kg	State variable
V_{Gi}	Gas volume i	m^3	$V_{G1} = const$
V_L	Volume occupied by liquid	m^3	
V_{LR}	Volume of liquid in riser	m^3	
V_T	Total volume in riser	m^3	
P_i	Pressure in volume i	$\frac{N}{M^2}$	
ρ_{Gi}	Gas density in volume i	$\frac{kg}{m^3}$	
ρ_L	Liquid density	$\frac{kg}{m^3}$	Constant
$\bar{\rho}$	Average density in riser	$\frac{kg}{m^3}$	
ρ_T	Density upstream valve	$\frac{kg}{m^3}$	
v_{G1}	Gas velocity at lowpoint	$\frac{m}{s}$	
$v_{mix,out}$	Liquid velocity through choke valve	$\frac{m}{s}$	
w_{G1}	Internal gas mass flowrate	$\frac{Kg}{s}$	
$w_{G,out}$	Gas mass flowrate through choke valve	$\frac{Kg}{s}$	
$w_{L,out}$	Liq. mass flowrate through choke valve	$\frac{Kg}{s}$	
α_L	Average liq. frac. in riser, volume basis	-	
α_{LT}	Liq. frac. upstream valve, volume basis	-	
α_L^m	Liq. frac. upstream valve, mass basis	-	
α_{LT}^*	Liq. frac. upstream valve without entr.	-	
h_1	Liquid Level upstream the dip	m	
H_1	Critical liquid level	m	Constant
H_2	Height of riser	m	Constant
r	Radius of pipe	m	Constant
A_1	Area in horizontal plane, V_1	m^2	Constant
A_2	Cross section area, V_2	m^2	Constant
$\hat{A}$	Gas flow area at lowpoint	m^2	
L_3	Length of horizontal top section	m	Constant
θ	Feed pipe inclination	rad	Constant
R	Gas Constant	$8314\frac{J}{K \cdot Kmol}$	Constant
g	Spesific gravity	$9.81\frac{m}{s^2}$	Constant
T	System Temperature	K	Constant
M_G	Molecular weight of Gas	$\frac{Kg}{Kmol}$	Constant
$w_{G,in}$	Mass rate of gas into system	$\frac{Kg}{s}$	Disturbance
$w_{L,in}$	Mass rate of liquid into system	$\frac{Kg}{s}$	Disturbance
P_0	Pressure after choke valve	$\frac{N}{M^2}$	Disturbance
z	Valve Position	-	Input
K_1	Choke valve constant	-	Tuning param.
K_2	Gas Flow constant	-	Tuning param.
K_3	Friction parameter	-	Tuning param.
n	w^n in the friction expression	-	Tuning param.

Appendix C

Simulations

This appendix contains all the simulations with the controllers designed in chapters 5 and 6 with all three models used in this thesis (the three-state model from chapter 3, the two-fluid model from chapter 2 and OLGA). The controller parameters and closed loop norms, calculated based on the three-state model, are given for each controller.

C.1 SISO PID-controllers

Table C.1: Tuning parameter and achieved closed loop norms for SISO PID control

y	Minimized	K_c	$\tau_I[s]$	$\tau_D[s]$	$\tau_F[s]$	$\|S\|_\infty$	$\|T\|_\infty$	$\|KS\|_\infty$
P_I	$\|S\|_\infty$, $\|KS\|_\infty$ [a]	-0.098bar^{-1}	600	14.2	6.9	**1.26**	1.91	**0.29**
P_I	$\|T\|_\infty$	-0.20bar^{-1}	600	14.3	12.3	1.60	**1.44**	0.50
P_{Rb}	$\|S\|_\infty$, $\|KS\|_\infty$ [a]	-0.16bar^{-1}	600	0	0.9	**1.03**	1.52	**0.30**
P_{Rb}	$\|T\|_\infty$	-0.30bar^{-1}	600	0	2.0	1.11	**1.25**	0.45
Q	$\|S\|_\infty$ [b]	120$\frac{m^3}{(bar\cdot s)}$	∞	0	145	**1.00**	1.34	0.31
Q	$\|T\|_\infty$	270$\frac{m^3}{(bar\cdot s)}$	∞	0	135	1.00	**1.16**	0.63
Q	$\|KS\|_\infty$	55$\frac{m^3}{(bar\cdot s)}$	∞	0	135	1.35	2.02	**0.15**

[a] The controller that minimizes $\|KS\|_\infty$ is not unique; these parameters minimize $\|S\|_\infty$ whilst achieving $\min_K(\|KS\|_\infty)$

[b] Design not unique, these parameters achieves $\|S\|_\infty = 1$ with minimal input usage

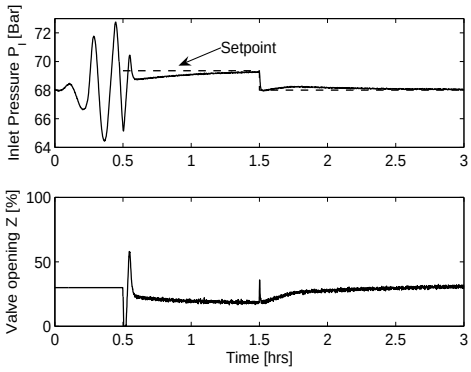

(a) Simplified model, $\|S\|_\infty$ minimized

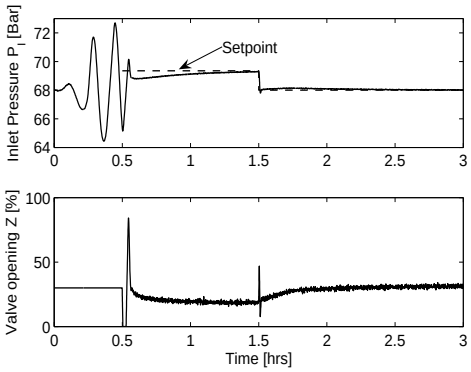

(b) Simplified model, $\|T\|_\infty$ minimized

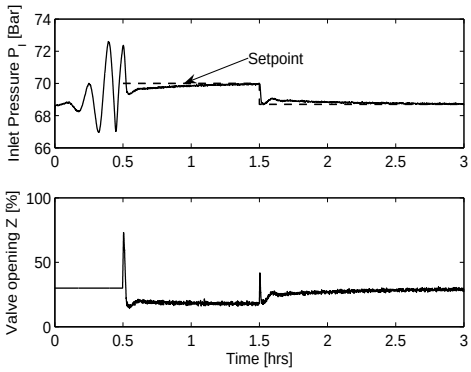

(c) Two-fluid model, $\|S\|_\infty$ minimized

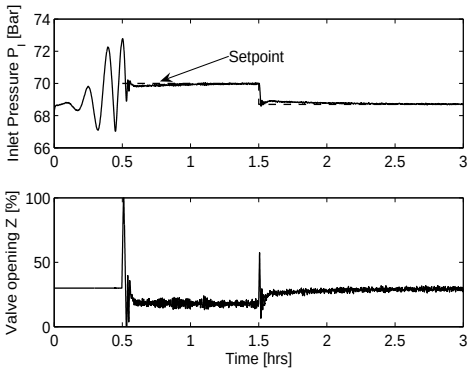

(d) Two-fluid model, $\|T\|_\infty$ minimized

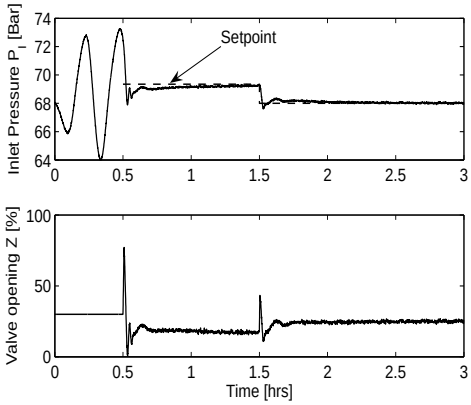

(e) OLGA model, $\|S\|_\infty$ minimized

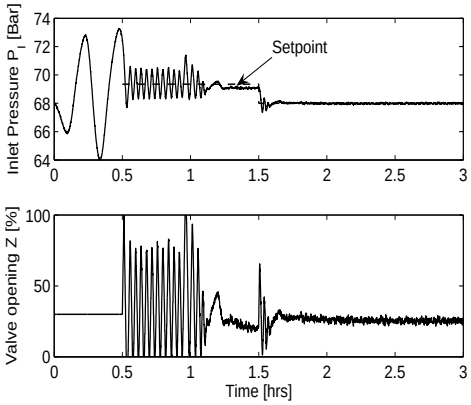

(f) OLGA model, $\|T\|_\infty$ minimized

Figure C.1: Anti-slug control ($y = P_I$)

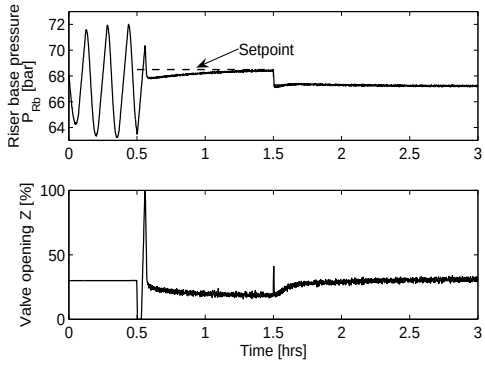

(a) Simplified model, $\|S\|_\infty$ minimized

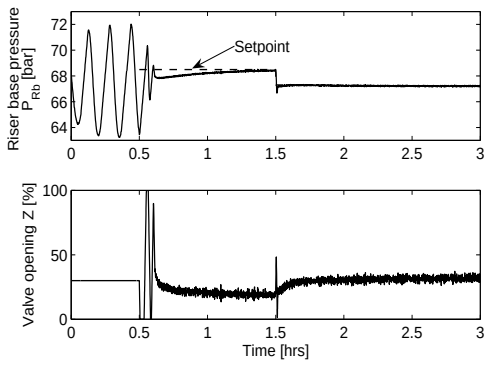

(b) Simplified model, $\|T\|_\infty$ minimized

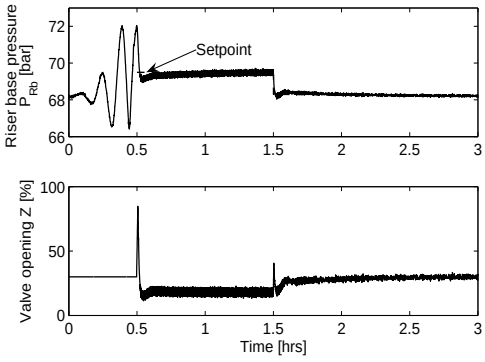

(c) Two-fluid model, $\|S\|_\infty$ minimized

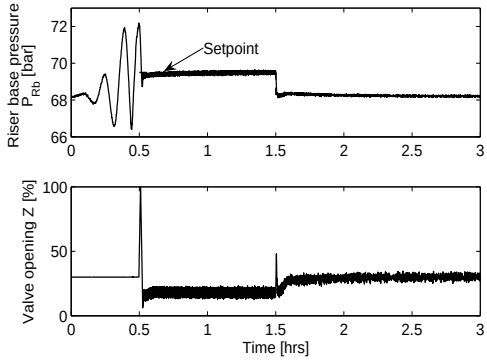

(d) Two-fluid model, $\|T\|_\infty$ minimized

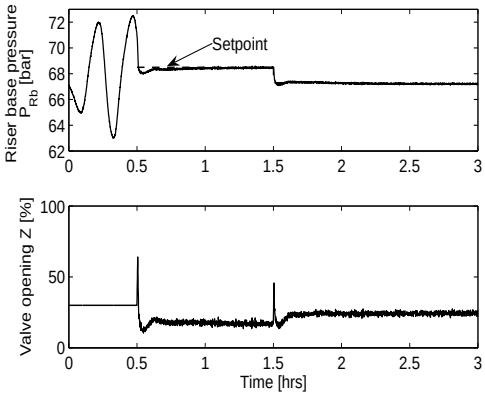

(e) OLGA model, $\|S\|_\infty$ minimized

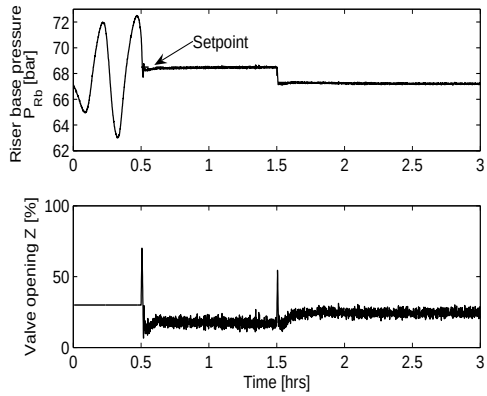

(f) OLGA model, $\|T\|_\infty$ minimized

Figure C.2: Anti-slug control ($y = P_{Rb}$)

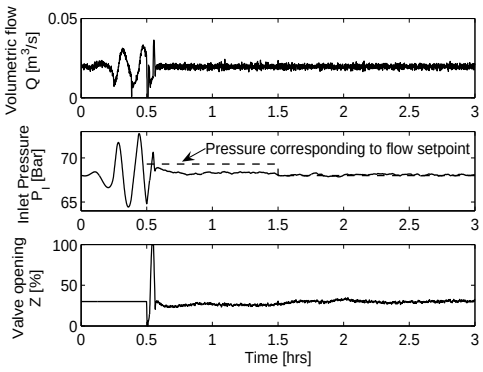

(a) Simplified model, $\|S\|_\infty$ minimized

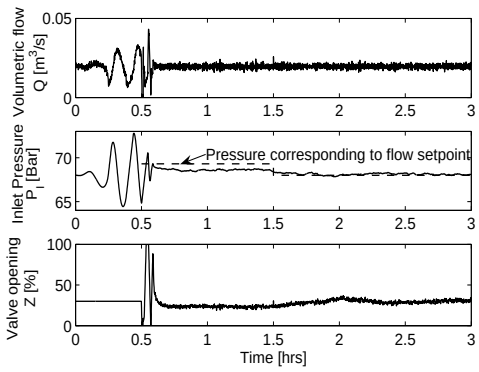

(b) Simplified model, $\|KS\|_\infty$ minimized

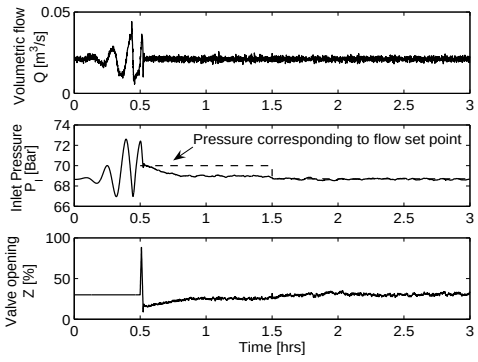

(c) Two-fluid model, $\|S\|_\infty$ minimized

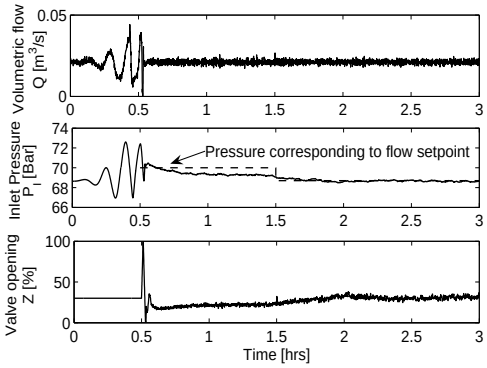

(d) Two-fluid model, $\|KS\|_\infty$ minimized

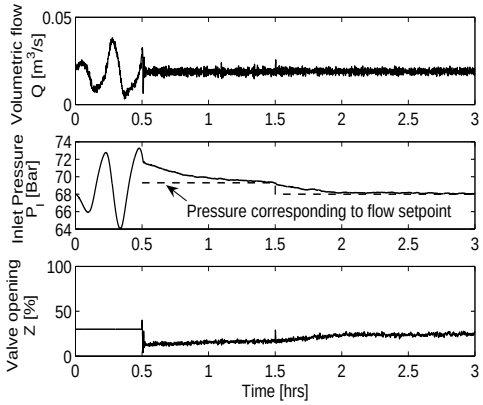

(e) OLGA model, $\|S\|_\infty$ minimized

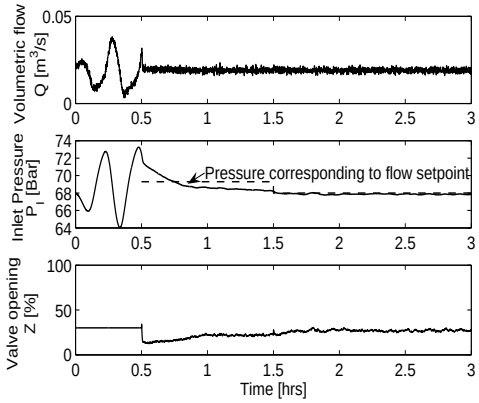

(f) OLGA model, $\|KS\|_\infty$ minimized

Figure C.3: Anti-slug control ($y = Q$)

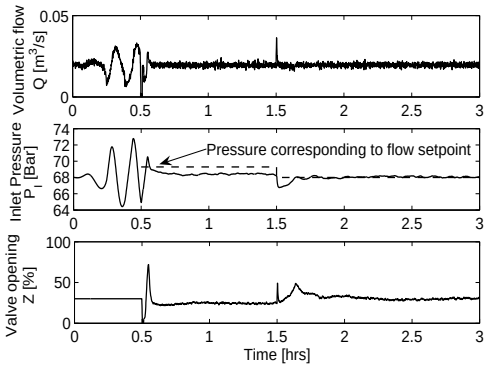

(a) Simplified 3-state model, $\|T\|_\infty$ minimized

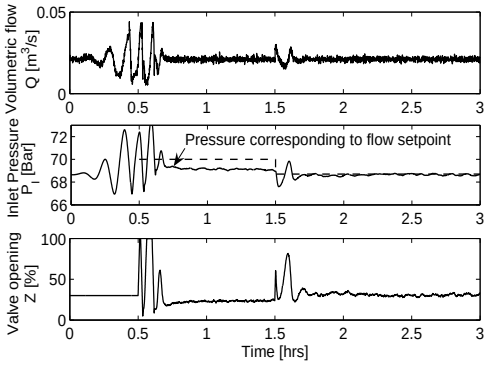

(b) Two-fluid model, $\|T\|_\infty$ minimized

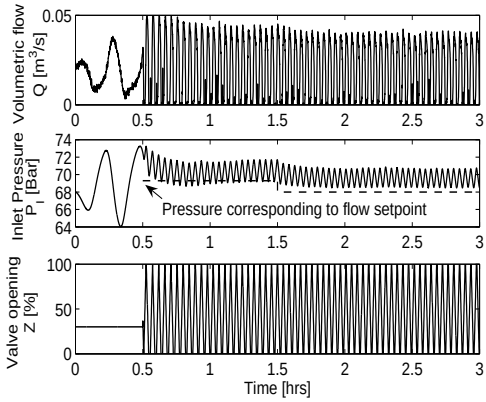

(c) OLGA model, $\|T\|_\infty$ minimized

Figure C.4: Anti-slug control ($y = Q$)

C.2 Cascade controllers

Table C.2: Tuning parameter and achieved closed loop norms for SISO PID control

y	K_{c1}	$\tau_{I1}[s]$	$\tau_{F1} = \tau_{F2}[s]$	$K_{c1}[s/m^3]$	$\|S\|_\infty$	$\|T\|_\infty$	$\|KS\|_\infty$
$[P_1\ Q]$	-0.001 $\frac{m^3}{(bar \cdot s)}$	600	135	55	1	1.9	0.29
$[DP\ Q]$	-0.00015 $\frac{m^3}{(bar \cdot s)}$	600	135	55	1.42	2.1	0.16
$[Z\ Q]$	-0.002 $\frac{m^3}{s}$	600	135	90	1.14	1.54	1.42

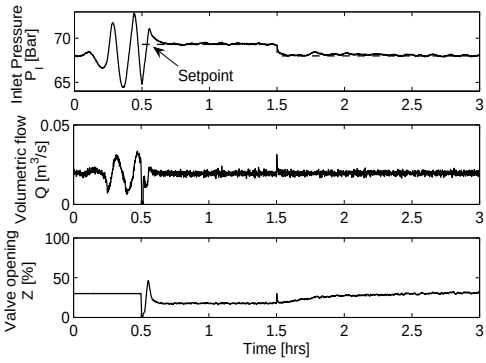

(a) Simplified 3-state model

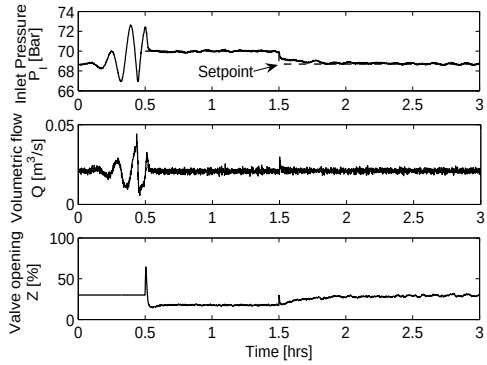

(b) Two-fluid model

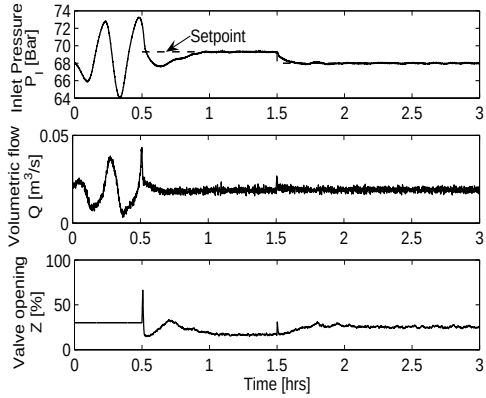

(c) OLGA model

Figure C.5: Anti-slug control ($y_1 = P_I,\ y_2 = Q$)

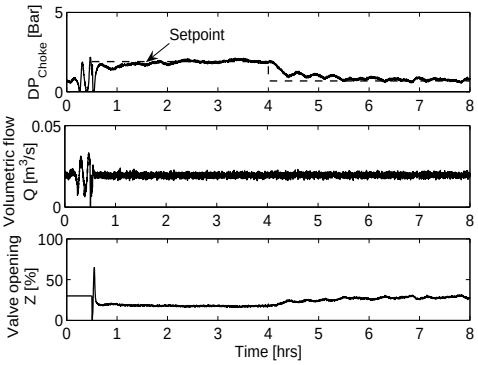

(a) Simplified 3-state model, $y_1 = DP,\ y_2 = Q$

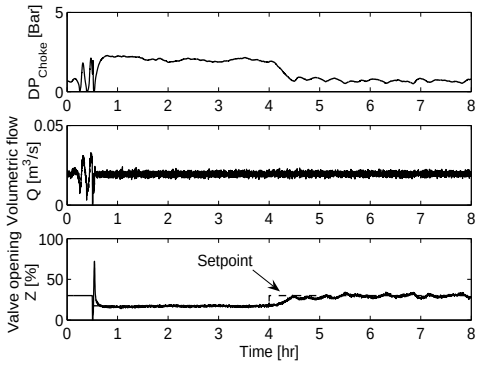

(b) Simplified 3-state model, $y_1 = Z,\ y_2 = Q$

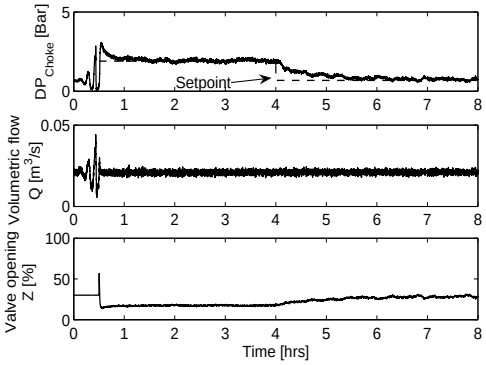

(c) Two-fluid model, $y_1 = DP,\ y_2 = Q$

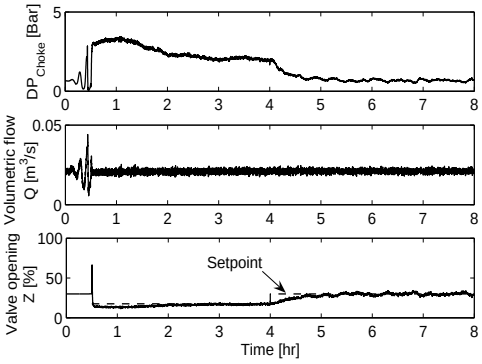

(d) Two-fluid model, $y_1 = Z,\ y_2 = Q$

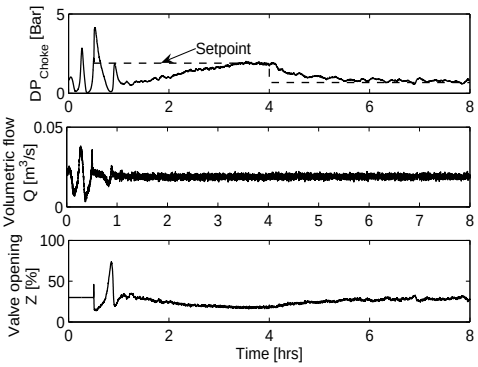

(e) OLGA model, $y_1 = DP,\ y_2 = Q$

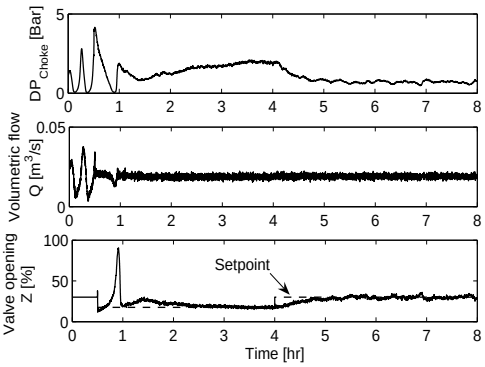

(f) OLGA model, $y_1 = Z,\ y_2 = Q$

Figure C.6: Anti-slug control ($y = Q$)

C.3 Model based controllers

Table C.3: Closed loop norms and bandwidth for model-based controllers

	$\|S\|_\infty$	$\|T\|_\infty$	$\|KS\|_\infty$	ω_B
$\mathcal{H}_\infty$ controller, $y = P_I$	1.48	1.35	0.43	
$\mathcal{H}_\infty$ controller, $y = [DP\ Q]$	1.27	0.94	0.37	0.0025
$\mathcal{H}_\infty$ controller, $y = [Z\ Q]$	1.16	0.91	0.91	0.0010
LQG controller, $y = [DP\ Q]$	14	13	0.43	0.0004

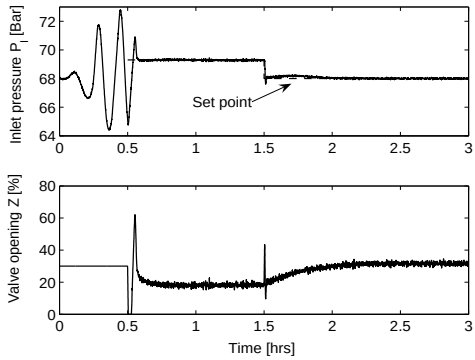

(a) Simplified 3-state model

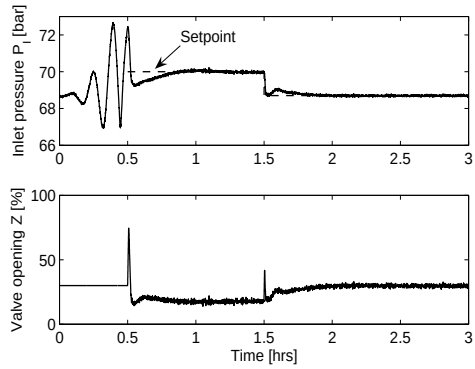

(b) Two-fluid model

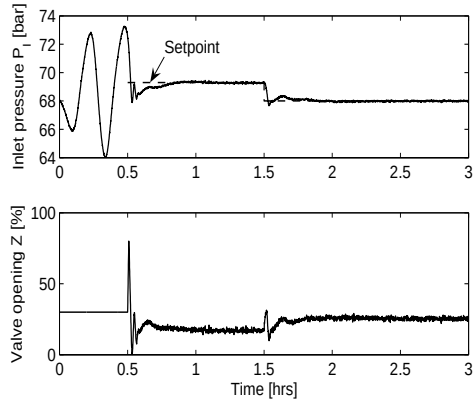

(c) OLGA model

Figure C.7: Anti-slug $\mathcal{H}_\infty$ control with $y_1 = P_I$

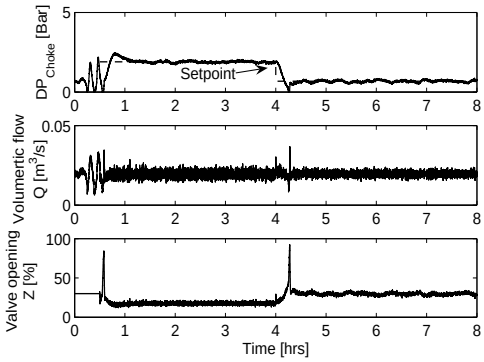

(a) Simplified 3-state model, $y = [DP\ Q]$

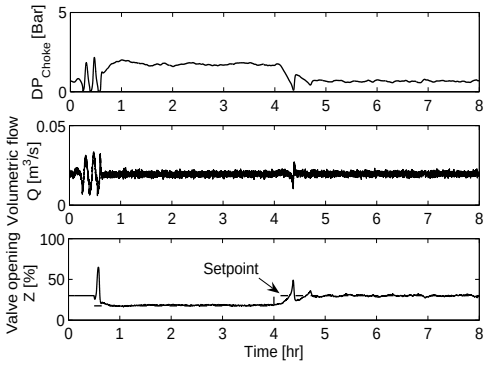

(b) Simplified 3-state model, $y = [Z\ Q]$

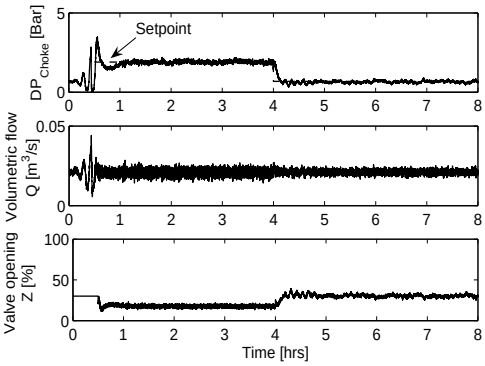

(c) Two-fluid model, $y = [DP\ Q]$

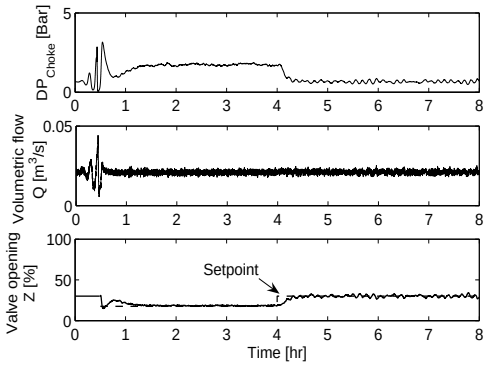

(d) Two-fluid model, $y = [Z\ Q]$

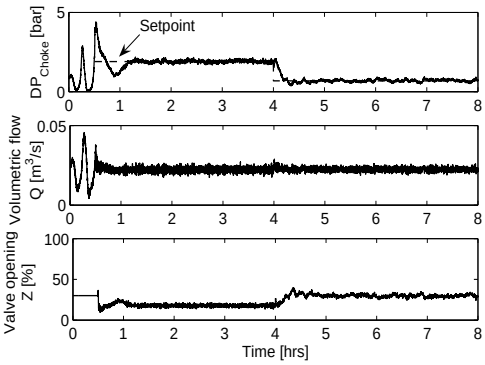

(e) OLGA model, $y = [DP\ Q]$

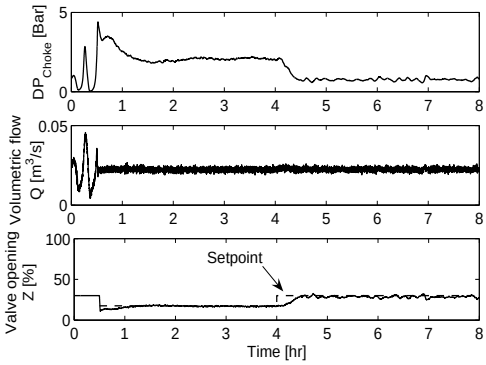

(f) OLGA model, $y = [Z\ Q]$

Figure C.8: Anti-slug MISO $\mathcal{H}_\infty$ control

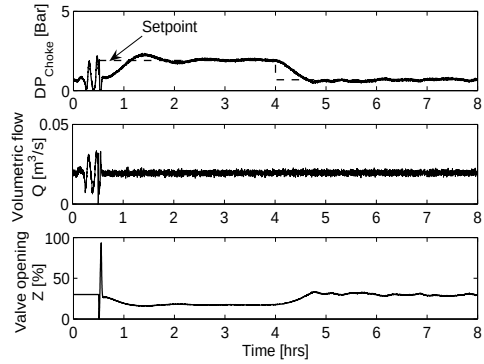

(a) Simplified 3-state model

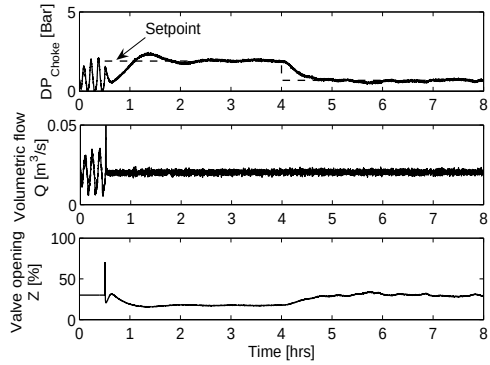

(b) Two-fluid model

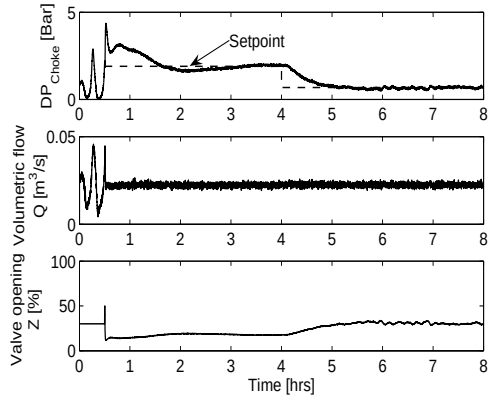

(c) OLGA model

Figure C.9: LQG Anti-slug control with $y = [DP\ Q]$